Indian J Pure & Appl Phys, Vol 21 No. 12 pp. 683-754
DECEMBER 1983
CODEN: IJOPAU ISSN: 0019-5596
21(12) 683-754 (1983)

INDIAN JOURNAL OF PURE & APPLIED PHYSICS

Published by
PUBLICATIONS & INFORMATION DIRECTORATE, CSIR
NEW DELHI
in association with
THE INDIAN NATIONAL SCIENCE ACADEMY, NEW DELHI

CSIR SCIENTIFIC PERIODICALS

JOURNAL OF SCIENTIFIC & INDUSTRIAL RESEARCH (Monthly)

With a fine record of over 45 years' service to the scientific community, this journal has grown into India's leading general science periodical. Intended to fulfil the responsibility of helping the research workers to keep themselves abreast of current developments in various fields of science and technology, the journal carries editorial features highlighting important scientific events in India and abroad, articles on science policy and management of science review articles on topics of current research interest, technical reports on international and national conferences, reviews of scientific and technical publications, and notes on major advances in various fields.

Annual subscription	Rs 120.00	$ 40.00	£ 23.00
Single copy	12.00	4.00	2.30

INDIAN JOURNAL OF CHEMISTRY (Monthly)

Section A: Started in the year 1963, the journal is devoted to papers in Inorganic, Physical, Theoretical and Analytical Chemistry.

Annual subscription	Rs 160.00	$ 53.00	£ 30.00
Single copy	16.00	5.30	3.00

Section B: This journal is devoted to papers in Organic Chemistry, including Medicinal Chemistry.

Annual subscription	Rs 160.00	$ 53.00	£ 30.00
Single copy	16.00	5.30	3.00

INDIAN JOURNAL OF PURE & APPLIED PHYSICS (Monthly)

Started in the year 1963, this journal is devoted to original research communications (full papers and short communications) in all conventional branches of physics (except radio and space physics).

Annual subscription	Rs 180.00	$ 60.00	£ 34.00
Single copy	18.00	6.00	3.40

INDIAN JOURNAL OF RADIO & SPACE PHYSICS (Bimonthly)

The journal, which is being published beginning from March 1972, is intended to serve as a medium for the publication of the growing research output in various areas of radio and space physics, such as ionospheric propagation, magnetosphere, radio and radar astronomy, physics and chemistry of the ionosphere; neutral atmosphere; airglow, winds and motion in the upper atmosphere; stratosphere-mesosphere coupling, ionosphere-magnetosphere coupling; solar-terrestrial relationship, etc.

Annual subscription	Rs 100.00	$ 34.00	£ 19.00
Single copy	20.00	6.80	3.80

INDIAN JOURNAL OF TECHNOLOGY (INCLUDING ENGINEERING) (Monthly)

This journal publishes papers reporting results of original research of applied nature pertaining to unit operations, heat and mass transfer, products, processes, instruments and appliances, etc. The journal is of special interest to research workers in departments of applied sciences in universities, institutes of higher technology, commodity research laboratories, industrial cooperative research institutes, and industrial research laboratories.

Annual subscription	Rs 120.00	$ 40.00	£ 23.00
Single copy	12.00	4.00	2.30

INDIAN JOURNAL OF EXPERIMENTAL BIOLOGY (Monthly)

This journal, devoted to the publication of research communications in the fields of experimental botany, zoology, microbiology, pharmacology, endocrinology, nutrition, etc., is the only one in India with such a wide coverage and scope.

Annual subscription	Rs 180.00	$ 68.00	£ 34.00
Single copy	18.00	6.80	3.40

INDIAN JOURNAL OF BIOCHEMISTRY & BIOPHYSICS (Bimonthly)

This journal, published in association with the Society of Biological Chemists (India), Bangalore, is the only research journal in India devoted exclusively to original research communications in biochemistry and biophysics.

Annual subscription	Rs 65.00	$ 23.00	£ 12.00
Single copy	13.00	4.60	2.40

INDIAN JOURNAL OF MARINE SCIENCES (Quarterly)

Commencing publication from June 1972, this journal is devoted to research communications (full papers and short communications) pertaining to various facets of marine research, viz. biological, physical, geological and chemical oceanography.

Annual subscription	Rs 90.00	$ 30.00	£ 17.00
Single copy	26.00	8.70	5.00

RESEARCH AND INDUSTRY (Quarterly)

Intended to serve as a link between science and industry, this journal is addressed primarily to technologists, engineers, executives and others in industry and trade. It publishes informative original articles containing practical details of processes and products devoted in India, which show promise of ready utilization, and technical digests on new processes, products, instruments and testing methods which are of interest to industry. Developments in Indian industry are regularly reported.

Annual subscription	Rs 70.00	$ 23.00	£ 13.00
Single copy	22.00	7.00	4.00

INDIAN JOURNAL OF TEXTILE RESEARCH (Quarterly)

Commencing publication from March 1976, this journal is devoted to the publication of papers reporting results of fundamental and applied researches in the field of textiles.

Annual subscription	Rs 50.00	$ 17.00	£ 10.00
Single copy	15.00	5.00	3.00

MEDICINAL & AROMATIC PLANTS ABSTRACTS (Bimonthly)

Carries informative abstracts of scientific papers published in important Indian and foreign journals relating to different aspects of medicinal and aromatic plants. Each issue contains about 350 abstracts with a subject index.

Annual subscription	Rs 120.00	$ 40.00	£ 23.00
Single copy	24.00	8.00	4.60

INDUSTRIAL NEWS DIGEST (Monthly)

Provides technical and techno-economic information for industrialists, prospective entrepreneurs and experts in both government and private agencies dealing with the management and planning of industry. Each issue carries at least one profile on a particular industry.

Annual subscription	Rs 40.00	$ 13.00	£ 8.00
Single copy	4.00	1.30	0.80

CURRENT LITERATURE ON SCIENCE OF SCIENCE (Monthly)

Carries abstracts, digests, book reviews, news & notes and R&D statistics with emphasis on problems of S&T in developing countries, it also covers the areas of science policy, R&D planning and management, technology transfer, technology assessment and science and society.

Annual subscription	Rs 100.00	$ 30.00	£ 12.00

Please contact

Manager (Sales & Advertisement)
PUBLICATIONS & INFORMATION DIRECTORATE, CSIR
Hillside Road, New Delhi-110012

RENEWAL NOTICE

Your subscription which expires with the despatch of December 1983 issue of the journal, stands for renewal. We request you to be so good as to return the enclosed order form duly filled early, so as to ensure continuity in despatch.

Manager (Sales & Advertisement)

DATED:

The Manager (Sales & Advertisement)
PUBLICATIONS & INFORMATION DIRECTORATE
HILLSIDE ROAD, NEW DELHI-110012 (INDIA)

Dear Sir,

Please renew my subscription/enrol me as subscriber to:

			Rs.	$	£
1	Journal of Scientific & Industrial Research	(Monthly)	120.00	40.00	23.00
2	Indian Journal of Chemistry, Section A	(Monthly)	160.00	53.00	30.00
3	Indian Journal of Chemistry, Section B	(Monthly)	160.00	53.00	30.00
4	Indian Journal of Experimental Biology	(Monthly)	180.00	68.00	34.00
5	Indian Journal of Technology	(Monthly)	120.00	40.00	23.00
6	Indian Journal of Pure & Applied Physics	(Monthly)	180.00	60.00	34.00
7	Indian Journal of Biochemistry & Biophysics	(Bimonthly)	65.00	23.00	12.00
8	Indian Journal of Radio & Space Physics	(Bimonthly)	100.00	34.00	19.00
9	Indian Journal of Marine Sciences	(Quarterly)	90.00	30.00	17.00
10	Indian Journal of Textile Research	(Quarterly)	50.00	17.00	10.00
11	Research & Industry	(Quarterly)	70.00	23.00	13.00
12	Current Literature on Science of Science	(Monthly)	100.00	30.00	12.00
13	Medicinal & Aromatic Plants Abstracts	(Bimonthly)	120.00	40.00	23.00
14	Industrial News Digest	(Monthly)	40.00	13.00	8.00

(Please tick off the periodicals you would like to subscribe).

for one year from January 1984 for which I/we have remitted to you a sum of Rs .....£ ..... $ ..... by Cheque/Demand Draft No. ..... dated ..... in favour of PUBLICATIONS & INFORMATION DIRECTORATE, NEW DELHI.

COMPLETE MAILING ADDRESS

Name .....

Address .....

Country/State .....

(Signature)

Note:

1. Subscribers at annual rates for all the periodicals are enlisted for the full volumes, i.e. for the period from January to December only.
2. The Cheque/Demand Draft may plese be drawn in favour of "PUBLICATIONS & INFORMATION DIRECTORATE, NEW DELHI". Banking charges shall be borne by the subscriber. For inland outstation cheques please add Rs. 3.50. For foreign cheques please add $ 1.00 or £ 0.45.
3. The supply will commence on receipt of subscription in advance.

Indian Journal of Pure & Applied Physics

Published by the Publications & Information Directorate, CSIR, Hillside Road, New Delhi 110012
Editor-in-Chief : Y R Chadha

The Indian Journal of Pure & Applied Physics is issued monthly. The Directorate assumes no responsibility for the statements and opinions advanced by contributors. The editorial staff in its work of examining papers received for publication is assisted, in an honorary capacity, by a large number of distinguished scientists, working in various parts of India.

Communications regarding contributions for publication in the journal should be addressed to the Editor, Indian Journal of Pure & Applied Physics, Publications & Information Directorate, Hillside Road, New Delhi 110012.

Correspondence regarding subscriptions and advertisements should be addressed to the Sales & Distribution Officer, Publications & Information Directorate, New Delhi 110012.

Annual Subscription	**Single Copy**
Rs. 120.00 £20.00 $45.00	Rs. 12.00 £2.00 $4.50

50% Discount is admissible to research workers and students and 25% discount to non-research individuals, on annual subscription. Payments in respect of subscriptions and advertisements may be sent by cheque, bank draft, money order or postal order marked payable *only* to **Publications & Information Directorate, New Delhi 110012.** Claims for missing numbers of the journal will be allowed only if received within 3 months of the date of issue of the journal plus the time normally required for postal delivery of the journal and the claim.

Corrigendum

Paper entitled, "Red Edge Effect in Excited State Protonic Transfer Reaction in Alkaline Aqueous Solutions of β-Naphthylamine" Vol. 20 (No. 9) (Sept) 1982, pp. 728-732.

The authors have now found that Eq. (5) is not applicable for reaction 3 listed in the paper, since back-reaction is unaffected by $[OH^-]$. Hence Eq. (1) is sufficient to give the forward rate constant. The red edge effect, therefore, depends only on change in proton transfer rate (k). The value of k comes out to be $4 \times 10^9\ M^{-1}\ s^{-1}$ for short wavelength excitation.

Errata

Paper entitled, "Calculations of Geometry & Molecular Properties by Semiempirical Molecular Orbital Method (SINDO)" Vol. 21 (No. 10) (Oct), pp. 605-608.

In Table 1, the values of net charges under the column headings X_1, X_2 and X_3 are to be corrected as follows:

Molecule	X_1	X_2	X_3
HBeH	−0.229	0.458	−0.229
HBH	−0.105	0.209	−0.105
HCH T	0.046	−0.092	0.046
HCH S	0.0006	−0.0011	0.0006
HNH	0.118	−0.235	0.118
HOH	0.194	−0.387	0.194
OOO	−0.145	0.291	−0.145
OCO	−0.273	0.545	−0.273
HCN	0.019	0.119	−0.138

Indian Journal of Pure & Applied Physics

VOLUME 21 NUMBER 12 DECEMBER 1983

CONTENTS

Continued overleaf

CONTENTS

*The author for correspondence is indicated by the (*) mark in case of papers with more than one author.

Indian Journal of Pure & Applied Physics
Vol. 21, December 1983, pp. 683-685

A Mechanism for Drag on Zinc Dislocations

RAHUL BASU*
California Institute of Technology, Pasadena, California, USA

Received 28 *January* 1983

Experimental data for dislocation mobilities in zinc single crystals are analyzed. A drag model is formulated for the low-stress regions after slip occurs and for the high-stress regions after stage I-stage II transition. It is found that the drag approaches an asymptotic value at high velocities starting from an initially high value. The significance of this value is discussed regarding the formation of Zn-N interstitial molecules that impede the free flight of dislocations on slip systems in zinc single-crystals.

1 Introduction

Although dislocations have been studied extensively over the past three decades, quantitative understanding of the basic scientific principles is still lacking. It has generally been held that dislocations move by carrying the cloud with them, and at high stresses 'breakaway' occurs—since the 'Cottrell atmosphere' was propounded[1-3]. The author has performed an extensive study using the concepts of Seeger[4] and Dorn and Rajnak[5], together with experimental data from research performed in the laboratory. It is found that in the case of zinc crystals, the motion of dislocations above a certain stress and velocity causes chemical formation of Zn_3N_2 and Zn_2N_2 molecules, which obstruct further motion[6,7]. In the same study it was found that there are two mechanisms for drag—one controlled by Peierls forces below a certain transition stress, and another controlled by the molecular interaction forces between zinc and nitrogen at stresses above this magnitude. Also, an asymptotic drag was obtained at high stresses, which may be caused by constraining chemical and electronic forces or by lattice forces during 'free flight' as in the model of Ashby[3]. It is now attempted to show that the variations in drag coefficient (B) are due to chemical and electronic interactions.

2 Analysis

Zinc single crystals were prepared and tested at various stresses with a Hopkinson's apparatus and subsequently etched with chemicals and photomicroscopically examined[6,7]. The dislocations were observed on the basal (screw component) and pyramidal (edge component) planes. Experimental results obtained are presented in Tables 1 and 2.

From a heuristic analysis, it is obvious that prior to any interaction with interstitials and precipitates, the only resistance faced by the dislocation in its initial motion is that of lattice friction, together with superimposed stress fields from other defects. In a pure and perfect crystal, this is the force obtained by solving the wave equation in a crystalline symmetry. This can be a formidable task, and resort to the digital computer is to be taken. Simpler methods have been devised which are described in Ref. 6. This force required to move a dislocation past one-half a lattice spacing is the Peierls force. When the crystal is doped, or contains unintentional additions such as nitrogen in zinc, it varies with the nature and concentration of the solute. An approximate value is given by the CRSS (critical

Table 1—Damping Coefficients Calculated from Various Stress-Velocity Measurements

V, cm/s	10	1	0.1	0.01
τ, 10^6 dyn/cm^2	24.08	19.8	14	10
B_{screw}, 10^{-2} dyn/cm^2	6.38	52.47	371	2650
B_{edge}, 10^{-2} dyn/cm^2	13.6	111.87	791	5650
(τ-6.9), 10^6 dyn/cm^2	17.18	12.9	7.1	3.1
B_{screw}, 10^{-2} dyn/cm^2	4.55	34.19	188.15	82.5
B_{edge}, 10^{-2} dyn/cm^2	9.71	72.89	401.15	1751.5

Note: The first two rows of the table give experimental values of velocity and stress, pairwise. The 5th row gives stress values after subtraction of a constant value, and rows 6 and 7 give the recalculated damping coefficients obtained from the new stress.

Table 2—Damping Coefficients above the Transition Stress (28.875×10^6 dyn/cm^2)

V, cm/s	100	1000
τ_{edge}, 10^6 dyn/cm^2	100	390
τ_{screw}, 10^6 dyn/cm^2	100	810
B_{edge}, 10^{-2} dyn.s/cm^2	5.65	2.20
B_{screw}, 10^{-2} dyn.s/cm^2	2.65	2.15

Note: The top row gives two velocities selected from region II of the figure. Corresponding stresses are read off from the figure. Subsequently, the damping coefficients are calculated as explained in the text.

* Present address: Gas Turbine Research Establishment, Bangalore 560075

resolved shear stress), where deformation is initiated. Extrapolation of the shear stress-velocity data of Table 1 gives this to be 6.9 Mdyn/cm^2 at room temperature.

The drag model used is given as

$$BV = \tau b \quad \ldots (1)$$

where B is the drag coefficient, V the dislocation velocity, τ the applied shear stress and b the relevant Burgers vector. The effect of the CRSS of 6.9 Mdyn/cm^2 can be eliminated by using a new stress after subtraction of this component.

The results are presented in Table 1. However, it is seen that the variation in B is not regulated by this, although it is altered. Here the drag increases with stress and velocity, because of increasing interaction with interstitials present everywhere in the lattice.

A model for this region, given by data in Table 2, may be represented as

$$BV = (\tau - y)b \quad \ldots (2)$$

where y is a stress to be determined. A study of the values given in Table 2 shows that an asymptotic value appears to be reached at high velocity. Eq. (2) is then solved for B for the edge and screw components, giving for y a value of approximately 19 Mdyn/cm^2. This is close to the measured transition stress of 24 Mdyn/cm^2 and indicates the controlling stress for this region to be that which causes the change in deformation mode of the crystal, namely line pinning.

From a more detailed study including lattice energy and dynamics it is found that the average line tension is 5.4×10^{-5} dyn and the perturbation potential produces a force or tension of 2.7×10^{-9} dyn (Ref. 6). The distance between each pair of inclusions is 10 μm and the arc length of contact between line and inclusion was found to be 12.4 Å. The value of line tension was also calculated by work principles and found to be nearly equal to that calculated with the use of differential equations of motion and was found to be 5.565×10^{-5} dyn (or erg/cm). Actually the prior value is the theoretical value assuming full contact between line and precipitate (inclusion), and the value obtained from work principles takes the velocity as constant, with no deceleration during approach of the line to the inclusions.

Now from the drag relation [Eq. (2)]

$$BV = \tau b$$

so at transition

$$BV = 24 \times 2.65 \times 10^6 \times 10^{-8} = 4.55 \times 10^{-1} \text{ dyn/cm} \quad \ldots (3)$$

where $b = 2.65$ Å for the screw component. Hence the force over the arc of contact with the inclusion (known to be 12.4 Å) is approximately 5.6×10^{-8} dyn. Similarly, at the asymptotic drag, where assuming contact still exists between line and precipitate,

$$BV = 2.096 \times 10^{-2} \times 1000 = 20.96 \text{ dyn/cm}$$

and the tension over the arc of contact is therefore equal to

$$20.96 \times 12.4 \times 10^{-8} = 2.6 \times 10^{-6} \text{ dyn(approx.)} \quad \ldots (4)$$

Comparison of these values with the earlier calculations shows that, at transition, the tension over the arc of contact is comparable within a factor of 10 with the perturbation force known to be 2.7×10^{-9} dyn, and that at sufficiently high stress (asymptotic region), the constant contact stress is within a factor of 10 of the line tension calculated as 5.4×10^{-5} dyn. This is a sufficiently good indication that the line remains pinned at the high stresses and that breakaway does not occur. The value obtained at transition found to agree with the calculated tension due to perturbational forces shows that at transition the interaction is primarily that of the second-order Fourier component. This is, of course, a repulsive force and is electronic in nature, depending also on the neighbour-to-neighbour bond strengths.

Alternatively, we may recalculate the arc length of contact using the new forces per unit length by using Eqs (3) and (4). From Eq. (3) one obtains a length of 1.5 Å, using 6.9×10^{-9} dyn and from Eq. (4) an arc length of 256 Å, using 5.4×10^{-5} dyn. These are tensions obtained from work principles in both cases[6]. This result may be interpreted as follows: full contact does not occur between line and precipitate, as the line does not travel the full distance at constant velocity due to deceleration from repulsive forces. Alternatively, full contact occurs, but only over a small arc length. The first explanation is more reasonable from physical principles. In the asymptotic region, the line tension is less by a factor of 10, or it would appear that the arc length of contact is 256 Å or 96 atomic spacings of zinc. The inclusion is then a cluster of 32 (Zn_3N_2).

Line tension could be less through escape mechanisms also, i.e. by cutting through the inclusion or by other cloud interactions with lattice drag included. However, from the results obtained at transition, and the gradual decrease in B (Tables 1 and 2), it is more probable that increasing contact occurs with maximum restraining force at stresses lying in the asymptotic region. Hence, the experimental results do not cover the fracture and breakaway region.

3 Conclusion

Calculations using the dynamic parameters of velocity and drag, rather than the static calculations done earlier[6], show that the values obtained are consistent within a factor of 10. Furthermore, it is

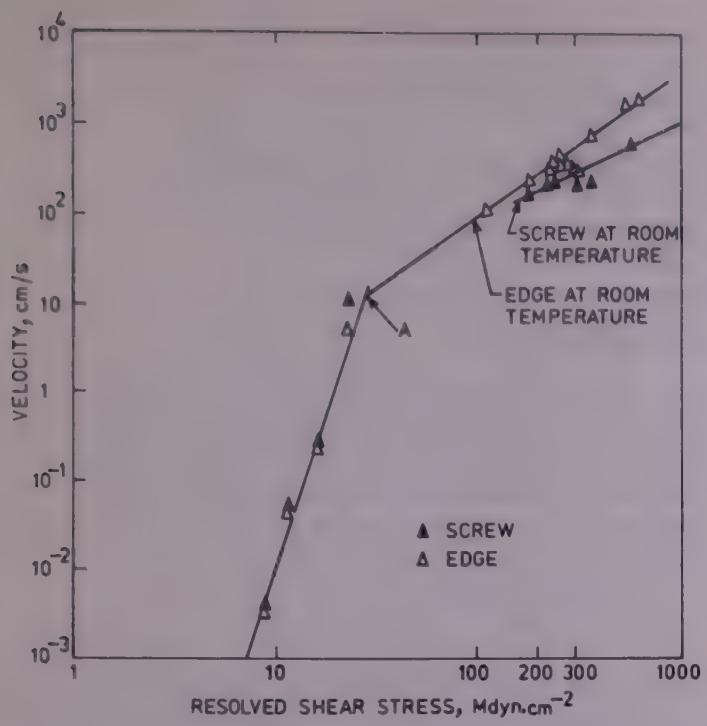

Fig. 1—Stress-velocity curve for dislocations in zinc single crystals

found that full contact does not occur at the transition stress (point A in Fig. 1) rather it occurs at asymptotic stress and velocity. This is logical considering the electronic repulsion force involved. An important feature would seem to be the divergence between the screw and edge components in the stress-velocity curve (Fig. 1).

This can only be analyzed by using drag concepts and the difference in b for the two components. Here $b = 2.65$ Å for screw and 5.65 Å for edge component respectively—and these values were used in the tabulation of B_{edge} and B_{screw} in Tables 1 and 2 by substitution of experimental values of stress and velocity in Eq. (1), and the refined values from Eq. (2). Earlier it was estimated that this was due to different molecular forces on the two slip systems. However, as it is now found that full contact may not occur at transition stress, it is possible that some different mechanisms (perhaps dissipation) may be occurring simultaneously.

References

1 Cottrell A H, *Dislocations and plastics flow in crystals* (Oxford University Press, New York) 1953.

2 Haasen P,'Interaction of dislocations and foreign atoms', in *Proc Symp Internal Stresses and Fatigue in Metals*. Detroit and Warren, Michigan, 1958 (Elsevier, New York) 1959, 205-219.

3 Frost H J & Ashby M F, *J Appl Phys (USA)*, **43** (1971) 5273.

4 Seeger A, *Philos Mag (GB)*, **1** (1956) 651.

5 Dorn J E & Rajnak S, *Trans TMS-AIME*, **230** (1964) 1052.

6 Basu R, *J Phys & Chem Solids, (GB)*, **42** (1981) 799.

7 Basu R, *Phys Status Solidi a, (Germany)*, **63** (1981) K153.

Indian Journal of Pure & Applied Physics
Vol. 21, December 1983, pp. 686-690

Mössbauer Study of $Zn_{0.1}Ni_{0.9+x}Sn_xFe_{2-2x}O_4$ Ferrites

R K PURI, USHA VARSHNEY & R G MENDIRATTA
Department of Physics, Indian Institute of Technology, Delhi, Hauz Khas, New Delhi 110016

Received 8 *November* 1982

The Mössbauer spectra of ^{57}Fe in the polycrystalline solid solutions of tetravalent tin-substituted nickel zinc ferrites ($Zn_{0.1}Ni_{0.9-x}Sn_xFe_{2-2x}O_4$ with $x=0.1$ to 0.9 varying in steps of 0.1) have been studied at room temperature. The spectra elucidate such aspects as ionic distribution from internal magnetic field and occupancy ratio, spin correlation time and anisotropy energy with increasing tin concentration. The results have been explained on the basis of Neal's molecular field model for low tin-concentration samples, whereas the results for samples of high tin-concentration could be explained from Ishikawa's hypothesis of super-paramagnetic clusters. A transition was observed from a magnetically ordered state to a paramagnetic state for $x > 0.7$ which has been explained on the basis of chemical disorder present in the ferrites by considering charge and point symmetry about Fe^{3+} ions.

1 Introduction

A number of workers have shown that the tetravalent impurities substituted in the ferrite matrix could be exploited to upgrade the electric and magnetic properties of ferrites due to inherent property of tetravalent impurities to localize the charge carriers. It has been reported that impurities like silica[1,2], titanium[1,3], germanium[2] and tin[4], when added to various ferrites, promote coarse crystallization and grain growth as well as increase the resistivity and magnetic quality factor of the basic ferrite. Varshney *et al.*[5] have reported that increased substitution of tetravalent tin in nickel zinc ferrites increases its resistivity by a large factor and significantly influences other electrical and magnetic properties. The present Mössbauer study of tetravalent tin-substituted, nickel zinc ferrite is aimed at elucidating such aspects as the site occupancy, ionic distribution from internal magnetic field, and spin correlation time and anisotropy energy obtained from relaxation effects.

2 Experimental Details

The polycrystalline solid solutions of

$Zn_{0.1}Ni_{0.9+x}Sn_xFe_{2-2x}O_4$

($x=0.1$ to 0.9 varying in steps of 0.1) ferrites were prepared by the conventional ceramic technique involving slow annealing in air. The desired quantity of the analytical grade NiO, ZnO, Fe_2O_3 and SnO_2 metal oxides were wet-blended with deionized water in an agate mortar and pestle. The mixed powder was calcined for 4 hr at 1000°C in an alumina crucible to improve homogenization of the constituents. The mixture was wet-milled again with deionized water to reduce the particle size and the wet powder was dried at 350°C. Polyvinyl alcohol (10% by weight) was mixed as an adhesive and the pulverized powder was granulated through the sieves of 85 to 120 mesh (B.S.S.) and compressed to pellets of 15 mm diameter under a pressure of 3 ton/in^2. The pellets were finally sintered for 2 hr at 1300°C in an alumina combustion boat and were cooled in air to room temperature at the rate of 100°C/hr. The surfaces of the pellets were rubbed with an abrasive paper. The X-ray diffraction analysis, using Fe(K_α) radiations with Mn filter and Debye Scherrer camera, confirmed single-phase spinel structure in all the compositions except for $x=0.8$, 0.9, where an additional phase was observed due to the presence of unreacted stannic oxide.

The Mossbauer spectra were recorded at room temperature on Nuclear Data 512 Channel Analyzer operating in the multiscaling mode in conjunction with a constant acceleration electromechanical drive using a 20 mCi ^{57}Co source in the rhodium matrix.

The experimental spectra, which were computer analyzed using a standard non-linear least squares fit program, are shown as solid lines in Fig. 1. The intensities and widths of these Lorentzian lines were allowed to vary freely, subjected only to the constraints $I_j = I_{7-j}$ and $\Gamma_j = \Gamma_{7-j}$ of the component spectrum of the sextets where I_j is the intensity of the jth line and Γ_j is the width of the jth line.

3 Results and Discussion

The Mössbauer spectra of each of the specimens, with tin concentration varying from $x=0.1$ to 0.7, have been resolved into two sextets. These sextets have been assigned A site or B site on the basis of their respective values of isomer shift as well as internal magnetic field. For specimens having $x=0.1$ to 0.5, the sextets corresponding to A and B sites have been identified as hyperfine sextets without any relaxation effects. The spectra of specimens having $x=0.6$ and 0.7 showed relaxation effects at B site whereas A site

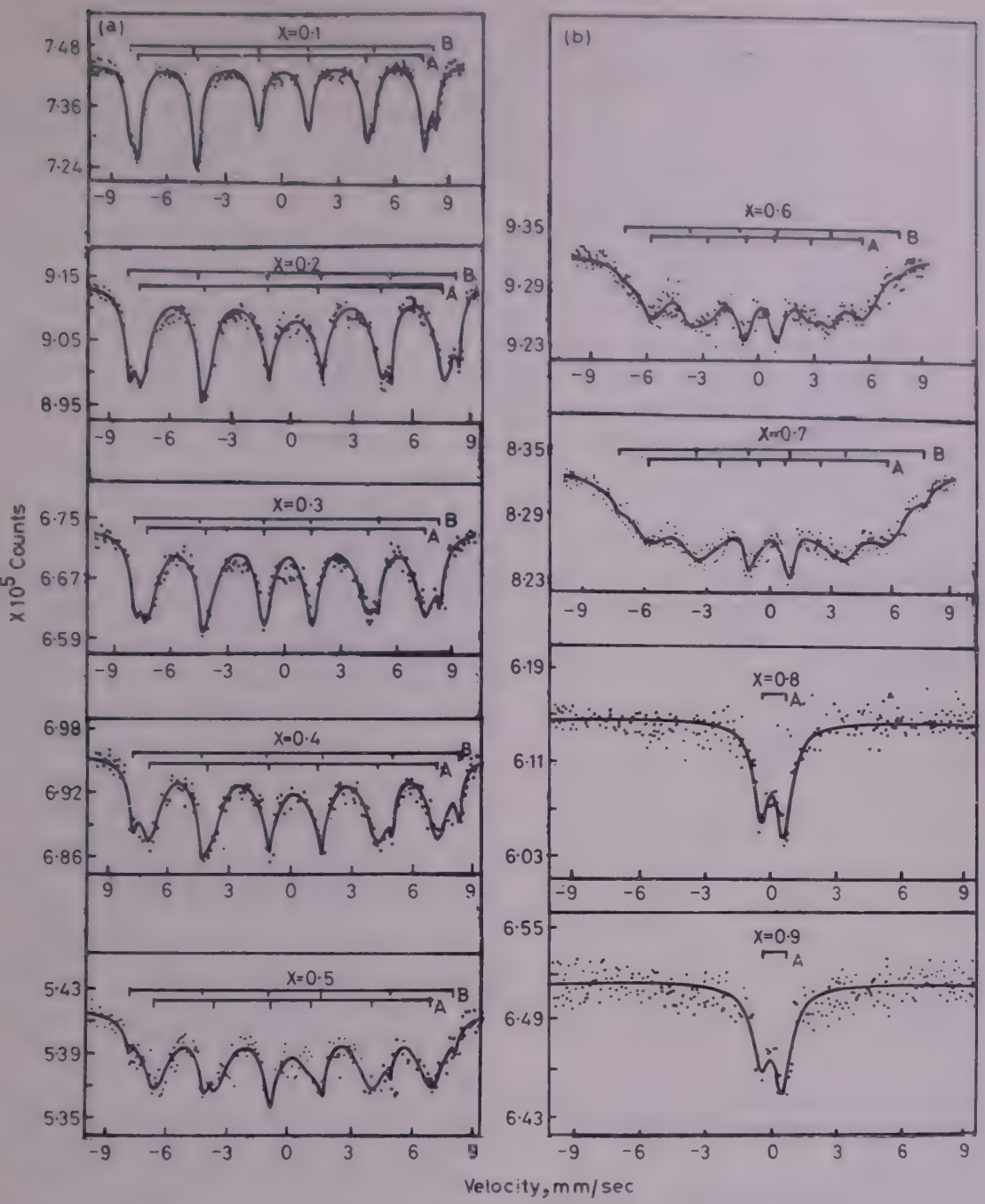

Fig. 1—Mössbauer spectra of $Zn_{0.1}Ni_{0.9+x}Sn_xFe_{2-2x}O_4$ ($x=0.1$ to 0.9 in steps of 0.1) at 300 K

sextets were observed without any relaxation effects. The spectra of specimens having $x=0.8$ and 0.9, however, showed quadrupole doublet corresponding to A site Fe^{3+} ions.

The values of isomer shift relative to natural iron and line widths for all specimens are shown in Table 1. It shows no systematic change of isomer shift at A and B sites with increase of tin concentration, indicating that the *s*-electron charge distribution of Fe^{3+} ions is not influenced by the increased substitution of tin ions. The difference in isomer shift due to A site and B site can be attributed to the slight Sp^3 covalency present at the A site ions[6,7].

The variation of nuclear magnetic field at A site and B site with tin concentration has been estimated within an experimental error of 5 kOe and is shown in Fig. 2. It shows that for samples having tin concentration less than 0.5, the nuclear magnetic field at A site decreases significantly as compared to that at B site. The internal magnetic field, however, decreases significantly at both A as well as B sites for samples having $x=0.6$ and 0.7.

The observed variation of internal magnetic field as a function of tin concentration can be interpreted to derive the following ionic distribution for samples having $x=0.1$ to 0.5:

$$(Zn^{2+}_{0.1}\,Fe^{3+}_{0.9})\,[Ni^{2+}_{0.9+x}Sn^{4+}_{x}Fe^{3+}_{1.1-2x}]O^{2-}_{4}$$

where the metallic cations enclosed by parenthesis occupy A site while the ions enclosed by the square bracket occupy B site such that Sn^{4+} ions mainly occupy B site wherein two Fe^{3+} ions are replaced by

Table 1—Values of Isomer Shift w.r.t. Natural Iron, Full Width at Half Maxima (FWHM), Spin Correlation Time, and Anisotropy Energy (K) for Various Samples

x	Isomer shift, mm/sec		FWHM, mm/sec		Spin correlation time sec/mm	$K \times 10^3$ erg/cm^3
	A-site	B-site	A-site	B-site		
0.1	0.11±0.01	0.23±0.01	0.55	0.37	—	—
0.2	0.14±0.02	0.23±0.02	1.19	0.38	—	—
0.3	0.12±0.02	0.26±0.02	1.39	0.37	—	—
0.4	0.12±0.02	0.27±0.02	1.55	0.40	—	—
0.5	0.12±0.02	0.21±0.03	1.69	0.42	—	—
0.6	0.07±0.05	0.23±0.06	2.08	0.88	2.58	4.21
0.7	0.08±0.04	0.23±0.05	2.66	1.15	2.39	4.19
0.8	0.09±0.01	—	0.84	—	—	—
0.9	0.04±0.01	—	0.97	—	—	—

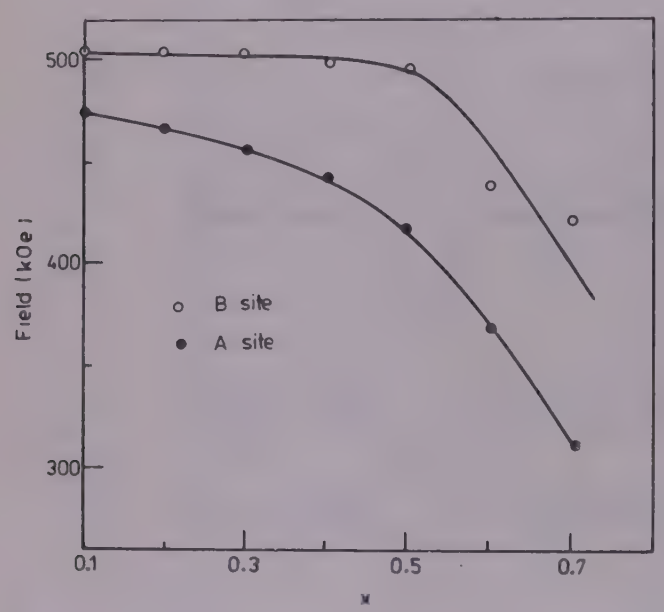

Fig. 2—Nuclear magnetic field at ^{57}Fe nuclei at octahedral (B) site and at tetrahedral (A) site versus tin concentration x

Sn^{4+} and Ni^{2+} ions at the octahedral site. The preference of Ni^{2+} ions for octahedral site is due to favourable fit of its charge distribution in the crystal field of octahedral site whereas Zn^{2+} ions have got a marked preference for tetrahedral coordination to form covalent bonds involving Sp^3 hybrid orbitals.

The ionic distribution, derived from the variation of magnetic field, can be explained on the basis of Neel's molecular field model[8] with distant-neighbour exchange interactions wherein AB interactions are stronger than AA or BB exchange interactions. In the spinel structure, each ion at A site is surrounded by twelve B site ions while the ion at the B site has got six A site and six B site neighbours. Sn^{4+} and Zn^{2+} ions, being diamagnetic, do not participate in the exchange interactions. The substitution of two Fe^{3+} ions by Sn^{4+} and Ni^{2+} ions preferentially at B site, leads to an average net reduction of number of $Fe^{3+}_A - O - Fe^{3+}_B$ bonds which A site Fe^{3+} ions will experience. The increase in Sn^{4+} concentration, therefore, results in larger reduction of average nuclear magnetic field at A site. As A site Fe^{3+} ions are not affected due to the increased substitution of tin ions, the magnetic field at B sublattice is not reduced. Since the two sublattices must be treated as a coupled system, the rapid decrease in the average A site magnetization weakens AB interactions which slightly reduce the magnetic field at B site. A larger decrease in the magnetic field at A site than that at B site Fe^{3+} nuclei is thus expected. The observed variation in magnetic field follows a trend similar to that predicted from ionic distribution.

The above mentioned ionic distribution is further confirmed from the occupancy ratio of B to A site Fe^{3+} ions as a function of tin concentration. It is obvious that Sn^{4+} primarily occupies B site for samples having $x=0.1$ to 0.5. Also the observed variations in the line width, as given in Table 1, show that the line widths of the sextets corresponding to A site increase with increased tin concentration unlike that at B site. It is expected that for samples with $x \leq 0.5$, tin ions, primarily going to B site, should alter the environment around the A site Fe^{3+} ions. One does not, however, expect any appreciable change of environment around B site Fe^{3+} ions for these specimens because a negligible amount of tin is present at A site. The ionic distribution is thus in accordance with the observed variation in line width.

For the samples with tin concentration, $x=0.6$ and 0.7, the variation of internal magnetic field at A and B sites can be explained from the following ionic distribution:

$$(Zn^{2+}_{0.1}\,Fe^{3+}_{0.9-Z}\,Sn^{4+}_{Z})[Ni^{2+}_{0.9+x}\,Sn^{4+}_{x-Z}\,Fe^{3+}_{1.1-2x+Z}]O^{2-}_{4}$$

wherein Z Sn^{4+} ions enter A site and $(x-Z)$ Sn^{4+} ions go to B site, such that $Z=0.1$ and 0.2 for $x=0.6$ and 0.7 respectively.

The rapid decrease in the magnetic field at A site can be attributed to the fact that AB exchange interactions as experienced by the A site Fe^{3+} ions become too weak to participate in the ferrimagnetic array and hence AA interactions start playing a dominant role. The increased tin concentration at A site, therefore, reduces the magnetic field.

The variation of the magnetic field at B site in samples with $x=0.6$ and 0.7 can be explained on the basis of Ishikawa's hypothesis[9] of super-paramagnetic clusters. When tin starts going to A site also, the probability that all the B site magnetic ions to be surrounded by the non-magnetic Zn^{2+} and Sn^{4+} ions increases, thus resulting in the formation of isolated super-paramagnetic clusters at B site. It, therefore, breaks the long-range order between the magnetic ions. The spins inside the cluster are assumed to form the collinear ferrimagnetic array. The formation of these super-paramagnetic clusters is further confirmed from the calculations of the super-paramagnetic spin correlation time which has been found to be a real quantity for specimens with $x=0.6$ and 0.7.

The spin correlation time is given as[10,11]:

$$\tau_s=\frac{2(2S_{16}^2-2.016\ S_{34}^2)^{1/2}}{S_{34}(S_{16}^2-40.32\ S_{34}^2)^{1/2}}$$

where S_{16} is the separation between the first and the sixth line and S_{34} is the separation between the third and the fourth line. In the presence of super-paramagnetic effect, the internal field at the nucleus fluctuates[10,11] at the rate given by $\tau_s=\tau_0\exp(KV/kT)$, where K is the uniaxial anisotropy per unit volume, V the effective particle volume, $\tau_0\cong 10^{-12}$sec, and $\tau_s=1/\omega_s$ where ω_s is the spin flip-flop frequency. The values of the spin-correlation time and anisotropy energy, obtained at B site for $x=0.6$ and 0.7, are listed in Table 1. The addition of nonmagnetic Sn^{4+} ion results in the weakening of various magnetic bonds at the octahedral site. It is, therefore, easier for the magnetic domains to fluctuate from one direction of an easy magnetization to another without causing change in the spin state of any particular ion in the cluster. The increase of the diamagnetic tin ions results in an increase of the spin flip-flop frequency and decrease in the anisotropy energy. The observed variation, as seen from Table 1, is in accordance with these predictions. The above mentioned ionic distribution for $x=0.6$ and 0.7 is further supported by the observed behaviour of the occupancy ratio, which indicates that Sn^{4+} ions go to A sublattice also apart from going to B sublattice.

An anomalously large increase in the line width at A site with $x=0.6$ and 0.7 is probably also due to the presence of clusters of various dimensions at the B site. It may lead to different magnetic field at the iron nuclei at A site resulting in an overlap of unresolved sextets. It is, however, difficult to draw any such conclusions about the B site because of the presence of relaxation effects.

The spectra of specimens with $x=0.8$ and 0.9, as shown in Fig. 1, clearly show the presence of a quadrupole doublet which is attributed to tetrahedral Fe^{3+} ions on the basis of the isomer shift of the observed doublet. The absence of any signal due to B site Fe^{3+} ions indicates that negligible amount of iron ions are present at the B sublattice. It is inferred that the amount of diamagnetic tin is sufficiently large to break the short-range order, thus removing the hyperfine field at B site and giving rise to the paramagnetic ordering of the Fe^{3+} ions at the A site. The appearance of the electric field gradient at A site for these specimens may be due to the presence of Ni^{2+} ions in the octahedral sublattice. These Ni^{2+} ions present at B site, being nearest neighbour to Fe^{3+} ions at A site, would generate an electric field gradient at A site which results in the appearance of a paramagnetic doublet. Daniel and Rosencwaig[12] have reported that the Ni^{2+} ions, going to B site in nickel zinc ferrites, increase the electric field gradient. An overall cubic symmetry is maintained due to Ni^{2+} as well as Sn^{4+} ions going to the lattice site simultaneously up to $x\leq 0.7$. This symmetry is, however, lost for samples with Sn^{4+} up to $x\leq 0.7$, exhibiting Zeeman hyperfine additional phase. It has been inferred from scanning electron micrographs and X-ray diffraction results that an additional phase is present which has been attributed to the presence of unreacted SnO_2.

A transition takes place from a magnetically ordered state to a paramagnetic state for $x>0.7$. The Mössbauer spectra of nickel zinc ferrite, substituted with Sn^{4+} up to $x\,[0.7$, exhibiting Zeeman hyperfine pattern, show negligible quadrupole shift for both the tetrahedral and octahedral sites, whereas in passing from a magnetically ordered state to a paramagnetic state, the samples with $x=0.8$ and 0.9 show sizable quadrupole splitting at A site equal to 1.07 ± 0.2 mm/sec and 1.07 ± 0.03 mm/sec respectively. The absence of quadrupole splitting in the spectra showing Zeeman pattern followed by sudden appearance of quadrupole splitting in nickel zinc ferrites has been interpreted by Daniel and Rosencwaig[12] on the basis of the chemical disorder present in such ferrites, by considering the charge and point symmetry about Fe^{3+} ions. Such ferrite systems, being chemically disordered in both the sublattices, may experience a distribution of electric field gradient of varying magnitude, direction, sign and symmetry. Thus for an overall cubic symmetry of the spinel ferrite, there may exist approximately equal probability for shifts of opposite sign which may result in producing negligible

quadrupole splitting in the magnetic spectra of such ferrite systems which explains such a transition.

References

1 Styntjes T G W, *Proceedings of the international conference on ferrites, Japan*, 1970 (Science Council of Japan), 1971, 194.

2 Santosh Kumari, *The effect of dopants* SiO_2, GeO_2 *and* SnO_2 *on the microstructure and magnetic properties of* Mn-Zn *ferrites*, Ph D thesis, University of Delhi, 1978.

3 Franken P E C & Van Deveren H, *Ber Dtsch Keram Ges* (*Germany*), **45** (1978) 287.

4 Gallagher P K, Johnson (Jr) D W, Schreiber (Jr) H & Vogel E H, *J Solid State Chem* (*USA*), **35** (1980) 215.

5 Varshney Usha, Puri R K, Rao K H & Mendiratta R G, *Ferrites: Proceedings of the third international conference, Kyoto, Japan*, 1980 (Science Council of Japan), 1981, 267.

6 Goodenough J B & Losh A L, *Phys Rev* (*USA*), **98** (1955) 391.

7 Hudson A & Whitefield H J, *Mol Phys* (*GB*), **12** (1967) 1965.

8 Neel L, *Ann Phys* (*France*), **3** (1948) 137.

9 Ishikawa Yoshikazu, *J Phys Soc Jpn* (*Japan*), **17** (1962) 1877.

10 Raj P & Kulshreshtha S K, *Phys Status Solidi A* (*Germany*), **4** (1971) 501.

11 Bhargava S C & Zeeman N, *Phys Rev B* (*USA*), **21** (1980) 1717.

12 Daniel J M & Rosencwaig A, *Can J Phys* (*Canada*), **48** (1970) 381.

Indian Journal of Pure & Applied Physics
Vol. 21, December 1983, pp. 691-693

Applicability of Onsager's Theory to the Transport Phenomena of Ions in Solutions

HAIMANTI CHAKRABARTI & S N CHANGDAR
Nuclear Physics Laboratory, Bose Institute, Calcutta 700009

Received 7 *January* 1982; *accepted* 15 *July* 1983

Self-diffusion coefficient of Tl in thallous sulphate solution has been determined over a wide range of concentrations using a method based on radioactive tracer technique. The solute and solvent columns are of equal length and the detector is placed vertically over the diffusion column. The measurement of diffusion is made over a restricted region and the diffusion coefficients thus obtained are utilized to show the applicability of Onsager's theory of diffusion of ions in solutions.

1 Introduction

For more than a century, the diffusion phenomenon has been extensively investigated by several groups of workers. The field of application of such investigations is wide and at the same time has a great variety. The importance of the study of this common (but as yet not completely understood) phenomenon, springs from its close relationship with the dynamics of the molecules. Moreover, the measured diffusion coefficients can be used as a fundamental tool in correlating the experimental findings with various theories of the liquid state. Though diffusion data[1-4] are available in plenty, most of them suffer from various inconsistencies due to the inherent slowness of the process in liquid state. Fortunately, there are a few methods which permit rapid and consistent measurement of the diffusion coefficients with moderate accuracy.

We have developed a radioactive tracer technique[5] in our laboratory for the determination of the self- and mutual-diffusion coefficients of liquids. The experimental geometry consists of equal lengths of solute (radioactive) and solvent (nonradioactive) columns with the detecting device placed vertically over it. This technique is superior to others because it is free from the zero-time correction. This paper reports the results of experimentally determined self-diffusion coefficient values of Tl in Tl_2SO_4 solution over a wide range of concentrations. The data are used to check the applicability of Onsager's theory of diffusion of ions in solutions.

2 Principle of Measurement

The theory is based on the Fourier series solution[6] of Fick's second law of diffusion for a unidirectional flow:

$$\frac{\partial C(x,t)}{\partial t} = D\frac{\partial^2 C(x,t)}{\partial x^2} \qquad \ldots (1)$$

Eq. (1) is a second-order inhomogeneous equation. Assuming that variables are separable, we seek a solution of the form:

$$C = A(x)B(t) \qquad \ldots (2)$$

so that $$A\frac{dB}{dt} = DB\frac{d^2A}{dx^2}$$

or $$\frac{1}{B}\frac{dB}{dt} = \frac{D}{A}\frac{d^2A}{dx^2} = -\lambda^2 D$$

hence

$$C = \sum_{m=1}^{\infty} (a_m \sin \lambda_m x + b_m \cos \lambda_m x)e^{-\lambda m^2 Dt} \qquad \ldots (3)$$

where a_m, b_m and λ_m can be solved knowing the initial and final boundary conditions.

In our experiment, the region $x=l$ to $x=0$ is occupied by a solution of concentration C_0, while the region $x=2l$ to $x=l$ is occupied by a solution of concentration zero.

$$\therefore C = \frac{C_0}{2} + \frac{2C_0}{\pi}\sum_{s=1}^{\infty}\frac{1}{s}\cos\frac{s\pi x}{2l}\exp\left(-\frac{s^2\pi^2 Dt}{4l^2}\right)$$

If the time of observation is such that $(\pi^2 Dt/4l^2) > 0.5$, then, based on the first approximation, C can be expressed as:

$$C = \frac{C_0}{2} + \frac{2C_0}{\pi}\cos\left(\frac{\pi x}{2l}\right)\exp(-kt) \qquad \ldots (4)$$

Now Eq. (4) can be modified to conform to data obtainable with our experimental arrangement as follows:

$$N_t = A_1 - B_1 \exp(-kt) \qquad \ldots (5)$$

At $t=\alpha$, when the solute and solvent columns are uniformly mixed $N=N_0$ and $N_0=A_1$. Eq (5) can now be rewritten as:

$$N_0 - N_t = B_1 \exp(-kt) \qquad \ldots (6)$$

where N_t is the count rate at time t, N_0 is the count rate when the solute and solvent columns are completely mixed up. B_1 is a constant (depending on the geometry) which gets eliminated when the ratios of $(N_0 - N_t)$ at different values of t are taken. The value of D can be estimated by noting the variation of $(N_0 - N_t)$ with time.

3 Experimental Details

A sliding-cell technique has been utilized for the measurement of the diffusion coefficient in the aqueous thallous sulphate solution to get an insight into the process of migration of an ion in solutions. This method is based on the radioactive tracer technique. The diffusion cell consists of two stainless steel slabs of equal dimension which are placed in a brass vessel. The lower steel slab is kept fixed with respect to the brass vessel with the help of an attaching hook. But the upper steel slab could be slowly moved with respect to the lower one by means of a sliding screw arrangement. The central cavity L [Fig. 1(b)] in the lower slab, together with the hole M in the upper slab, constitutes the diffusion column proper. There is another hole N in the upper slab for filling L with the radioactive solute. The whole arrangement is shown in Fig. 1(a).

The diameter of the diffusion column is 0.6 cm, a value larger than that for most of the diffusion cells normally used. It has been done so as to make the curvature of the open liquid surface negligible. The cavity is accurately machined at the bottom to have as flat a surface as possible so that the depth of the different points did not differ by more than 1 %.

The mechanical vibrations are eliminated by taking proper precautions. The photomultiplier tube (5819 type) is coupled to an anthracene counter and then connected to a highly stable electronic circuit. The stability of this electronic circuit is checked to within ± 0.1 % error for a period of 24 hr. It is clear from the working formula that for the sake of simplicity, we are taking solute and solvent columns to be of equal heights.

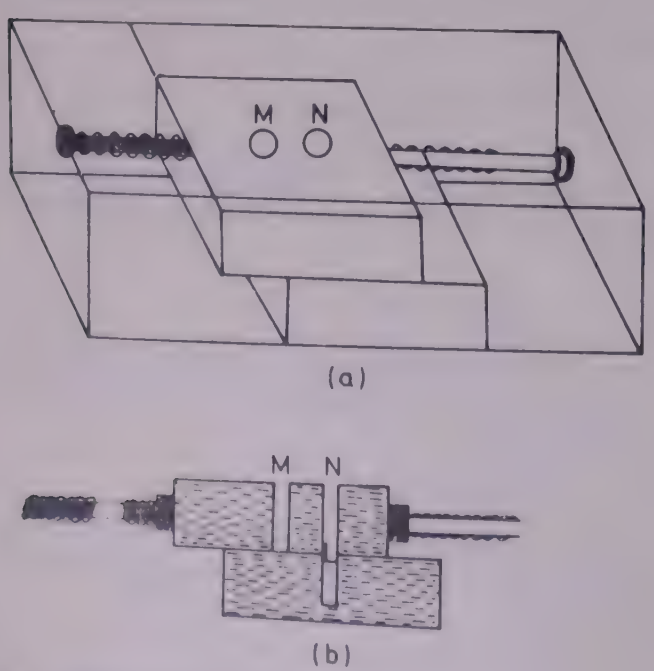

Fig. 1—Sketch of sliding cell [(a) Whole arrangement; (b) cross-sectional views; L central cavity in lower slab; M central cavity in upper slab; and N another hole in upper slab]

For the measurement of the self-diffusion coefficient of Tl, diffusion cells with diffusion column length 2.5 cm and diameter 0.6 cm were used. Tl_2SO_2 solutions of different concentrations were prepared by the weighing method. The lower cavity was filled up with the radioactive solute having ^{204}Tl as the tracer through the other hole of the upper slab. Then by a sliding screw arrangement, the solvent columns were superposed on the solute column, when diffusion gets started. Readings were generally taken every $\frac{1}{2}$ hr from the start of the diffusion process. The measurements were made for a wide range of concentrations from 0.5 mg/cc to 100 mg/cc.

4 Results and Discussion

From observed variation of N_t with t, $\log_e (N_0 - N_t)$ was plotted against t and found to be nearly linear. The variation of D with the concentration is shown in Fig. 2.

Diffusion data in electrolytic solution are available in plenty but most of these diffusion coefficients reported have been obtained by conventional experimental methods which give rather inconsistent results. The main aim of an experimental study in electrolytic solutions is to get an insight into the process of migration of ions in solution. With this aim in view, we have measured the diffusion coefficients of Tl ion in aqueous thallous sulphate solutions over an extended range of concentration. The percentage of ionization of thallous sulphate in aqueous solution in the concentration range studied by us (0.5 mg/cc to 100 mg/cc) is 95 to 85 %. This means that thallous sulphate readily ionizes in aqueous solutions. Initially Tl^+ and $(TlSO_4)^-$ ions are formed and the ionization constant for this stage is 0.23. In the next stage $(TlSO_4)^-$ ions break into Tl^+ and $(SO)_4^{--}$ ions and the ionization constant at this stage is 0.014. The aqueous solution has a neutral reaction. There is no evidence of the existence of free sulphuric acid in the solution which exhibits the characteristic reactions of thallous salts. These salts have a tendency to form ions with double charges (Tl_2^{2+}) as in the case of Hg salts.

We have tested the validity of Onsager's theory[7] in this particular case. Onsager's theoretical formula for

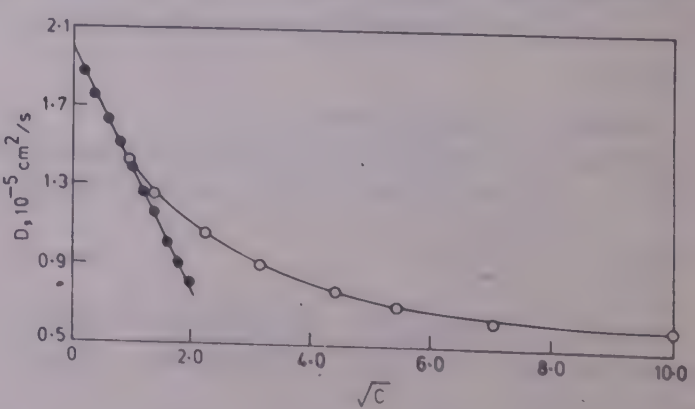

Fig. 2—Plot of D versus $\sqrt{C}$ (C in mg cc)

the dependence of the diffusion coefficient (D) on concentration of a uni-univalent electrolyte can be written as follows:

$$\frac{D}{D_0}-1=-(t^- - t^+)^2\frac{b^+ + b^-}{2a}\frac{\kappa a}{1+\kappa a} + \frac{e^2}{2\varepsilon kTa}\cdot\frac{b^+ + b^-}{2a}\cdot(\kappa a)^2\cdot\varphi(\kappa a) \quad \ldots (7)$$

where t^+, t^- denote the transport numbers; ε the permittivity of water; b^+, b^-, the effective ionic radii calculated from Stoke's law, κ the mean thickness of the ionic atmosphere in the Debye-Hückel theory and a the mean ionic diameter in the same theory. Values of b^+ and b^- can be calculated from the formulae:

$$b^+ = \frac{F^2}{6\pi N\eta t^+ \dot{\lambda}}, \quad b^- = \frac{F^2}{6\pi N\eta t^- \dot{\lambda}}$$

The term $\beta c^{1/2}$ in the denominator of Debye-Hückel formula for $\log f$ is the same as κa. The coefficient β is proportional to a and is unity when a is 3.08 Å. The function φ is defined by[8]:

$$\varphi(y)=\frac{e^{2y}}{(1+y)^2}\int_{2y}^{\infty}\frac{e^{-t}}{t}dt$$

We can reduce Eq. (7) to a simple limiting law. Onsager's limiting law regarding the diffusion coefficient of tracer ion of jth kind is

$$D_j=\omega_j\left[kT-\frac{\kappa e_j^2}{3D}(1-\sqrt{d(\omega_j)})\right] \quad \ldots (8)$$

which on simplification becomes[9]

$$D_j=\frac{kT\dot{\lambda}_j}{|Z_j|F}-\frac{\dot{\lambda}_j^0|Z_j|F}{3ND}\times 2.694\times 10^6+\sqrt{\frac{4\pi}{DRT}}[1-\sqrt{d(\omega_j)}]\sqrt{\sum_i C_i Z_i^2} \quad \ldots (9)$$

For diffusion of tracer ions of species No. 1, in a salt solution containing ions of species Nos 1 and 2, we have $C_1|Z_1|=C_2|Z_2|$. For uni-univalent electrolyte, $|Z_1|=|Z_2|=1$ and

$$d(\omega_j)=\frac{1}{2}\left[\frac{1}{2}+\frac{\dot{\lambda}_2^0}{\dot{\lambda}_1^0+\dot{\lambda}_2^0}\right]$$

If we now substitute $\dot{\lambda}_1^0=74.7$ for Tl ion and $\dot{\lambda}_2^0=79.8$ for $\frac{1}{2}SO_4$ ion we obtain

$$D\times 10^5=1.99-0.574\sqrt{C} \quad \ldots (10)$$

The theoretical variation D with $\sqrt{C}$ corresponding to Eq. (10) is seen to be in close agreement with the experimentally obtained variation at lower concentrations.

So far as dilute solutions are concerned, the diffusion data indicate that the fully hydrated thallium ion is completely embedded in water molecules. Since the average distance between ions in solutions of low concentrations is very large, the hydration as well as the interaction between the hydrated ion and the surrounding solvent water molecules remain essentially the same irrespective of change in concentrations, provided the solutions are dilute. The only effect of increasing the salt concentrations in this range, then, is to increase the interionic attraction due to long-range electrostatic forces. While measuring diffusion coefficients of the tracer element in liquid solutions, it is always assumed that the activity coefficient of the diffusing tracer ion is constant along the diffusion path. Onsager has shown that the diffusion potential and electrophoretic effect are both negligibly small, and in dilute solutions the decrease in diffusion coefficient with increasing salt concentrations can be completely attributed to the relaxation effect of the ion atmosphere. If this assumption is valid in the transport of ions in dilute solutions, the D versus, $C^{1/2}$ curve should give a straight line in the lower concentration range. Our experimental results (Fig. 2) confirm the validity of this assumption in the range of dilute solutions. Therefore it can be said that Onsager's concept of liquid diffusion coupled with Debye-Hückel theory is successful in explaining the transport properties in liquid solutions.

References

1 Spitzer J J, *J Chem Soc Faraday Trans I (GB)*, **74** (1978) 756; **72** (1976) 2108; **73** (1977) 1066; **74** (1976) 2385; **74** (1978) 2418.

2 Paterson R, *J Chem Soc Faraday Trans I (GB)*, **74** (1978) 2896; **74** (1978), 2885; **74** (1978) 103.

3 Anderson J, *J Chem Soc Faraday Trans I (GB)*, **73** (1977) 1973.

4 Tyrrell H J, *Diffusion and heat flow in liquids* (Butterworths, London) 1961, Ch 7.

5 Changdar S N, *Proc Nucl Phys and Solid State Phys Symp, Madurai* (Department of Atomic Energy, Govt of India, Bombay), **3** (1970) 347.

6 Crank J, *The mathematics of diffusion* (Clarendon Press, Oxford), 1964, 15.

7 Onsager L, *Ann New York Acad Sci (USA)*, **46** (1945) 241.

8 Harned H S & Owen B B, *Physical chemistry of electrolytic solutions* (Reinhold, New York), 1950, 130.

9 Wang J H, *J Am Chem Soc (USA)*, **74** (1952) 1184.

Indian Journal of Pure & Applied Physics
Vol. 21, December 1983, pp. 694-697

Dielectric Relaxation & Dipole Moment of N, N-Dimethylacetamide

J S DHULL & D R SHARMA
Electronics Research Laboratory, Department of Physics, Himachal Pradesh University, Simla 171 005

Received 14 *June* 1982; *accepted* 8 *April* 1983

Using standing wave techniques, dielectric constant (ε') and dielectric loss (ε'') of dilute solutions of N, N-dimethylacetamide (N, N-DMA) in carbon tetrachloride, dioxane and benzene have been measured at 9.987 GHz at 25, 35, 45 and 55°C. Following the single-frequency concentration variational method, dielectric relaxation time (τ) and the dipole moment (μ) of DMA have been evaluated. For N, N-DMA in benzene solution, solute-solvent type of molecular association has been proposed. Energy parameters (ΔF_ε, ΔH_ε and ΔS_ε) for the dielectric relaxation of N, N-DMA in carbon tetrachloride, dioxane and benzene solutions have been calculated from the Eyring's rate equations and compared with the corresponding viscosity parameters. A comparison between these two sets of parameters shows that the dielectric relaxation, like viscosity, can also be considered as a rate process.

1 Introduction

Amides have attracted the attention of a number of research workers[1-4] in different fields because of their high dielectric constant and their biological applications. N, N-dimethylacetamide [N, N-DMA] is an important non-aqueous solvent. Dielectric relaxation data obtained using microwave absorption studies are expected to throw light on various types of molecular associations because of the ability of the microwave technique to detect weak molecular interactions. This paper reports results of dielectric relaxation and dipole moment studies of N, N-DMA in carbon tetrachloride, dioxane and benzene solutions at four different temperatures.

2 Experimental Details

The samples of N, N-DMA (E Merck) was kept over a molecular sieve (4°Å) for 48 hr and then distilled through a long vertical fractionating column and the middle fraction was used. Benzene (BDH AnalaR) and dioxane (E Merck) were purified by refluxing over sodium metal for 6-8 hr and then distilling through a long vertical fractionating column. The middle fraction of both these solvents was used. Carbon tetrachloride (BDH AnalaR) was distilled through a long vertical fractionating column and the middle fraction was used for the present studies.

X-band microwave bench was used to measure the wavelength in the dielectric and voltage standing wave ratio (VSWR) using a short-circuiting plunger. A range of N, N-DMA concentrations was prepared in carbon tetrachloride, dioxane and benzene and the measurements were made at 25, 35, 45 and 55°C by circulating thermostated water around the dielectric cell. The temperature control of the thermostat (MLW-Baureihe U7^c, German make) was ±0.05°C. The precision of the equipment was tested by measuring the dipole moments of purified acetone, methanol and pyridine. The values of our measured dipole moment were found to be within ±2% in agreement with the values known in literature[5,6]. The viscosity and density of carbon tetrachloride, dioxane and benzene at various temperatures were measured using a Ubbelohde viscometer and a pyknometer respectively.

3 Results and Discussion

The values of dielectric constant (ε') and the dielectric loss (ε'') of the dilute solutions of N, N-DMA in carbon tetrachloride, dioxane and benzene presented in Table 1 were calculated following the method of Heston *et al.*[7] using the following equations:

$$\varepsilon' = (\lambda/\lambda_c)^2 + (\lambda/\lambda_d)^2 \quad \ldots (1)$$

$$\varepsilon'' = (2/\pi)(\lambda/\lambda_d)^2(\lambda_g/\lambda_d)(d\rho/dn) \quad \ldots (2)$$

where λ, λ_c, λ_g and λ_d are the wavelength in the free-space, the cut-off wavelength, the waveguide wavelength and the wavelength in the dielectric-filled waveguide of the cell respectively. The term ρ represents the inverse of the standing-wave ratio. The accuracy of measurement of ε' and ε'' was about 1% and 5% respectively.

The values of relaxation time (τ) and the dipole moment (μ) listed in Table 1 were determined by the single-frequency concentration variational method of Gopala Krishna[8] using the following relations:

$$X = \frac{\varepsilon'(\varepsilon'+1)+\varepsilon''^2-2}{(\varepsilon'+2)^2+\varepsilon''^2} \quad \ldots (3)$$

$$Y = \frac{3\varepsilon''}{(\varepsilon'+2)^2+\varepsilon''^2} \quad \ldots (4)$$

$$\tau = \frac{\lambda}{2\pi C}\left(\frac{dY}{dX}\right), \quad \ldots (5)$$

Table 1—Dielectric Constant (ε'), Dielectric Loss (ε''), Relaxation Time (τ) and Dipole Moment (μ) of N,N-DMA in Different Solutions at Different Temperatures

Temp °C	Conc. of N,N-DMA (Weight fraction)	ε'	ε''	$\tau \times 10^{12}$ s	μ Debye
	Solvent: Carbun tetrachloride				
25	0.0020	2.269	0.0307		
	0.0044	2.338	0.0605	6.77	3.65
	0.0073	2.414	0.0974		
	0.0091	2.465	0.1111		
35	0.0020	2.263	0.0295		
	0.0044	2.325	0.0532	6.63	3.67
	0.0073	2.392	0.0876		
	0.0091	2.443	0.1021		
45	0.0020	2.251	0.0251		
	0.0044	2.312	0.0506	6.13	3.67
	0.0073	2.374	0.0760		
	0.0091	2.427	0.0959		
55	0.0020	2.231	0.0236		
	0.0044	2.289	0.0442	5.63	3.67
	0.0073	2.354	0.0703		
	0.0091	2.405	0.0826		
	Solvent: Dioxane				
25	0.0028	2.263	0.0338		
	0.0046	2.86	0.0516	8.76	3.69
	0.0070	2.324	0.0687		
	0.0091	2.355	0.0886		
35	0.0028	2.249	0.0317		
	0.0046	2.278	0.0459	8.12	3.69
	0.0070	2.311	0.0636		
	0.0091	2.343	0.0787		
45	0.0028	2.239	0.0294		
	0.0046	2.69	0.0424	7.48	3.69
	0.0070	2.300	0.0565		
	0.0091	2.333	0.0736		
55	0.0028	2.223	0.0275		
	0.0046	2.256	0.0377	6.69	3.69
	0.0070	2.286	0.0505		
	0.0091	2.319	0.0673		
	Solvent: Benzene				
25	0.0022	2.320	0.0166		
	0.0064	2.377	0.0381	6.53	3.37
	0.0083	2.401	0.0518		
	0.0106	2.429	0.0637		
35	0.0022	2.296	0.0152		
	0.0064	2.349	0.0361	5.42	3.58
	0.0083	2.379	0.0451		
	0.0106	2.414	0.0594		
45	0.0022	2.274	0.0139		
	0.0064	2.324	0.0299	4.62	3.65
	0.0083	2.359	0.0387		
	0.0106	2.401	0.0494		
55	0.0022	2.258	0.0126		
	0.0064	2.311	0.0252	3.82	3.69
	0.0083	2.339	0.0354		
	0.0106	2.392	0.0456		

and

$$\mu^2 = \frac{9kT}{4\pi N}\cdot\frac{M}{d}\left\{1+\left(\frac{dY}{dX}\right)^2\right\}\left(\frac{dX}{dW}\right) \quad \ldots (6)$$

where d is the density of the solvent and M and W are the molecular weight and the weight fraction of N, N-DMA in the solution respectively. All other symbols have their usual significance.

Energy parameters for the dielectric relaxation (ΔF_ε, ΔH_ε and ΔS_ε) of the N, N-DMA solutions in carbon tetrachloride, dioxane and benzene and the corresponding viscosity parameters for the viscous flow (ΔF_η, ΔH_η and ΔS_η) of carbon tetrachloride, dioxane and benzene presented in Table 2 were calculated using the Eyring equations[9] for the rate process:

$$\tau = \frac{h}{kT}\exp\left(\frac{\Delta F_\varepsilon}{RT}\right) \quad \ldots (7)$$

$$\Delta F_\varepsilon = \Delta H_\varepsilon - T\Delta S_\varepsilon \quad \ldots (8)$$

$$\eta = \frac{hN}{V}\exp\left(\frac{\Delta F_\eta}{RT}\right) \quad \ldots (9)$$

and

$$\Delta F_\eta = \Delta H_\eta - T\Delta S_\eta \quad \ldots (10)$$

where V is the molar volume of the solvent and all other symbols have their usual meaning. As demanded by Eqs (7) and (9), the plots of log (τT) versus $1/T$ and log (η) versus $1/T$ were linear in each case, which showed the applicability of these equations to our relaxation time and the viscosity data. ΔH_ε and ΔH_η were evaluated from the slopes of these linear plots.

The dipole moments of N, N-DMA in carbon tetrachloride, dioxane and benzene are close to the literature value of the unassociated N, N-DMA molecule[10]. This pleads for the monomer structure of

Table 2—Values of Relaxation Time (τ), Free-Energies (ΔF_ε, ΔF_η), Enthalpies (ΔH_ε, ΔH_η), Entropies (ΔS_ε, ΔS_η), α the Debye Factor ($\tau T/\eta$) and the Kalman Factor ($\tau T/\eta\alpha$)

Temp. °C	$\tau\times10^{12}$ s	ΔF_ε	ΔF_η	ΔH_ε	ΔH_η	ΔS_ε	ΔS_η	$\alpha=\frac{\Delta H_\varepsilon}{\Delta H_\eta}$	$\frac{\tau T\times10^8}{\eta}$	$\frac{\tau T\times10^8}{\eta\alpha}$
				N,N-DMA in carbon tetrachloride						
25	6.77	2.21	3.18			−3.6	−2.2		22.71	1.72
35	6.63	2.29	3.22			−3.7	−2.3		25.95	1.84
45	6.13	2.34	3.25	1.14	2.52	−3.8	−2.3	0.454	28.26	1.86
55	5.63	2.38	3.28			−3.8	−2.3		30.25	1.87
				N,N-DMA in dioxane						
25	8.76	2.37	3.26			−3.6	−0.81		22.62	1.73
35	8.12	2.42	3.27			−3.7	−0.81		25.47	1.77
45	7.48	2.47	3.28	1.28	3.02	−3.7	−0.82	0.424	28.15	1.79
55	6.69	2.49	3.29			−3.7	−0.82		29.85	1.76
				N,N-DMA in benzene						
25	6.53	2.19	2.91			0.30	−1.31		32.44	20.23
35	5.42	2.17	2.93			0.40	−1.33		32.08	19.77
45	4.62	2.16	2.95	2.29	2.52	0.40	−1.35	0.908	31.80	19.36
55	3.82	2.13	2.97			0.50	−1.37		30.59	18.41

[ΔF_ε, ΔF_η, ΔH_ε, ΔH_η are in kcal/mol and ΔS_ε, ΔS_η are in cal/mol°C]

N, N-DMA in carbon tetrachloride, dioxane and benzene solution. Dipole moments of N, N-DMA in carbon tetrachloride and dioxane solution were found to remain constant with the temperature whereas the μ value was lower and found to increase with rise in the temperature of benzene solution. This can be attributed to the solute-solvent association of N, N-DMA in benzene solution due to the interaction of π-delocalized electron cloud of the benzene ring with the fractional positive charge on the site of the nitrogen atom of the amide group of N, N-DMA molecule. This is shown in Fig. 1. The value of the dipole moment increases with temperature because of the breaking of the solute-solvent association with temperature and it approaches the value corresponding to that of the unassociated molecule.

The observed higher value of the dielectric relaxation time of N, N-DMA in dioxane than that in carbon tetrachloride and benzene solutions can be explained on the basis that the viscosity of dioxane is higher than those of carbon tetrachloride and benzene. Decrease of dielectric relaxation time with temperature for N, N-DMA in dioxane and carbon tetrachloride solutions can be explained on the basis of the Debye theory[11]. Appreciably higher rate of decrease of relaxation time with temperature was found for N, N-DMA in benzene than in carbon tetrachloride and dioxane solutions. This further supports solute-solvent type of molecular association already proposed for N, N-DMA in benzene solution. Higher rate of decrease of dielectric relaxation time with temperature is because of increased thermal molecular energy (Debye theory)[11] and breaking of solute-solvent type of

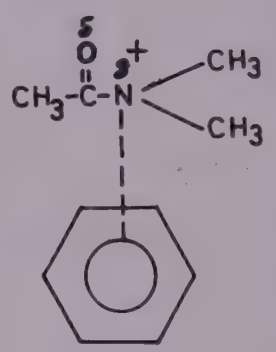

Fig. 1—Solute-solvent molecular association of N,N-DMA in benzene solution

molecular association for N, N-DMA in benzene solution.

In all the solvents, i.e. carbon tetrachloride, dioxane and benzene, the free-energy of activation (ΔF_ε) for the dielectric relaxation of N, N-DMA is less than the free-energy of activation (ΔF_η) for the viscous flow. This difference in these two sets of parameters is because of the fact that the dielectric relaxation process involves the rotation of the molecules whereas viscous flow involves the rotational as well as translational motion of the molecules. The value of α (ratio of enthalpy energy for dielectric relaxation process to enthalpy energy for viscous flow) is indicative of the solvent environment around the solute molecules. It is established that the molecules for which $\alpha>0.5$ do not behave as solid phase rotator and the molecules for which $\alpha<0.45$ behave as solid phase rotator. It is interesting to note that the value of α for N, N-DMA in benzene solution (Table 2) is greater than 0.5 ($\alpha=0.908$), while for N, N-DMA in dioxane and in carbon tetrachloride solutions it is less than 0.5 (being 0.424 and 0.454 respectively). According to the above classification, N, N-DMA molecules in benzene

solution do not behave as solid phase rotator whereas they behave as solid phase rotator in dioxane and carbon tetrachloride solutions. This difference in behaviour of N, N-DMA molecules may be attributed to the proposed solute-solvent association of N, N-DMA molecules in benzene solution and to the involved solvent effect. From Table 2 it is found, that the Debye factor ($\tau T/\eta$) varies appreciably with the variation in temperature whereas the Kalman factor ($\tau T/\eta\alpha$) remains nearly constant with temperature. This supports the view that Kalman and Smyth equation[12] is a better representation of the relaxation mechanism. It may be suggested that η^{α} is the measure of the internal resistance experienced by the molecular dipoles under the action of an applied field.

Entropy of the system is a measure of the orderly nature of the system. For a particular process, if the environment of the system is cooperative, the activated system becomes more stable than the normal system and the change in entropy is negative. In the same sense, if the environment of the system is obstructive to the process, the activated system becomes more unstable than the normal system and the environment of the system tends to bring the activated system back to the normal state. In this case, change in entropy for the process becomes positive. In the present study, change in entropy for the dielectric relaxation process is found to be negative for N, N-DMA in carbon tetrachloride and dioxane but positive for N, N-DMA in benzene solution. This may indicate the existence of cooperative orientations of the molecules resulting from the steric forces in carbon tetrachloride and dioxane solutions whereas for N,N-DMA in benzene solution, because of proposed solute-solvent association, the existing solvent environment around N, N-DMA molecules gets modified and the change in entropy for the system becomes positive.

Acknowledgement

The authors are grateful to Prof. A W Joshi for providing necessary experimental facilities. The authors are thankful to Dr K C Sharma and Dr D S Gill for valuable discussions and help. One of the authors (JSD) is grateful to the Himachal Pradesh University, Simla, for the award of a research fellowship.

References

1 Kumlar W D & Porter C W, *J Am Chem Soc (USA)*, **56** (1934) 2549.
2 Bates W W & Hobbs M E, *J Am Chem Soc (USA)*, **73** (1951) 2151.
3 Sato K & Nishioka A, *Bull Chem Soc Jpn (Japan)*, **44** (1971) 52.
4 Bass S J, Nathan W I, Meighan R M & Cole R H, *J Phys Chem (USA)*, **68** (1964) 509.
5 Pimental G C & Mc Clellan A L, *The hydrogen bond* (Reinhold Publishing Co, New York), 1960, 15.
6 Smyth C P, *Dielectric behaviour and structure* (McGraw Hill, New York), 1955, 48.
7 Heston W M (Jr), Franklin A D, Hennely E J & smyth C P, *J Am Chem Soc (USA)*, **72** (1950) 3443.
8 Gopala Krishna K V, *Trans Faraday Soc (GB)*, **33** (1957) 767.
9 Eyring H, Classtone S & Laidler K J, *The theory of rate process* (McGraw Hill, New York), 1941.
10 Zabicky J, *The chemistry of amides* (Interscience Publishers, New York), 1970.
11 Debye P, *Polar molecules* (Chemical Catalog, New York), 1929.
12 Kalman O F & Smyth C P, *J Am Chem Soc (USA)*, **82** (1960) 783.

Indian Journal of Pure & Applied Physics
Vol. 21, December 1983, pp. 698-701

Magnetic Resonance Studies on Dichlorotribenzoxazole Copper(II) & Dichlorodibenzoxazole Copper(II)

K V R CHARY*, K V G REDDY & B A SASTRY
Solidstate & Molecular Physics Laboratory, Department of Physics, Osmania University, Hyderabad 500007
and
G PONTICELLI & R PINNA
Istituto Di Chimical Generale, Inorganica Ed Analitica, Universita Di Cagliari, via Ospedale 72, 09100 Cagliari, Italy

Received 15 *June* 1983

Proton magnetic resonance and electron spin resonance studies have been carried out on the title compounds to elucidate the molecular motion and coordination behaviour of these complexes. From the temperature dependence of the proton second moment (S_2) of these complexes, the lattices are found to be rigid below 300 and 275 K in the case of $Cu(BO)_3Cl_2$ and $Cu(BO)_2Cl_2$ [BO = Benzoxazole] respectively. The observed low values of S_2 at higher temperatures are ascribed to the general reorientation of these molecules whose activation energies have been calculated to be 28.0 kJ mol^{-1} and 10.0 kJ mol^{-1} for $Cu(BO)_3Cl_2$ and $Cu(BO)_2Cl_2$ respectively. The ESR studies in polycrystalline samples indicate that the unit cell of $Cu(BO)_2Cl_2$ contains magnetically equivalent molecules and copper(II) has nitrogen coordination which is tallying with the earlier conclusions based on IR studies. ESR studies in N,N'-dimethylformamide (DMF) solutions indicate that the solute-solvent interaction in the case of $Cu(BO)_2Cl_2$ is strong unlike in the case of $Cu(BO)_3Cl_2$

1 Introduction

Benzoxazole (BO) ligands are known for their coordinating ability with number of transition metal ions and hence form many interesting complexes. These complexes have been prepared and characterized by IR and other spectroscopic techniques[1-3]. On the basis of such techniques[3] it is found that the chromophore around copper(II) in $Cu(BO)_3Cl_2$ is trigonal pyramidal formed with the three nitrogens of the three benzoxazole molecules (Fig. 1) arranged in a plane with the two chlorine atoms arranged on either side of this plane. Similar studies[1,2] in the case of $Cu(BO)_2Cl_2$ have shown that the chromophore around copper(II) is a square planar formed with the two nitrogen atoms of the benzoxazole rings and two chlorine atoms. To the best of our knowledge, no magnetic resonance studies have been made so far on any one of the benzoxazole complexes of copper(II). These characteristic features of the structure prompted us to take up the present investigation to elucidate the molecular motion and coordination behaviour of these complexes.

2 Experimental Procedure

The two complexes under investigation were prepared using the literature methods[1,2]. The PMR studies at temperatures ranging from 77 to 370 K and 77 to 330 K on $Cu(BO)_3Cl_2$ and $Cu(BO)_2Cl_2$ respectively were made using a laboratory made wide line NMR spectrometer at a fixed radio frequency of 12.0 MHz along with its variable-temperature assembly whose details are given in our earlier publication[4]. The errors in the second moment and temperature measurement are about ± 1 and ± 2.5 K respectively. The unit of the second moment is 10^{-2} $(mT)^2$.

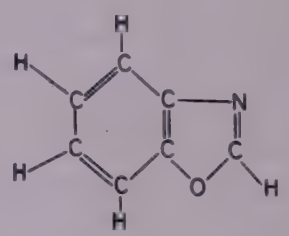

Fig. 1—Structural formula of benzoxazole

The X and Q-band ESR spectra of these complexes in polycrystalline and solution (5×10^{-4} M) forms were recorded using Varian E-4 X-band and E-112 Q-band spectrometers respectively. The magnetic field modulation frequencies were 100 kHz and 70 kHz in the case of X and Q-bands respectively. The ESR spectra of these complexes in polycrystalline form are recorded at room temperature in X and Q-bands whereas the spectra in N,N'-dimethylformamide (DMF) solution form were recorded at liquid nitrogen temperature in X-band. DPPH is used as a g-marker. The error in g and A (hyperfine separation) measurements are about ± 0.001 and 0.2 mT respectively.

*Present address: Chemical Physics Group, Tata Institute of Fundamental Research, Bombay 400005

3 Results and Discussion

3.1 Proton Magnetic Resonance Studies

The recorded first derivative PMR signals of $Cu(BO)_3Cl_2$ and $Cu(BO)_2Cl_2$ were used to calculate the values of the proton second moment (S_2) by standard methods[5]. The variation of S_2 of these two complexes with temperature is shown in Fig. 2.

From Fig. 2 it is evident that the S_2 of $Cu(BO)_3Cl_2$ is constant at 4.5 ± 1 in the temperature range 77-300 K and a rapid fall in S_2 from the above value to 1.5 ± 1 is noticed between 300 and 315 K. Thereafter, S_2 is found to be fairly constant.

From Fig. 2 it can be seen that S_2 of $Cu(BO)_2Cl_2$ is almost constant at 6 ± 1 in the temperature range 77-275 K and a rapid fall in S_2 from 5.8 ± 1 to 1.5 ± 1 is noticed in the temperature range 275-305 K. Thereafter, S_2 is found to fall slowly to 0.9 ± 1 in the temperature range 305-330 K.

In order to find the temperature up to which the lattices of the two complexes are rigid, the theoretical value of S_2(rig) has to be compared with the experimental value of S_2 at the low temperatures. But due to the absence of the crystal structure and the positional coordinates of the hydrogen atoms of these molecules, we could not calculate the theoretical second moment. Since there is no functional group in either complex to contribute more to the S_2 value and also because the interatomic distance between the two neighbouring hydrogen atoms itself will be[6] definitely more than 2.5 Å in the benzene ring and the hydrogen atom of the oxazole ring is much more remote, the low values of S_2 at 77 K are justified for a rigid lattice.

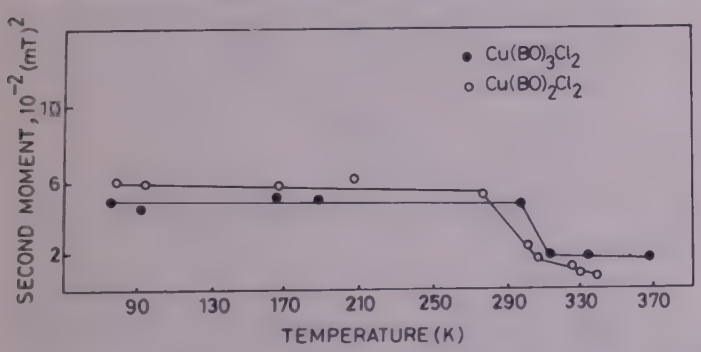

Fig. 2—Variation of proton second moment of $Cu(BO)_3Cl_2$ & $Cu(BO)_2Cl_2$ with temperature

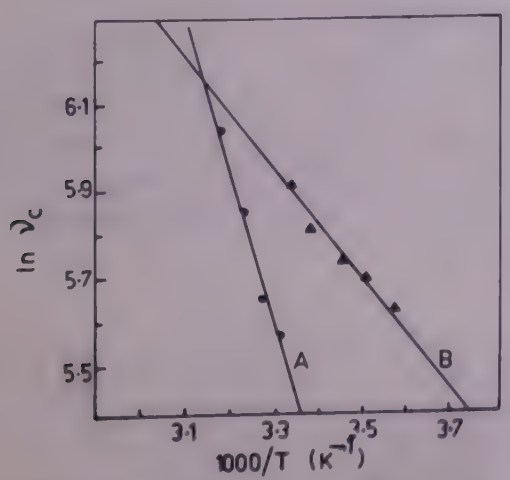

Fig. 3—Plot of $\ln \nu_c$ vs $1000/T$ for $Cu(BO)_3Cl_2$ (A) and $Cu(BO)_2Cl_2$ (B)

The second moment transitions at high temperatures in both these complexes are the result of some kind of molecular motion. Since the S_2 values at higher temperature are very low ($\sim 1.5 \pm 1$), this can be ascribed to the onset of general molecular reorientations[6].

The correlation frequencies and activation energies associated with the above molecular motions are calculated from the experimental S_2 values using the standard expression given below:

$$\ln \nu_c = \ln \frac{\nu M^{\frac{1}{2}}}{2} - \ln \tan \frac{\pi}{2}\left[\frac{M - M_{HT}}{M_{LT} - M_{HT}}\right] \quad \ldots (1)$$

The constants in the above expression have their usual meanings[7-9]. These reorientation frequencies are assumed to fit the Arrhenius' equation $\nu_c = \nu_0 \exp(-E_v/RT)$. A plot of $\ln \nu_c$ against $10^3/T$ yields a straight line (Fig. 3, curves A and B) from which the activation energies (E_v) can be calculated. In the case of $Cu(BO)_3Cl_2$ it comes out to be 28.6 kJ mol^{-1} and 10.0 kJ mol^{-1} in the case of $Cu(BO)_2Cl_2$. The error in the value of E_v is found to be ± 1 kJ mol^{-1}.

3.2 Electron Spin Resonance Studies

From the *X*-band ESR spectra of these complexes in polycrystalline form (Fig. 4, curves A and B) it is evident that no useful information can be obtained. But the *Q*-band spectrum of $Cu(BO)_2Cl_2$ (Fig. 4, curve D) indicates rhombic symmetry. Since the value of $G\left[\frac{g_3 - 2}{\frac{1}{2}(g_2 - g_1) - 2}\right]$ is coming out to be 5.0, the principal

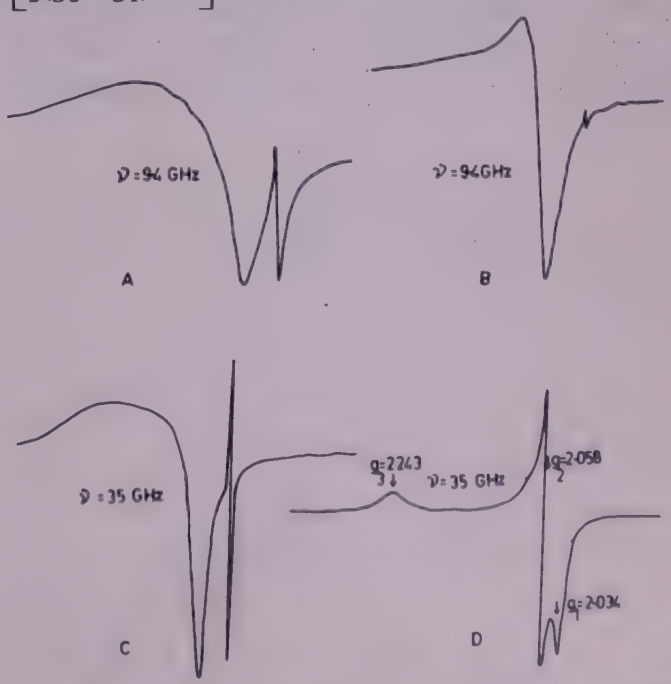

Fig. 4—ESR spectra in polycrystalline samples of $Cu(BO)_3Cl_2$ (A & C) and $Cu(BO)_2Cl_2$ (B & D)

g values may correspond to the molecular g values[10-13] which indicates that the unit cell contains one or more than one magnetically equivalent ions. The g values also indicate nitrogen coordination which is in agreement with the conclusions of the IR studies[3].

Since the information about the nature of the chromophore around copper(II) is not completely obtainable from ESR studies in polycrystalline form, ESR studies have been extended to DMF solutions at 300 and 77 K.

The frozen DMF solution of $Cu(BO)_2Cl_2$ is indicating the existence of two species (Fig. 5). The g and A values are calculated from these spectra, following methods reported in literature[14]. These values are given below:

$Cu(BO)_3Cl_2$:

$g = 2.133$; $a = 5.0$ mT

$g_\parallel = 2.252$ $g_\perp = 2.066$

$A_\parallel = -16.5$ mT; $A_\perp = +0.75$ mT

$Cu(BO)_2Cl_2$:

$g = 2.158$; $a = 5.5$ mT

$g_\parallel = \begin{cases} 2.379 \text{ (Species-I)} \\ 2.333 \text{ (Species-II)} \end{cases}$

$A_\parallel = \begin{cases} -11.5 \text{ mT (Species-I)} \\ -12.0 \text{ mT (Species-II)} \end{cases}$

$g_\perp = 2.077$; $A_\perp = 2.4$ mT

The g and A values of the $Cu(BO)_2Cl_2$ in DMF are indicating oxygen coordination which is different from the conclusion drawn from IR studies. Therefore, similar to some isoxazole complexes[15-17] here also strong solute-solvent interaction may exist resulting in an oxygen coordination due to the attachment of DMF molecules in the coordination position of the complex. On the other hand, in the case of $Cu(BO)_3Cl_2$, the g values are indicating nitrogen coordination of this complex indicating the absence of strong solute-solvent interaction.

Fig. 5 –ESR spectra of $Cu(BO)_3Cl_2$ (A) and $Cu(BO)_2Cl_2$ (B) in frozen DMF solution

The g and A values and the shape of the frozen solution spectra of both the complexes are indicating that the unpaired electron is in $d_{x^2-y^2}$ ground state and the metal-ligand bond is covalent. The ground state of the unpaired electron in the MO can be written as:

$$B_{1g} = \alpha|x^2 - y^2> - \tfrac{1}{2}\alpha'(-\sigma_x^a + \sigma_y^b + \sigma_x^c - \sigma_y^d) \quad \ldots (2)$$

The constants have their usual meanings[18]. Here, the ligand orbitals involved in the in-plane bonding are taken to be SP^2 hybrid orbitals. The σ-bond parameter (α^2) and isotropic contact term (K) can be calculated using the following equation which is derived from the equations of Maki and McGarvey[18] when the complex is square planar:

$$\alpha^2 = \frac{7}{4}\left[\frac{|A_\parallel|}{P} - \frac{|a|}{P} + \frac{2}{3}g_\parallel - \frac{5}{21}g_\perp - \frac{6}{7}\right] \quad \ldots (3)$$

$$\frac{K}{P} = \kappa = \frac{|a|}{P} + \Delta g = \alpha^2\kappa_0 \quad \ldots (4)$$

The constants have their usual meanings[14]. When the apical positions are also occupied by the ligand atoms, 4s admixture in the ground state arises due to the bonding of the apical ligand atoms with the copper(II). A detailed discussion about 4s mixing in the ground state of copper(II) is given in our earlier publication[14]. In the presence of 4s admixture, the expressions for $\alpha^2 f^2$ and α^2 will be given as[19]:

$$\alpha^2 f^2 = \frac{7}{4}\left(\frac{|A_\parallel|}{P} - \frac{|a|}{P} + \frac{2}{3}g_\parallel - \frac{5}{21}g_\perp - \frac{6}{7}\right) \quad \ldots (5)$$

$$\alpha^2 = \frac{|a|}{P\kappa_0} + \frac{\Delta g}{\kappa_0} + \frac{(1-f^2)0.0975}{P\kappa_0}$$

where f^2 is the fraction of the 3d-character in copper 3d-4s ground state.

The values of α^2, κ and f^2 in the case of $Cu(BO)_3Cl_2$ are coming out to be respectively 0.74, 0.32, 0.985. These values indicate moderately strong axial bonds.

Acknowledgement

We thank Prof. M Suryanarayana, Head of the Department of Physics for his interest in the present investigation. We express our gratitude to Prof. K Venkata Ramiah for his constant encouragement. We are grateful to the University Grants Commission, New Delhi, for the financial assistance given to carry out this work.

References

1 Duff E J & Hughes M N, *J Chem Soc A (GB)*, (1968) 2144.
2 Duff E J, *J Inorg & Nucl Chem (GB)*, 32 (1970) 3103.
3 Ponticelli G, Istituto Di Chimical Generale, Inorganica Ed Analitica, Universita Di Cagliari, via Ospedale 72, 09100 Cagliari, Italy, Private communication, 1982.
4 Chary K V R, Reddy K V G, Sastry B A & Ponticelli G, *Indian J Phys*, (1983), in press.

5 Andrew E R, *Phys Rev* (*USA*), **91** (1953) 425.
6 Slitcher C P, *Principles of magnetic resonance* (Harper and Row, New York) 1964, 61.
7 Bloemburgen N, Purcell E M, Pound R V, *Phys Rev* (*USA*), **74** (1948) 1184.
8 O'Reilly D E & Tsang T, *J Chem Phys* (*USA*), **46** (1967) 1298.
9 Abragam A, *Principles of nuclear magnetism* (Oxford University Press, Oxford) 1961, 456.
10 Procter I N, Hathaway B J & Nicholis P, *J Chem Soc A* (*GB*), (1968) 1678.
11 Tomlinson A A G & Hathaway B J, *J Chem Soc A* (*GB*), (1968) 1685.
12 Tomlinson A A G & Hathaway B J, *J Chem Soc A* (*GB*), (1968) 1905.
13 Bew M J, Hathaway B J & Fereday R J, *J Chem Soc A* (*GB*), (1972) 1229.
14 Sastry B A, Asadullah S Md, Ponticelli G & Massacessi M, *J Chem Phys* (*USA*), **70** (1979) 2834.
15 Sastry B A, Asadullah S Md, Reddy K V G *et al.*, *J Mol Struct* (*GB*), **55** (1979) 143.
16 Sastry B A, Asadullah S Md, Ponticelli G & Massacessi M, *J Inorg & Nucl Chem* (*GB*), **42** (1980) 833.
17 Ponticelli G, Pelizzi G, Sastry B A *et al.*, *Indian J Pure & Appl Phys*, **18** (1980) 212.
18 Maki A H & McGarvey B R, *J Chem Phys* (*USA*), **29** (1958) 31, 35.
19 Kuska H A, Rogers M T & Drullinger R E, *J Phys Chem* (*USA*), **71** (1967) 109.

Indian Journal of Pure & Applied Physics
Vol. 21, December 1983, pp. 702-707

Calculation of Skyshine Spectrum & Exposure due to a Cobalt-60 Gamma Source

J SWARUP
Health Physics Division, Bhabha Atomic Research Centre, Bombay 400085
and
S MINATO
Government Industrial Research Institute, Nagoya, 1 Hirate-Cho, Kita-ku, Nagoya, Japan-462

Received 24 *June* 1983

Multiply-scatter spectra of gamma rays from a point source of 1250 keV energy are calculated by Monte Carlo method in infinite air, air over ground and infinite ground media. The calculations are carried out for narrow vertical direction as well as for omni-direction for different distances (15-405 m) from the source, and for different source and detector heights (25-125 m) above ground. The spectra calculated with respect to number of scatterings in the media show that a maximum is obtained between 47 and 95 keV energy after 5 scatterings. The maximum of this energy-band is seen in all the calculated spectra. The media behave as if there is a preferential transmission band of this energy. The scattered flux beyond 45 m distance from the source meets all important requirements of diffusion theory and can be represented by diffusion equation. It is shown that with measurements carried out only in vertical direction, total exposure at different distances can be estimated.

1 Introduction

With the increase in use of nuclear energy, it is necessary to estimate the exposure on general public near a nuclear installation. Air-scattered gamma-rays (skyshine) play an important role in this exposure. A knowledge of skyshine spectrum under conditions of air over ground helps in estimating the exposure.

A gamma-photon loses its identity as to its primary energy, after a few Compton scatterings and the emergent or reflected spectrum from a thick medium has a peak in the low energy region which is not affected much by the energy of the primary source and the thickness of the medium[1]. The contribution of primary or near-primary radiation to total exposure dose reduces with increase in distance according to inverse square law and exponential attenuation in the medium but the multiply-scatter radiation persists in the medium at large distances also. Thus, at large distances, the low energy component of the multiply-scatter spectrum cannot be ignored for estimating the exposure on nearby public.

In the present study, the multiply-scatter spectra for a cobalt-60 source are calculated in air over ground medium down to 20 keV energy for different distances and heights of the source, and compared with measurements and calculations available in literature. The exposures due to scattered radiation in different configurations are also calculated.

The Monte Carlo method used here is a modified version of that developed by Nakamura and Hyodo[2]. The outline of the method is as follows. The trajectory of a photon undergoing multiple scattering is assumed to depend only on the probabilities of photoelectric absorption, Compton scattering and pair production. Coherent scattering events are disregarded because the probabilities of these interactions are very small in the energy range considered in this calculation. Photon path lengths between successive interaction sites in the two-medium geometry (air-ground) are determined precisely according to the Monte-Carlo sampling technique. Cross-section data used here are taken from the work of Hubbell[3]. The densities of soil (assumed to be represented by SiO_2) and air are taken to be uniform and equal to 1.6 and 0.001205 g/cm^3, respectively. Each spectrum is calculated with 70,000 histories.

2 Results

A cobalt-60 point-source of strengrh 1 photon/s of energy 1250 keV is assumed to be kept in air and scattered spectra are calculated at different distances in the range 15-405 m at intervals of 15 m each. The calculations are carried out for 3 sets as given below:

(1) source and detector both at ground level, (2) source and detector both raised to the same heights successively from 25 m to 125 m in steps of 25 m each, and (3) detector at ground level and the source raised from 25 to 125 m heights in the same steps of 25 m each.

Similar calculations are carried out for infinite air and infinite ground media. Calculations in the latter medium are carried out up to 45 cm distance in steps of 1.33 cm each.

Experimental measurements of air-scattered spectra in vertically downward direction showing a maximum between 50 and 90 keV energy have been reported elsewhere[4]. Miyasaka *et al.*[5] and Nason *et al.*[6] have also reported the maximum between these energies.

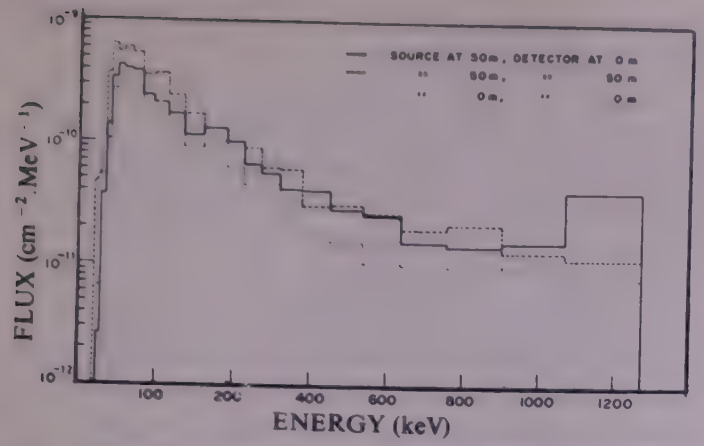

Fig. 1—Omni-directional spectra at 345 m distance for all the three configurations

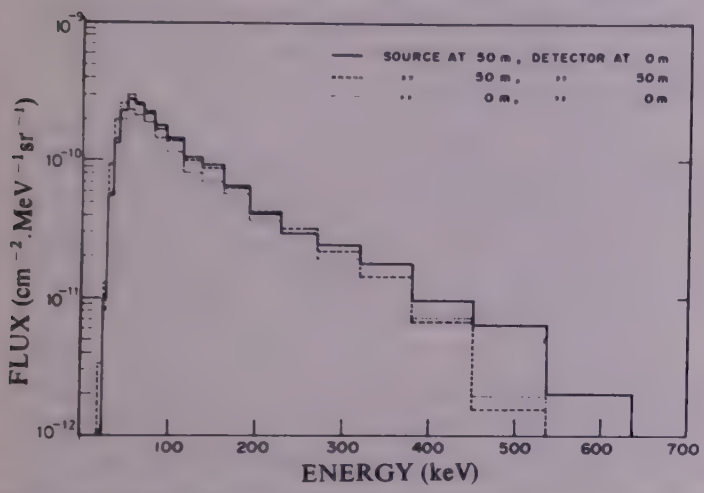

Fig. 2—Spectra in vertically downward direction at 165 m distance for all the three configurations

The present calculations show a maximum between 47 and 95 keV for infinite air and air-ground media. The calculations of the scattered spectra for each of the above mentioned sets, therefore, are carried out for vertically downward direction for comparison with experiment along with that for omni-direction. For both these directions, peak fluxes for energy between 47 and 95 keV, and their respective exposures at different distances are calculated along with exposures due to total scattered spectra from 20 keV to the primary energy. Typical omni-directional spectra for 345 m distance are shown in Fig. 1, and those in vertical direction at 165 m distance are shown in Fig. 2.

It has been reported earlier[1] that the low energy peak in aluminium medium starts building up after the fifth scattering. To understand after how many scatterings, the low energy peak is generated in infinite air, the spectra with number of scattering events are calculated at a plane parallel to the air-ground interface placed at the detector height, and are shown in Fig. 3. It is seen that the peak starts building up after the fifth scattering event in inifinite air.

In the scattered spectrum of infinite ground medium, though higher flux is seen to occur between 47 and 95 keV energy, the peak is at somewhat higher energy

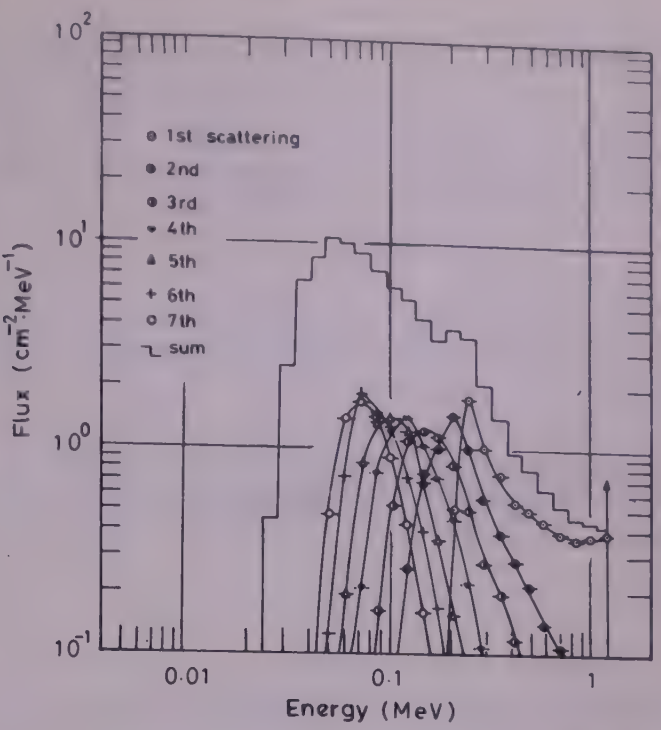

Fig. 3—Omni-directional spectra with number of scatterings in infinite air

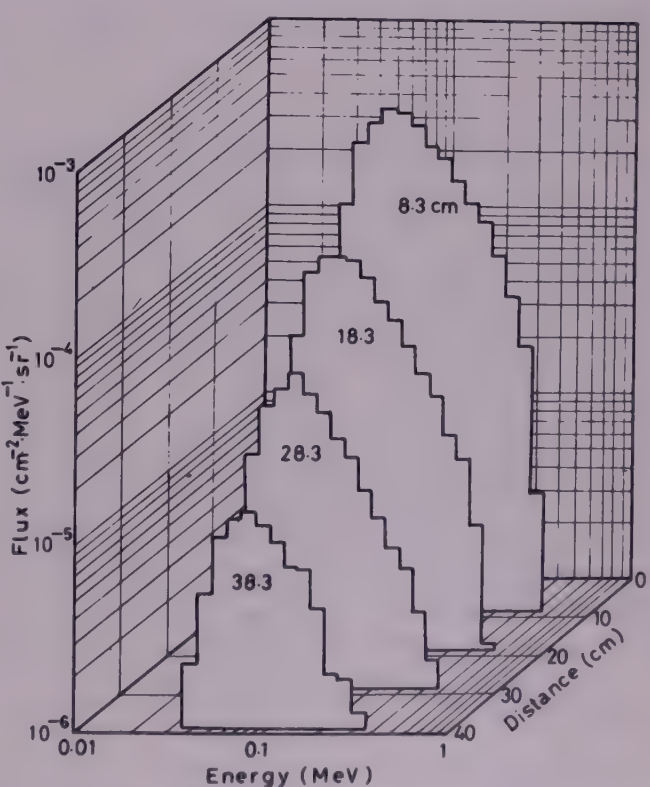

Fig. 4—Spectra in vertically downward direction in infinite ground at different distances

in comparison to that in infinite air between 67 and 80 keV (Fig. 4). For this medium too, the spectra with number of scattering events show that the peak starts building up after fifth scattering event in vertical as well as in omni-directional spectra. It may be concluded from the above that for the low energy peak to develop, a minimum number of five scatterings in the medium is required.

3 Discussion

It is observed that the scattered-energy spectra in all the three above mentioned sets of calculations are essentially of the same pattern having a maximum between 47 and 95 keV. In the following, some important observations are elucidated.

3.1 The Scattered Flux

The variation of omni-directional flux with distance from the source is shown in Fig. 5 for air-ground medium with source and detector at ground level. Similar curves are obtained for all the sets of calculations. The shape of this curve suggests that the flux can be represented by a formula used for particle diffusion, i.e. the flux (φ) at a distance r is represented by:

$$\varphi = \frac{S}{4\pi Dr} e^{-kr} \quad \ldots (1)$$

where D is the diffusion constant, S the source term and $k = \sqrt{\sum_a / D}$, $\sum_a$ being macroscopic absorption cross-section, in this case of photons, the photo-electric cross-section. Nakamura and Hyodo[2] have also given a similar formula. The diffusion constant, D is given by:

$$D = \frac{1}{3[\sum_a + (1 - \overline{\cos\theta})\sum_s]} \quad \ldots (2)$$

where $\sum_s$ is Compton scattering cross-section without coherent scattering. As mentioned in the earlier paper[1], the value of $(1 - \overline{\cos\theta})$ is taken as 0.9. As the detector is assumed to be placed above ground, cross-sections are taken for infinite air medium. These values only in SiO_2 medium are taken for infinite ground medium. With these assumptions, the variation of D and k with photon energy is calculated and plotted for all the three media, namely, infinite air, air-ground and infinite ground. The least square method is used to obtain the values of k and D/S for the calculated flux. The energy (say E_{tr}) corresponding to the least-square calculated k is read from the curve of k vs E, and for this energy (E_{tr}), the value of D is determined from the curve of D vs E.

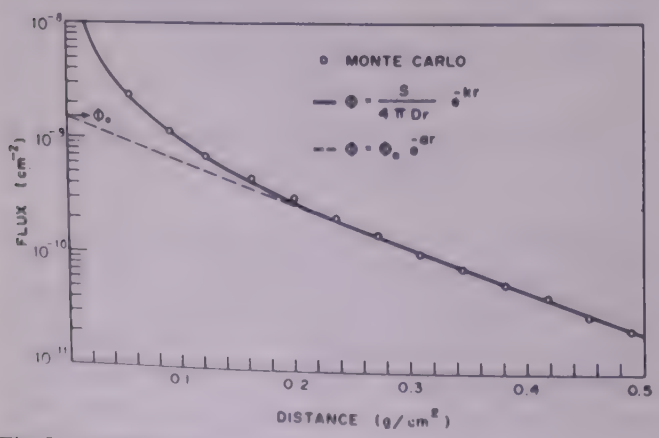

Fig. 5—Omni-directional flux with source and detector both at ground level at different distances

Thus, all the three terms k, S and D are determined. These are shown in Table 1.

It is seen from Fig. 5 that the variation of flux with distance can be expressed fairly accurately by Eq. (1) except that at 15 m (0.018 g/cm^2) distance which is too close to the primary source. The variation of flux at individual distances is not more than 10%.

While it is not suggested at the outset that the photons diffuse in the same way as particles, it is interesting to note from Table 1 that the energy E_{tr} is generally about 90 keV for infinite air and about 130 keV for ground media. This energy is very near the multiply-scatter energy of 70 ± 20 keV in infinite air reported elsewhere[4], and can be assumed as diffusion energy of multiply-scatter photons with the value of S giving the effective source term of the scattered photons of this energy.

At primary energy of 1250 keV, the photo-electric cross-section for infinite air medium is negligible in comparison to corresponding Compton cross-section and at around 80 keV energy it is about 4%. This meets the requirement of the diffusion theory that the diffusing medium should be a poor absorber.

As seen from Fig. 5, the flux at 15 m (0.018 g/cm^2) distance cannot be expressed by Eq. (1) along with the flux at other distances. This shows that the diffusion approximation of scattered photons is not valid near the source. This meets another requirement of the diffusion theory.

The ratio of vertical flux and the omni-directional flux both integrated for energies between 47 and 95 keV only, for infinite air and ground media, and when both source and detector are 100 m or 125 m above ground level, is found to be very near $1/4\pi$ for all the distances except at 15 m. This ratio for other configurations is more than $1/4\pi$, because a part of the omni-directional flux is absorbed by the ground. The vertical to omni-directional ratio of total scattered flux for other configurations is less than $1/4\pi$ at all the distsnces. Moreover, as reported elsewhere[4], the primary source in infinite air medium is surrounded by a halo comprising multiply-scatter photons of energy 70 ± 20 keV moving in all possible directions, and extending deep into the medium. This shows that the multiply-scatter photons are isotropically distributed in air for distances of 45 m (0.054 g/cm^2) and beyond, meeting yet another requirement of diffusion theory.

The multiply-scatter photons which form a peak in the scattered spectrum, thus, meet all important requirements of the diffusion theory. Thus, the scattered flux can be represented by the diffusion equation with an effective photon energy of 90 keV in infinite air medium, and 130 keV in infinite ground medium, as if a mono-energy group of photons diffuses in the medium.

Table 1—Values of k, E_{tr}, D, S, φ_0 and a for Omni-Directional and Vertical Fluxes

Source height m	Detector height m	Total scattered flux						Flux scattered between 47&95 keV energy					
		k cm²/g	E_{tr} MeV	D g/cm²	S	φ_0* cm⁻²	a cm⁻¹	k cm²/g	E_{tr} MeV	D g/cm²	S	φ_0* cm⁻²	a cm⁻¹
Omni-directional flux													
Infinite air													
—	—	0.038	0.100	2.40	0.45	2.53E-9	0.9311	0.026	0.124	2.60	0.086	5.87E-10	0.8642
Air-ground													
125	0	0.033	0.108	2.45	0.26	2.01E-9	0.9711	0.027	0.121	2.60	0.055	3.81E-10	0.8739
100	0	0.041	0.095	2.35	0.35	2.57E-9	1.0424	0.034	0.106	2.45	0.067	5.19E-10	0.9906
75	0	0.051	0.083	2.30	0.48	2.56E-9	1.0507	0.042	0.094	2.40	0.084	5.91E-10	1.0388
50	0	0.059	0.076	2.25	0.63	2.71E-9	1.0715	0.046	0.088	2.30	0.096	5.61E-10	1.0360
25	0	0.066	0.070	2.20	0.74	2.69E-9	1.0869	0.050	0.084	2.30	0.098	4.90E-10	1.0100
0	0	0.055	0.079	2.25	0.35	1.48E-9	1.0215	0.052	0.082	2.30	0.090	4.67E-10	1.0574
25	25	0.052	0.082	2.30	0.46	2.06E-9	1.0043	0.043	0.092	2.35	0.093	4.43E-10	0.9278
50	50	0.047	0.088	2.30	0.47	2.48E-9	0.9932	0.035	0.104	2.45	0.093	6.60E-10	0.9695
75	75	0.043	0.093	2.35	0.46	2.69E-9	0.9818	0.030	0.114	2.50	0.090	6.21E-10	0.9100
100	100	0.040	0.097	2.40	0.46	2.74E-9	0.9669	0.025	0.127	2.60	0.084	5.73E-10	0.8522
125	125	0.039	0.098	2.40	0.46	2.64E-9	0.9474	0.024	0.130	2.60	0.083	5.71E-10	0.8511
Infinite-ground													
—	—	0.053	0.124	2.55	0.71	2.81E-3	11.290	0.042	0.139	2.65	0.081	5.90E-4	11.453
Vertical flux													
Infinite-air													
—	—	0.037	0.101	2.40	0.023	1.25E-10	0.9067	0.027	0.121	2.60	0.0070	4.63E-11	0.8757
Air-ground													
125	0	0.042	0.094	2.40	0.024	1.38E-10	0.9729	0.030	0.114	2.50	0.0064	4.68E-11	0.9333
100	0	0.045	0.090	2.35	0.027	1.48E-10	0.9949	0.034	0.106	2.45	0.0073	5.16E-11	0.9588
75	0	0.047	0.087	2.30	0.029	1.53E-10	1.0133	0.039	0.098	2.40	0.0085	6.14E-11	1.0237
50	0	0.052	0.082	2.30	0.031	1.45E-10	1.0074	0.043	0.092	2.40	0.0094	5.81E-11	1.0174
25	0	0.054	0.080	2.30	0.032	1.40E-10	1.0256	0.047	0.087	2.30	0.0097	5.35E-11	1.0240
0	0	0.054	0.080	2.30	0.027	1.13E-10	1.0083	0.049	0.085	2.30	0.0089	4.14E-11	0.9895
Measurement[4]													
1.2	0.55	—	—	—	—	—	—	—	—	—	—	8.12E-11	1.118
25	25	0.048	0.086	2.30	0.027	1.26E-10	0.9773	0.042	0.094	2.35	0.0088	5.27E-11	0.9969
50	50	0.043	0.092	2.35	0.025	1.29E-10	0.9465	0.035	0.105	2.45	0.0080	5.64E-11	0.9755
75	75	0.040	0.096	2.40	0.024	1.25E-10	0.9187	0.031	0.112	2.50	0.0075	5.13E-11	0.9237
100	100	0.038	0.100	2.40	0.024	1.28E-10	0.9171	0.029	0.116	2.55	0.0073	4.91E-11	0.8988
125	125	0.038	0.100	2.40	0.023	1.21E-10	0.9024	0.028	0.118	2.55	0.0071	4.79E-11	0.8921
Infinite-ground													
—	—	0.048	0.130	2.60	0.023	1.29E-4	11.500	0.043	0.137	2.65	0.0069	4.97E-5	11.559

*E ±n represents $10^{\pm n}$

Table 2—Comparison of Primary Flux in Air ($\mu = 0.056$ cm^2/g)

Distance m	Theory* exp $(-\mu r)/4\pi r^2$	Monte Carlo*
75	8.5 E−10	10.0 E−10
165	9.6 E−11	9.9 E−11
255	2.2 E−11	2.5 E−11
345	6.5 E−12	7.4 E−12

*E ±n represents $10^{\pm n}$

As a measure of check for these calculations, in Table 2 the uncollided flux given by Monte Carlo method is compared with the theoretical flux ($e^{-\mu r}/4\pi r^2$), for four distances. The difference is due to the fact that the primary energy of 1.25 MeV has been taken as the mean value of the energy-bin (0.2 MeV) in the present calculations. With change in primary energy, effective energy is different from the mean energy within a bin.

3.1.1 *Comparison of flux with experimental data*—There is no direct measurement of omni-directional scattered flux available in literature. The comparison is, therefore, limited to scattered flux measured in vertically downward direction with energy-bins used in the present work. Moreover, comparison becomes somewhat difficult as most of the authors have ignored the assessment of low energy component of the scattered spectrum.

The skyshine spectrum of a 650 Ci cobalt-60 point source, measured at 155 m distance[4], is reduced to approximate energy-bins used in the present work. The comparison is shown in Fig. 6. It is observed that there is fairly good agreement between the two.

This agreement is confirmed by comparing the variation of low energy peak flux with distance. As reported elsewhere[4], the peak flux can be represented by $\varphi = \varphi_0 \exp(-ar)$ for measurements carried out between 150 m and 325 m distances in vertical direction where a has been defined as multiply-scatter coefficient of air and φ_0 as the flux of a virtual source of multiply-scatter radiation at the location of the primary source. As seen from Fig. 5, the calculated flux can also be represented by the above equation for distances beyond 150 m (0.18 g/cm^2). A least-square fit of the straight line portion of the curve shows that multiply-scatter coefficient, when both source and detector are at ground level, agrees to within 12% of the measured value (Table 1). When both source and detector are 125 m high, the value of a is almost the same as that for infinite air. The effect of ground-scattering becomes negligible at that height. Higher multiply-scatter coefficient for air-ground medium as compared to that for infinite air may be due to the absorption effect of ground at larger distances. The calculations in the ground medium are carried out only up to 45 cm depth under the assumption that the ground deeper than this does not contribute to skyshine spectrum.

3.1.2 *Comparison of exposure rate with experiment*—As mentioned above, Miyasaka *et al.*[5] and Nason *et al.*[6] have carried out detailed measurements of exposure in horizontal direction due to a cobalt-60 source collimated in vertically upward direction. The calculations in vertical direction are carried out according to the configuration of above experiments, i.e. half-angle of source-collimation as

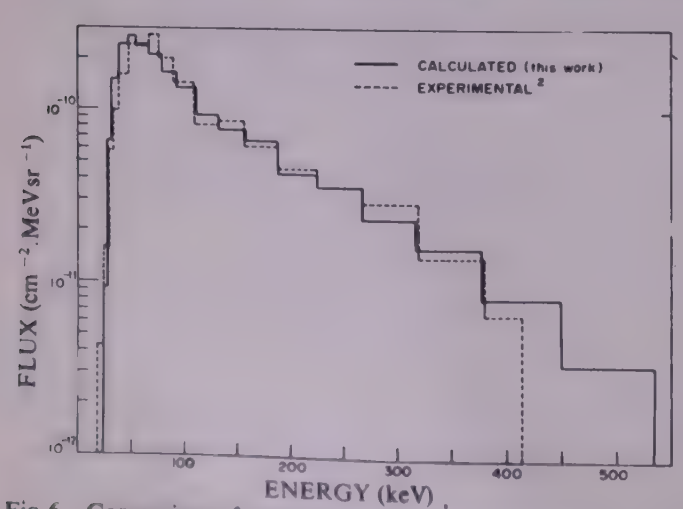

Fig. 6—Comparison of measured and calculated skyshine spectra in vertically downward direction at 155 m distance

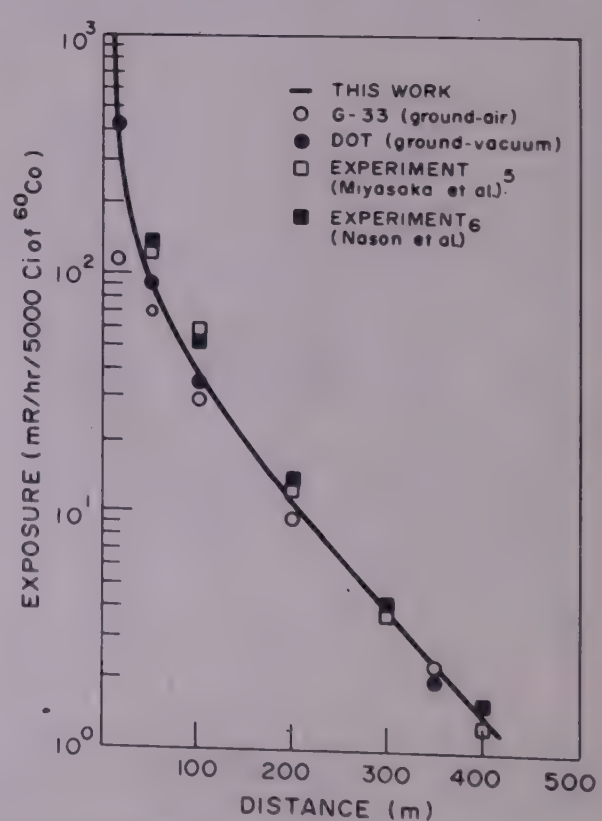

Fig. 7—Comparison of exposure rates (The calculations for G-33 and DOT are taken from Ref. 5)

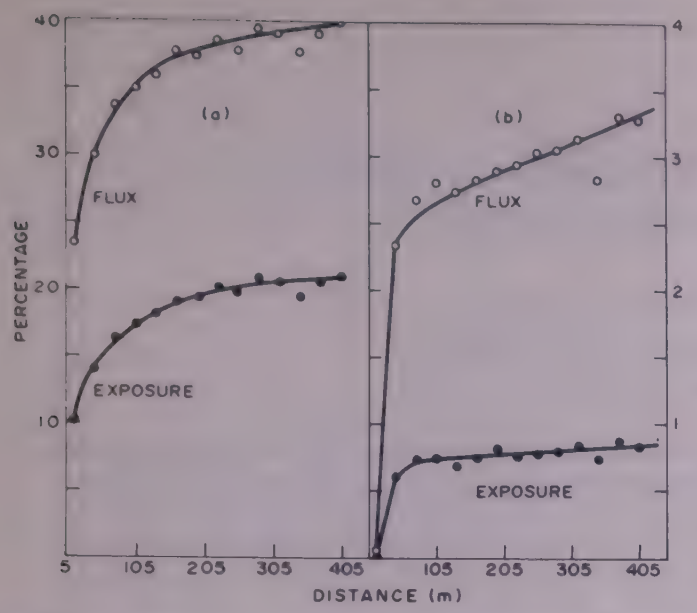

Fig. 8—Percentage contribution of multiply-scatter peak in vertical direction to total flux and exposure in (a) vertical, and (b) omni-direction, for source and detector at ground level

75°, source at 1.9 m height and detector 1 m high above the ground. The comparison of calculated exposure with the experiment is shown in Fig. 7. It is clear that the values calculated in this work are fairly close to the experimental values. This confirms the theory on which the present work is based.

3.2 Exposure at Large Distances

As the shape of the scattered spectrum in a particular configuration does not change with distance and in all the scattered spectra in air and ground a maximum is observed between 47 and 95 keV energy, it is concluded that the media behave as if there is a preferential band of transmission of the above energy, known as multiply-scatter energy. Moreover, as reported elsewhere[7], the scattered spectra of all gamma-energies show a maximum in the above energy band in air. At larger distances from a source, say, a nuclear installation, the contribution to exposure of nearby general public from this band in the scattered gamma-rays becomes more and more important.

To facilitiate the estimation of total flux and exposure from measurements of multiply-scatter part of the spectrum, their respective percentage contributions in vertical and omni-directions are shown in Fig. 8, for source and detector at ground level. If a vertically collimated detector sensitive to low energy band between 47 keV and 95 keV is used for measurements, it will detect about 20 % of the exposure per steradian in vertical direction and 0.8 % of that in omni-direction for distances up to 400 m for which these calculations are carried out. The contribution shows a tendency to rise at larger distances.

4 Conclusions

The scattered flux of a gamma source in infinite air, ground or air-ground medium can be represented by the diffusion equation. The multiply-scatter peak portion of the spectrum meets all important requirements of the application of the diffusion theory. Effective photon energy of diffusion is found to be around 90 keV in air and 130 keV in ground medium. Effective source term is found to be less than 1 with its value depending upon detector collimation.

The scattered spectra in air and ground are found to have a maximum between 47 and 95 keV energy. It takes more than five scatterings in the medium for the original photon of 1250 keV to degrade to this energy band. Air and ground media behave as if they have a preferential transmission band of this energy.

This work simplifies estimation of exposure dose to general public near a large gamma-source, say, a nuclear installation. Using the results of this work, the exposure can be estimated with measurements carried out in vertical direction only. This work also helps in estimating the exposure on ground due to a radioactivity-bearing cloud.

References

1 Minato S, *Nucl Sci & Engng (USA)*, **51** (1973) 52.

2 Nakamura T & Hyodo T, *J Nucl Sci Technol Jpn (Japan)*, **6** (1969) 143.

3 Hubbell J H, *Photon cross-sections, attenuation coefficients, and energy absorption coefficients from* 10 keV *to* 100 GeV (National Bureau of Standards, Washington, USA) Report, NSRDS-NBS, **29** (1969).

4 Swarup J, *Nucl Instrum & Methods (Netherlands)*, **172** (1980) 559.

5 Miyasaka S, Ryufuku H, Moriuchi S, Shimura S, Terada K, Yajima A, Kimura Y & Kadotani H, Publication (in Japanese) of Energy Soc Japan, **20** (1978) 485.

6 Nason R R, Shultis J K, Faw R E & Clifford C E, *Nucl Sci & Engng (USA)*, **79** (1981) 404.

7 Swarup J, *Indian J Pure & Appl Phys*, **17** (1979) 381.

Indian Journal of Pure & Applied Physics
Vol. 21, December 1983, pp. 708-715

Random Electrodynamics of Nonlinear Systems: Part II—The Hydrogen Atom

S SACHIDANANDAM & I V V RAGHAVACHARYULU
Bhabha Atomic Research Centre, Bombay 400085

Received 25 *October* 1982; *revised received* 23 *February* 1983

The hydrogen atom, immersed in the zero-point fields of Random Electrodynamics (RED), is examined from the classical point of view. The system is considered in stages, on the basis of the two time scales set by the physical processes at work. The optimal stochastic linearization technique is then applied to the equation governing short-term motion under equilibrium. The orbital frequency is determined by the driving fields. Over longer time scales, the system evolves into a spherically symmetric state, with the ensemble averages of energy and absolute value of angular momentum remaining constant at their short-term values.

1 Introduction

In continuation of our study of the Random Electrodynamics (RED) of nonlinear systems initiated in an earlier paper[1], we now discuss the physically interesting problem of the hydrogen atom. This basically nonlinear system in RED has continued to remain a frustrating challenge to workers in the field for a long time. Recent considerations by Claverie and Soto[2], making use of a formidable-looking Fokker-Planck type of equation, but employing simple perturbation techniques on elliptic orbits to evaluate the drift and diffusion coefficients, lead to a self-ionizing solution for the atom at the absolute zero of temperature. If this conclusion were indeed correct, RED should be considered a dead horse.

In our earlier paper[1], however, we underlined the fact that RED provides a meaningful classical covering theory for quantum phenomena, and the difficulties with regard to nonlinear systems are mathematical rather than physical. Indeed, we have substantiated this in the case of a slightly nonlinear oscillator for which we obtained results in essential agreement with quantum theory. This is achieved by taking a proper accounting of the nonlinear amplification of the effect of the driving fields on the natural periods of the system.

The main aim of this paper is to substantiate our theme in the case of the hydrogen atom also. We obtain a description of the ground state which, in a sense, bridges the gulf between the Bohr-orbit picture and the wavemechanical one, and provides a classical explanation of atomic stability.

An outline of the picture that emerges from our analysis is as follows: Suppose an ensemble of isolated hydrogen atoms were started off in the remote past with each atom having some negative value for its energy, i.e. with electrons in bound orbits. The emission of radiation by the (accelerated) charges causes a reduction in the orbit sizes, eccentricities, energies and angular momenta. The zero-point fields (ZPF) that are assumed to act on the charges tend to cause an increase in the same quantities. The size, shape and orientation of the orbits keep changing with a 'time-constant' approaching 10^{-9} sec as normal atomic dimensions and orbital periods (10^{-16}sec) are reached. The atoms reach equilibrium with radiation when the net rate of charge in the energy, the square of the angular momentum and the orbit size becomes zero on an average. As there is no fixed equilibrium plane for the orbit, the wobbling of the orbital plane persists even after equilibrium is attained. This brings about spherical symmetry over long times. The orbital frequencies being of the order of 10^{16}sec^{-1} while the rms angular velocity of the normal to the plane is 10^{9} radians/sec, an orbital plane can be considered as fixed during an intermediate time-scale. The scale of the ZPF (assumed to be determined by $\hbar$) fixes the root mean square orbit radius at the Bohr value and also brings about, via the wobbling of the orbit, the spherical symmetry of the *s*-state of wave mechanics over longer time scales ($>10^{-9}$sec).

The organization of the paper is as follows: We start with a review of the classical radiation-damped atom and a brief account of the ZPF. We then discuss the stochastic energy and angular momentum balance and the wobbling motion under equilibrium conditions. We proceed to determine the equilibrium orbit-size by the stochastic optimal linearization method which is further supported by a self-consistency argument. We conclude with a comparison of our RED description with those given by the Bohr model and wave mechanics.

2 The Atom in Classical Electrodynamics

Before taking up the study of the hydrogen atom immersed in the ZPF, we shall briefly recapitulate the

classical electrodynamical view[3] of it, because certain aspects of the damping fields have not received their due appreciation in the literature. An electron (charge e, mass m, and coordinate $\mathbf{r}_1$) and a proton (charge e, and mass M, and coordinate $\mathbf{r}_2$) satisfy, when they are assumed not to radiate, the Newtonian equations of motion

$$m\ddot{\mathbf{r}}_1 + e^2\mathbf{r}/r^3 = 0 \qquad \ldots (1)$$

$$M\ddot{\mathbf{r}}_2 - e^2\mathbf{r}/r^3 = 0 \qquad \ldots (1)$$

where $\mathbf{r} = \mathbf{r}_1 - \mathbf{r}_2$. The classical solution is in terms of the familiar Keplerian elliptic orbits confined to a plane normal to a constant angular momentem $\mathbf{L}$ with energy W. The eccentricity is given by

$$\varepsilon^2 = 1 - 2L^2|W|/\mu e^4 \qquad \ldots (2)$$

where μ is the reduced mass. The accelerated charges must radiate by the Larmor formula

$$-\frac{dW}{dt} = \frac{2}{3c^3}(e\ddot{\mathbf{r}}_1 + (-e\ddot{\mathbf{r}}_2)^2 \qquad \ldots (3)$$

where the wavelength of the radiation is very much greater than the separation between the charges. Now we postulate radiation reaction (RR) forces $\mathbf{F}_1^R$ and $\mathbf{F}_2^R$ acting on the electron and proton respectively so that the energy loss can be accounted for in terms of the work done by these forces: that is, we set

$$\frac{2e^2}{3c^3}\int_0^T (\ddot{\mathbf{r}}_1 - \ddot{\mathbf{r}}_2)^2 dt = -\int_0^T (\mathbf{F}_1^R.\mathbf{r}_1 + \mathbf{F}_2^R.\dot{\mathbf{r}}_2)dt \qquad \ldots (4)$$

Integrating the left hand side by parts, we have

$$\frac{2e^2}{3c^3}[(\dot{\mathbf{r}}_1 - \dot{\mathbf{r}}_2).(\ddot{\mathbf{r}}_1 - \ddot{\mathbf{r}}_2)]_0^T - \frac{2e^2}{3c^3}\int_0^T [(\ddot{\mathbf{r}}_1 - \ddot{\mathbf{r}}_2).(\dot{\mathbf{r}}_1 - \dot{\mathbf{r}}_2)dt$$

$$= -\int_0^T (\mathbf{F}_1^R.\mathbf{r}_1 + \mathbf{F}_2^R.\mathbf{r}_2)dt \qquad \ldots (5)$$

If the motion is periodic or very nearly so, the first term on the left can be set equal to zero. We shall verify shortly that damping time constant is indeed several orders of magnitude larger than orbital periods in our problem. We can then identify from Eq. (5) that

$$\mathbf{F}_1^R = \frac{2e^2}{3c^3}(\ddot{\mathbf{r}}_1 - \ddot{\mathbf{r}}_2)$$

$$\mathbf{F}_2^R = -\frac{2e^2}{3c^3}(\ddot{\mathbf{r}}_1 - \ddot{\mathbf{r}}_2) \qquad \ldots (6)$$

Now, by the incorporation of the reaction forces (6), Eq. (1) gets modified into

$$\left.\begin{aligned} m\ddot{\mathbf{r}}_1 - \frac{2e^2}{3c^3}(\ddot{\mathbf{r}}_1 - \ddot{\mathbf{r}}_2) + \frac{e^2\mathbf{r}}{r^3} = 0 \\ M\ddot{\mathbf{r}}_2 + \frac{2e^2}{3c^3}(\ddot{\mathbf{r}}_1 - \ddot{\mathbf{r}}_2) - \frac{e^2\mathbf{r}}{r^3} = 0 \end{aligned}\right\} \qquad \ldots (7)$$

Incidently, it is interesting to note that the radiation reaction force couples the motion of the two particles in addition to other forces that might act between them. This radiative coupling by the reaction force and also by the ZPF produces a quantum-like correlation among identical particles in a classical manner. Recently, Sachidanandam[4] has made a preliminary study of this phenomenon and identified it with Bose attraction for spin-zero particles.

The equation of motion for the relative coordinate $\mathbf{r}$ can be obtained from relations (7) as

$$\ddot{\mathbf{r}} - \tau\dddot{\mathbf{r}} + \frac{e^2\mathbf{r}}{\mu r^3} = 0 \qquad \ldots (8)$$

where $\tau = 2e^2/3\,\mu c^3$ which is of the order of 10^{-23}sec. In solving Eq. (8) the difficulties associated with the $\dddot{\mathbf{r}}$ term in the equation are well known[5,6]. They can be circumvented if the value of $|\tau\dddot{\mathbf{r}}|$ is orders of magnitude smaller than $|e^2\mathbf{r}/\mu r^3|$ so that we can perturbatively replace the third derivative by a lower-order one. If the initial orbit is taken to be circular, for simplicity, we can readily verify that

$$|\tau\dddot{\mathbf{r}}|/|e^2\mathbf{r}/\mu r^3| = \tau\Omega$$

$$\simeq 10^{-7} \qquad \ldots (9)$$

for a Bohr orbit.

If the motion is initially in a plane, it remains in the same plane in spite of the term $\dddot{\mathbf{r}}$.

We shall find presently that there is a wobbling motion of the orbital plane itself as a result of the ZPF and the time scale over which the wobbling occurs is much longer than orbital periods.

In the absence of these fields, Eq. (8) leads, when we treat $\tau\dddot{\mathbf{r}}$ as a perturbation, to a constancy in the direction of angular momentum $\mathbf{L}$ as its length shrinks by the orbit contraction due to radiation damping. We have, from Eq. (8),

$$\frac{d\mathbf{L}}{dt} = \mu\mathbf{r}\times\ddot{\mathbf{r}}$$

$$= \mu\tau\mathbf{r}\times\dddot{\mathbf{r}} \qquad \ldots (10)$$

On making use of the relation

$$\mathbf{r}\times\dddot{\mathbf{r}} = \frac{d}{dt}(\mathbf{r}\times\ddot{\mathbf{r}}) - \dot{\mathbf{r}}\times\ddot{\mathbf{r}}$$

$$\simeq -\dot{\mathbf{r}}\times(-e^2\mathbf{r}/\mu r^3) \qquad \ldots (11)$$

where in the last step we have replaced $\ddot{\mathbf{r}}$ by $-e^2\mathbf{r}/\mu r^3$, Eq. (10) now becomes

$$\frac{d\mathbf{L}}{dt} = -e^2\tau\mathbf{L}/\mu r^3 \qquad \ldots (12)$$

This shows that $\mathbf{L}$ remains unchanged in direction from the initial condition in spite of the damping force. However, the shape of the orbit within its plane gets

drastically altered by radiation reaction. The rate of change of L averaged over a period gives

$$\widetilde{\frac{dL}{dt}} = -(e^2 L/\mu)\tilde{\mathbf{r}}^{-3}$$
$$= -\tau e^2(\mu|W|^3)^{1/2} \quad \ldots (13)$$

where the time average ($\sim$), over an elliptic orbit, is taken only for r^{-3} on the right hand side since L changes very little in one period. In addition, the energy W changes according to the Larmor formula at the rate

$$\frac{dW}{dt} = -\frac{2e^2}{3c^3}\ddot{\mathbf{r}}^2$$
$$= -\mu\tau(e^2\mathbf{r}/r^3)^2$$
$$= -\mu\tau e^4/r^4 \quad \ldots (14)$$

The mean rate of change of energy is thus given by

$$\widetilde{\frac{d|\tilde{W}|}{dt}} = \frac{\tau e^6}{2L^5}(2\mu|\tilde{W}|)^{3/2}\left(3-\frac{2|\tilde{W}|L^2}{\mu e^4}\right) \quad \ldots (15)$$

Combining Eq. (13) and Eq. (14), we get

$$\widetilde{\frac{d|\tilde{W}|}{dt}} = -\frac{\mu e^4}{2L^3}\left(3-\frac{2|\tilde{W}|L^2}{\mu e^4}\right) \quad \ldots (16)$$

which on integration gives

$$|\tilde{W}| = \frac{\mu e^4}{2L^2}\left(1-\frac{L^3}{L_0^3}\right)+\frac{|W_0|L}{L_0} \quad \ldots (17)$$

where L_0 and W_0 are the initial values of L and W respectively.

Of significant interest for the development here is that Eq. (15) gives the limit of $|\tilde{W}|L^2$ as $\mu e^4/2$ when $L \to 0$. This means that the eccentricity $\varepsilon \to 0$, and the elliptic orbit not only shrinks in size but tends to become circular for small values of L. The final collapse of the orbit into a point is what led Bohr to postulate special nonradiating orbits to secure atomic stability.

3 ZPF as an Orbit-stabilizing Factor

The radiative collapse of a charged particle orbit can be arrested in the mean if there is a reservoir with which the system exchanges energy and comes to equilibrium. Since the radiation from the system escapes into the rest of the universe, the reservoir has to be of the same extent. Hence, we can imagine certain free radiation fields which satisfy the homogeneous Maxwell's equations to pervade the universe and play the role of reservoir. This is the basic idea of RED. The essential framework of this theory was outlined in our earlier paper[1]. The existence of a universal temperature-independent radiation called the zero-point fields (ZPF) is the only hypothesis added to the classical Maxwell-Lorentz electrodynamics. There exists a body of literature on the various arguments[7-9] in favour of the ZPF-assumption and on the progress of work in the field of RED[10-13]. We shall simply postulate the existence of the ZPF and look for the verifiable consequence of the resulting theory. Some of these, not covered in the reviews cited[10-13], have been dealt with in the report by Sachidanandam[4].

The simplest assumption one can make on the ZPF is that each of its Fourier components has an independent random phase. The randomness assumption is similar to that on the bath degrees of freedom when considering the dynamics of a Brownian particle. The independence of the phases can be justified on the basis of the smallness of the cross-section for photon-photon scattering, or in other words, by the linearity of the Maxwell equations.

We thus take the electric part of the ZPF to be given by

$$\mathbf{E}(\mathbf{r}, t) = \frac{1}{2}\int d^3k \sum_{\lambda=1}^{2} \mathbf{e}(\mathbf{k}, \lambda)\left(\frac{\hbar\omega}{2\pi^2}\right)^{1/2}$$
$$\times \{a_{\mathbf{k},\lambda}\exp(\mathrm{i}(\mathbf{k}.\mathbf{r}-\omega t)) + C.C\} \quad \ldots (18)$$

where $a_{\mathbf{k},\lambda} = \exp(\mathrm{i}\theta_{\mathbf{k},\lambda})$, with $\theta_{\mathbf{k},\lambda}$ being a random variable uniformly distributed in the interval $(0, 2\pi)$, independently for each wavevector $\mathbf{k}$ and polarization index λ. The usual orthogonality and closure properties hold for the polarization vectors $\mathbf{e}(\mathbf{k}, \lambda)$:

$$\mathbf{e}(\mathbf{k}, \lambda).\mathbf{e}(\mathbf{k}, \lambda') = \delta_{\lambda\lambda'}$$
$$\mathbf{e}(\mathbf{k}, \lambda).\mathbf{k} = 0 \quad \ldots (19)$$
$$\text{and} \sum_{\lambda=1}^{2} e_i(\mathbf{k}, \lambda)e_j(\mathbf{k}, \lambda) = \delta_{ij} - k_i k_j/k^2$$

In view of the independence of the phases, we have the following averages over the phases:

$$\langle a_{\mathbf{k},\lambda}\, a^{\dagger}_{\mathbf{k}',\lambda}\rangle = \delta_{\lambda\lambda'}\delta(\mathbf{k}-\mathbf{k}')$$
$$\langle a_{\mathbf{k},\lambda}\rangle = \langle a^{\dagger}_{\mathbf{k},\lambda}\rangle = 0$$

and

$$\langle a_{\mathbf{k},\lambda}\, a_{\mathbf{k}'\lambda'}\rangle = \langle a^{\dagger}_{\mathbf{k},\lambda}\, a^{\dagger}_{\mathbf{k}',\lambda'}\rangle = 0 \quad \ldots (20)$$

where $a^{\dagger}_{\mathbf{k},\lambda}$ is the complex conjugate of $a_{\mathbf{k},\lambda}$.

Making use of the above relations, one readily finds

$$\langle E_i(t)E_j(t')\rangle = \delta_{ij}\frac{2h}{3c^3}\int_0^{\infty}\omega^3\cos\omega(t-t')\,d\omega$$
$$= \delta_{ij}\frac{2\hbar}{3c^3}\int_{-\infty}^{\infty}|\omega^3|\cos\omega(t-t')\,d\omega \quad \ldots (21)$$

The spectrum of our noise source is thus quite non-white. This feature has its counterpart in our stochastic differential equations in the form of a damping term which is proportional not to the velocity but to the rate of change of acceleration. For practical calculations free of run-away solutions or preacelerations and divergent energies, one has to modify, on some physical

grounds, both the damping term of radiation reaction and the divergent spectrum of the fluctuating fields.

An agreeable feature to be noted about the assumed form of the random fields is the close parallel it has to the quantum representation of the free Maxwell fields. The field with a definite number $n_{\mathbf{k},\lambda}$ of photons (per unit volume) in the mode $(\mathbf{k},\lambda)$ is described in quantum theory by a decomposition exactly as in Eq. (18) with the amplitude multiplied by a factor $(2n_{\mathbf{k},\lambda}+1)^{1/2}$ which reduces to unity when each $n_{\mathbf{k},\lambda}$ is taken to be zero, i.e. the vacuum state (see Loudon[14] for a pictorial representation of such a state).

It is also worth noting that the quantum of action $\hbar$ enters our picture only as a constant that fixes the scale of the ZPF, once the existence of the latter is assumed on the basis of any of the arguments of Refs 7-9. The uncertainty relations are derived from the dynamics of particles in interaction with the ZPF rather than from any assumed commutators or the uncontrollable interactions with the measuring apparatus.

4 Combined Action of the Damping and the Fluctuating Fields

4.1 Equation of Relative Motion

When we incorporate the forces of the ZPF on the radiation-damped atom, Eqs (7) get modified into

$$m\ddot{\mathbf{r}}_1-\frac{2e^2}{3c^3}\dddot{\mathbf{r}}+\frac{e^2\mathbf{r}}{r^3}=e\mathbf{E}^\circ(\mathbf{r}_1) \qquad \ldots (22)$$

$$M\ddot{\mathbf{r}}_2+\frac{2e^2}{3c^3}\dddot{\mathbf{r}}-\frac{e^2\mathbf{r}}{r^3}=-e\mathbf{E}^\circ(\mathbf{r}_2) \qquad \ldots (23)$$

so that the relative coordinate satisfies

$$\ddot{\mathbf{r}}-\tau\dddot{\mathbf{r}}+\frac{e^2\mathbf{r}}{\mu r^3}=e\left(\frac{\mathbf{E}^\circ(\mathbf{r}_1)}{m}+\frac{\mathbf{E}^\circ(\mathbf{r}_2)}{M}\right) \qquad \ldots (24)$$

where $\tau=2e^2/3\mu c^3$ and μ is the reduced mass. In the point-dipole approximation, the equation reduces to

$$\ddot{\mathbf{r}}-\tau\dddot{\mathbf{r}}+\frac{e^2\mathbf{r}}{\mu r^3}=\frac{e}{\mu}\mathbf{E}^\circ(0)=\frac{e\mathbf{E}^\circ}{\mu}\ \text{(say)} \qquad \ldots (25)$$

It is to be noted that the essential nonlinearity in the r^{-3} term is what prevents this oscillator from having a zeroth approximation (unlike in the case of the slightly anharmonic oscillator[1]) wherein there is an orbital frequency independent of the orbit size and hence of the driving fields. Here we want to stress that the orbital frequency involves the driving fields in a fundamental way, and accordingly, we shall not treat the driving fields as a perturbation on pre-existing Keplerian orbits.

4.2 Stochastic Energy Balance between the Atom and the Radiation Fields

We shall now deduce the conditions under which the atom comes to equilibrium with radiation and acquires a stationary ensemble average value for its energy. The scalar product of $\mathbf{r}$ with Eq. (25) gives

$$\mu\dot{\mathbf{r}}.\ddot{\mathbf{r}}-\tau\mu\ddot{\mathbf{r}}.\ddot{\mathbf{r}}+\frac{e^2\mathbf{r}.\dot{\mathbf{r}}}{\mu r^3}=e\mathbf{E}^\circ.\mathbf{r} \qquad \ldots (26)$$

$$\text{i.e. } \frac{d}{dt}\left(\frac{1}{2}\mu\dot{\mathbf{r}}^2-\frac{e^2}{r}\right)=(e\mathbf{E}^\circ+\tau\mu\ddot{\mathbf{r}}).\dot{\mathbf{r}} \qquad \ldots (27)$$

Taking expectation values on both sides, we get

$$\left\langle\frac{dW}{dt}\right\rangle=\langle\mathbf{F}^{\mathrm{RED}}.\dot{\mathbf{r}}\rangle \qquad \ldots (28)$$

where W is the energy of the atom and $\mathbf{F}^{\mathrm{RED}}$ is the sum of the forces of ZPF and radiation reaction as on the right side of Eq. (27). For equilibrium on average, we require

$$\left\langle\frac{dW}{dt}\right\rangle_0=O \qquad \ldots (29)$$

which from Eq. (28) means that

$$\langle e\mathbf{E}^\circ.\dot{\mathbf{r}}\rangle_0=-\tau\mu\langle\ddot{\mathbf{r}}.\dot{\mathbf{r}}\rangle_0$$
$$=\tau\mu\langle\ddot{\mathbf{r}}^2\rangle_0 \qquad \ldots (30)$$

where the last line is identical to the Larmor formula for the rate of radiative energy loss from which we derived the reaction force term via Eq. (5). The subscript 0 on the expectation signs is meant to indicate the particular values of the relevant quantities obtaining at equilibrium. Let us assume, for the moment, that the equilibrium orbits are circular on an average with a root mean-square radius r_0 and mean orbital frequency Ω_0. We shall see below (Section 4.4) that this assumption can be justified on the basis of the existence of two widely differing time-scales in the problem and that r_0 and Ω_0 can be chosen in a stochastically optimal manner (Section 5).

To check whether Eq. (30) is indeed satisfied under these assumptions, we proceed as follows: We treat the average circular orbit as that of an isotropic two-dimensional oscillator with frequency Ω_0 and write its equation[3] as

$$\ddot{\mathbf{x}}-\tau\dddot{\mathbf{x}}+\Omega_0^2x=\frac{e}{\mu}E_x^0$$

$$\ddot{\mathbf{y}}-\tau\dddot{y}+\Omega_0^2y=\frac{e}{\mu}E_y^0 \qquad \ldots (31)$$

With E_x^0 and E_y^0 given by Eq. (18), the steady-state solution of the above can be written as

$$x=\frac{e}{2\mu}\sum_{\lambda=1}^{2}\int d^3k\left(\frac{\hbar\omega}{2\pi^2}\right)^{1/2}e_x(\mathbf{k}\lambda)$$

$$\times\left\{\frac{a_{\mathbf{k},\lambda}\exp(-i\omega t)}{\Omega_0^2-\omega^2-i\tau\omega^3}+C.C\right\} \qquad \ldots (32)$$

with a similar expression for y when e_x is replaced by e_y on the right side of Eq. (32). Making use of the expectation values defined by Eq. (20), we find

$$\langle x^2\rangle_0=\frac{e^2}{4\mu^2}\sum_{\lambda=1}^{2}\int d^3k\left(\frac{\hbar\omega}{2\pi^2}\right)\times e_x^2(\mathbf{k}\lambda)\frac{2}{(\omega^2-\Omega_0^2)^2+\tau^2\omega^6} \quad \ldots (33)$$

Using Eq. (19) for the sum over λ, integrating over the angles, and noting that $\omega^2=c^2.k^2$, we get

$$\langle x^2\rangle_0=\frac{\hbar\tau}{\mu\pi}\int_0^{\omega}\frac{\omega^3 d\omega}{(\omega-\Omega_0^2)^2+\tau^2\omega^6} \quad \ldots (34)$$

where use has been made again of the notation $\tau=2e^2/3\mu c^3$. The integration over ω is effected by noting that the integral is sharply peaked at $\omega=\Omega_0$ and hence we replace all ω by Ω_0 except where $\omega-\Omega_0$ occurs. Thus

$$\langle x^2\rangle_0=\hbar/2\mu\Omega_0 \quad \ldots (35)$$

In the evaluation of $\langle y^2\rangle$ we get the same integral as in Eq. (34) and hence we have

$$\langle r^2\rangle_0=\hbar/\mu\Omega_0 \quad \ldots (36)$$

Similarly, we get

$$\langle\dot{x}^2\rangle_0=\langle\dot{y}^2\rangle_0=\hbar\omega_0/2\mu \quad \ldots (37)$$

provided we eliminate the logarithmic divergence in the ultraviolet by a suitable cut-off (such as the pair-creation frequency) which incidentally provides a radiation correction to the right side of Eq. (37).

We can now compute the left side of Eq. (30) by noting that Eq. (32) implies

$$r_i=\frac{e}{2\mu}\int d^3k\left(\frac{\hbar\omega}{2\pi^2}\right)^{1/2}\sum_{\lambda=1}^{2}e_i(\mathbf{k}\lambda)\times\left\{\frac{-i\omega a_{\mathbf{k},\lambda}\exp(-i\omega t)}{\Omega_0^2-\omega^2-i\tau\omega^3}+\text{C.C}\right\} \quad \ldots (38)$$

where r_i stands for x and y. The rate at which the ZPF performs work on the atom is hence

$$\left\langle\frac{dW}{dt}\right\rangle_{\text{ZPF}}=\langle e\mathbf{E}^{\cdot}.\dot{\mathbf{r}}\rangle_0=\hbar\tau\Omega_0^5 \quad \ldots (39)$$

when Eq. (38) for $\dot{\mathbf{r}}$ and Eq. (18) for $\mathbf{E}^0$ are used, and the same steps as in obtaining Eqs (34)-(37) are followed. Similarly, the mean rate of change of the energy of the atom by emission of radiation is obtained by squaring the time derivative of Eq. (38) and taking the expectation values to give

$$\left\langle\frac{dW}{dt}\right\rangle_{\text{damping}}=-\tau\mu\langle\ddot{\mathbf{r}}^2\rangle=-\tau\mu\Omega_0^4\frac{\hbar}{\mu\Omega_0}=-\tau\hbar\Omega_0^3 \quad \ldots (40)$$

Eq. (30) is thus verified and we have a zero net exchange of energy in the mean between the atom and the radiation. The mean energy of the atom in equilibrium (at the zero of temperature) is thus given by

$$\langle W\rangle_0=\left\langle\frac{1}{2}\mu\dot{\mathbf{r}}^2-\frac{e^2}{r}\right\rangle=\frac{1}{2}\mu\Omega_0^2r_0^2-\frac{e^2}{r_0}=-e^2/2r_0 \quad \ldots (41)$$

if we evaluate $\langle\dot{\mathbf{r}}^2\rangle$ by the same procedure and assume $\langle r^{-1}\rangle_0=\langle r^2\rangle_0^{-1/2}$.

4.3 Mean-Square Value of the Angular Momentum in the Stationary State

The equation for the rate of change of angular momentum [Eq. (12)] gets modified in the presence of ZPF into

$$\mathbf{L}=-\frac{\tau e^2}{\mu r^3}\mathbf{L}+e\mathbf{r}\times\mathbf{E}^0=\mathbf{T}^R+\mathbf{T}^0 \quad \ldots (42)$$

where $\mathbf{T}^R$ is the torque due to radiation reaction, and $\mathbf{T}^0$ that on the dipole $e\mathbf{r}$ exerted by $\mathbf{E}^0$. On taking the inner product with $\mathbf{L}$, Eq. (42) yields

$$\frac{dL^2}{dt}=-2\tau\Omega\mathbf{L}^2+2\mathbf{L}.\mathbf{T}^0 \quad \ldots (43)$$

If $\langle\mathbf{L}^2\rangle$ has to remain constant at equilibrium we must have

$$\langle\mathbf{L}^2\rangle_0=\langle\mathbf{L}.\mathbf{T}^0\rangle_0/\tau\Omega_0^2 \quad \ldots (44)$$

Now $\langle\mathbf{L}.\mathbf{T}^0\rangle$ can be written out in detail as

$$\langle\mathbf{L}.\mathbf{T}^0\rangle_0=\langle e\mathbf{E}^0.\mathbf{L}\times\dot{\mathbf{r}}\rangle_0=e\mu\{\langle E_x^0\dot{x}y^2+E_y^0\dot{y}x^2\rangle_0-\langle x\dot{x}E_y^0y-y\dot{y}E_x^0x\rangle_0\} \quad \ldots (45)$$

for motion confined in the xy-plane. It can be seen that the second expectation bracket above vanishes identically and the remaining one gives

$$\langle\mathbf{L}.\mathbf{T}^0\rangle_0=e\mu\{\langle E_x^0\dot{x}\rangle_0\langle y^2\rangle_0+\langle E_y^0\dot{y}\rangle_0+\langle x^2\rangle_0\}=\tau\Omega_0^2\hbar/2 \quad \ldots (46)$$

upon using the values deduced earlier [Eqs (35) and (39)]. Putting this in Eq. (44) yields

$$\langle L^2\rangle_0=\hbar^2/2$$

As a check on the algebra above, we can directly compute the equilibrium value as

$$\langle L^2\rangle_0=\langle L_z^2\rangle_0=\mu^2\langle(x\dot{y}-y\dot{x})^2\rangle_0=\mu^2\{\langle x^2\rangle_0\langle\dot{y}^2\rangle_0+\langle y^2\rangle_0\langle\dot{x}^2\rangle_0\}=\hbar^2/2 \quad \ldots (48)$$

even though

$$\langle L_z\rangle_0=\mu\langle(x\dot{y}-y\dot{x})\rangle_0 \quad =0 \qquad \ldots (49)$$

4.4 Randomization of the Orbital Plane

We have been considering the atom in equilibrium with radiation as an essentially two-dimensional system. Classical Kepler motion is of course strictly two-dimensional. In quantum mechanics, the Kepler problem is irreducibly three-dimensional, because all the three components of **L** cannot be specified simultaneously, or equivalently, the uncertainty principle makes $\Delta p_z\to\infty$ if one takes $\Delta z\to 0$. The same is true in RED also, because the ZPF are isotropic, and the third component of field excites the degree of freedom normal to an initial orbital plane.

Now we investigate the nature of the motion of the orbital plane. The rate of change of the unit vector normal to the instantaneous plane of the orbit is given by

$$\frac{d}{dt}\left(\frac{\mathbf{L}}{L}\right)=\mathbf{L}\times(\dot{\mathbf{L}}\times\mathbf{L})/L^3$$
$$=\mathbf{L}\times(\mathbf{T}^0\times\mathbf{L})/L^3 \qquad \ldots (50)$$

where the last line follows from Eq. (42). Now,

$$\mathbf{T}^0\times\mathbf{L}=(e\mathbf{r}\times\mathbf{E}^0)\times\mathbf{L}$$
$$=-(\mathbf{L}.e\mathbf{E}^0)\mathbf{r} \qquad \ldots (51)$$

since **L**.**r** is zero by definition. Thus, we have,

$$\left\langle\left\{\frac{d}{dt}\left(\frac{\mathbf{L}}{L}\right)\right\}^2\right\rangle_0=\langle(\mathbf{L}\times\mathbf{T}^0)^2/L^4\rangle_0$$
$$=e^2\langle E_Z^{02}r^2/L^2\rangle_0 \qquad \ldots (52)$$

This indicates that an arbitrary initial orbit is subject not only to changes in size and shape within a plane but to a wobbling motion of the orbital plane itself. After the system attains equilibrium values of energy and angular momentum, the changes within the orbital plane are zero on the average but the wobbling of the plane persists. The equilibrium mean-square rate of change of $\mathbf{L}/L$ given by Eq. (52) can be evaluated approximately as follows:

$\langle E_z^{02}\rangle$ is the expectation value of one third of the energy density in the modes of the ZPF. This is actually infinite if the entire spectrum is taken into account. However, we restrict our consideration to the energy density in the spectral range $\Omega_0-\Delta\Omega/2$ to $\Omega_0+\Delta\Omega/2$ where $\Delta\Omega=\tau\Omega_0^2$ is the natural line-width of the atomic oscillator of centre frequency Ω_0. That is, the integral in Eq. (21), evaluated between these limits is as follows:

$$\langle E_Z^{02}\rangle\simeq\frac{\hbar}{3\pi c^3}\int_{\Omega_0-\Delta\Omega/2}^{\Omega_0+\Delta\Omega/2}\omega^3 d\omega$$
$$\simeq\frac{\hbar\tau}{3\pi c^3}\Omega_0^5 \qquad \ldots (53)$$

On using the relations

$$\langle r^2\rangle_0=\frac{\hbar}{\mu\Omega_0} \text{ and } \langle L^2\rangle_0=\hbar^2/2$$

deduced earlier, Eq. (52) and Eq. (53) give

$$\left\langle\left\{\frac{d}{dt}\left(\frac{\mathbf{L}}{L}\right)\right\}^2\right\rangle\simeq\frac{2}{\pi}\tau^2\Omega_0^4 \qquad \ldots (54)$$

The root mean-square angular velocity of the vector **L** is hence of the order of $\tau\Omega_0^2$ radian/sec (10^9sec^{-1}).

The in-plane components of the ZPF go into the determination of equilibrium orbit size and frequency in a fundamental way as we shall see below. The component normal to the plane keeps shuffling the latter and brings about spherical symmetry over large time scales ($>10^{-9}$sec) without affecting the fundamental periodicity of the orbital motion. The mean energy remains constant even as the wobbling takes place, once equilibrium with radiation is established.

5 Equilibrium Planar Motion over Time Intervals in the Range $\Omega_0^{-1}\le\Delta t\ll(\tau\Omega_0^2)^{-1}$

5.1 Optimal Linearization

The orbital periods in the atom are of the order of $\Omega_0^{-1}(10^{-16}\text{sec})$. The unit vector normal to the plane moves on an average through $\tau\Omega_0=10^{-7}$ radian in this period. Thus about 10^5 cycles of orbital oscillations take place without any appreciable wobbling of the orbital plane. The zero-point fields help maintain this 'steady state' motion. Because of the essential nonlinearity of Eq. (25), we determine the orbital frequency by applying the optimal stochastic linearization method. Calling the orbital plane in the intermediate time scale the xy-plane, which may actually be a different plane for each member of an ensemble started off in a remote past with planar orbits, we replace the equation

$$\ddot{r}_i-\tau\dot{\bar{r}}_i+\frac{e^2r_i}{\mu r^3}=\frac{e}{\mu}E_i^0 \qquad \ldots (55)$$

by

$$\ddot{r}_i-\tau\dot{\bar{r}}_i+\Omega^2r_i=\frac{e}{\mu}E_i^0 \qquad \ldots (56)$$

where r_i stands for x and y and $\mathbf{r}$ is the radius vector in the xy-plane. We compute the expectation values of functions of r from the solution of Eq. (56) in terms of the parameter Ω and then determine its value such that

$$f(\Omega)=\langle(\Omega^2\mathbf{r}-e^2\mathbf{r}/\mu r^3)^2\rangle \qquad \ldots (57)$$

is a minimum. In evaluating the expression on the right side of Eq. (57), we assume that we can set $\langle r^{-n}\rangle=\langle r^2\rangle^{-n/2}$. This assumption cannot be justified

mathematically but is satisfactory physically, because it leads to the absolute minimum value of $f(\Omega)$. We have

$$f(\Omega)=\langle r^2\Omega^4+e^4/\mu r^4-2\Omega^2e^2/\mu r\rangle$$
$$=\frac{\hbar}{\mu}\Omega^3+e^4\Omega^2/\hbar^2-\frac{2\Omega^2e^2}{\mu}\left(\frac{\mu\Omega}{\hbar}\right)^{1/2}$$
$$=(\Omega^{1/2}-\Omega_0^{1/2})^2\hbar\Omega^2/\mu \quad \ldots (58)$$

where we have written $\mu e^4/\hbar^3=\Omega_0$. Now

$$\frac{\mu}{\hbar}\frac{df}{d\Omega}=2\Omega(\Omega^{1/2}-\Omega_0^{1/2})^2+\Omega^{3/2}(\Omega^{1/2}-\Omega_0^{1/2}) \quad \ldots (59)$$

To find the turning points of $f(\Omega)$ we set the above equal to zero. The roots of the equation so obtained are $\Omega=0$, $\Omega=\Omega_0$ and $\Omega=\frac{4}{9}\Omega_0$. Checking the sign of $(d^2f/d\Omega^2)$, it is verified that only the first two roots correspond to the minima of $f(\Omega)$, which, incidentally, give the absolute minimum of the function, i.e. zero. Of these two roots, $\Omega=0$ corresponds to $\langle r^2\rangle^{1/2}\to\infty$ when the motion is hardly periodic and our equation of motion itself ceases to be valid. Hence, in this context, the only physically meaningful solution is $\Omega=\Omega_0$. This implies that on attainment of equilibrium, we obtain the 'Bohr orbit', with root mean-square radius

$$r_0=\langle r^2\rangle_0^{1/2}$$
$$=\hbar^2/\mu e^2 \quad \ldots (60)$$

in the same plane, if we look at the system for times larger than 10^{-16} sec but much smaller than 10^{-9}sec.

5.2 A Self-consistency Argument

In the minimization procedure above, we had set $\langle r^{-n}\rangle=\langle r^2\rangle^{-n/2}$. This cannot be justified within the preceding framework for the following reason: The moments generated by our solution [Eq. (32)] can be shown[1] to satisfy

$$\langle x^{2n}\rangle=\langle y^{2n}\rangle=\frac{(2n)!}{n!2^n}\langle x^2\rangle^n \quad \ldots (61)$$

which leads to

$$\langle r^{2n}\rangle=\langle(x^2+y^2)^n\rangle$$
$$=n!\langle r^2\rangle^n \quad \ldots (62)$$

The density function determined by these moments gives actually a divergent $\langle r^{-4}\rangle$. In view of this, it is desirable to have an alternative justification for the result given by Eq. (60). This is provided by a self-consistency argument. We first assume that in Eq. (56), $e^2/\mu r^3$ is replaced by

$$\Omega_0^2=\frac{e^2}{\mu r_0^3} \quad \ldots (63)$$

where $r_0=\langle r^2\rangle^{1/2}$ is to be calculated from Eq. (56) in terms of Ω_0. The calculated value, as we have seen, is given by Eq. (36) from which we have

$$\Omega_0^2=\frac{\hbar^2}{\mu^2r_0^4} \quad \ldots (64)$$

If we demand that Eq. (63) be consistent with Eq. (64), then there results

$$r_0=\frac{\hbar^2}{\mu e^2} \text{ and } \Omega_0=\frac{e^2}{r_0\hbar} \quad \ldots (65)$$

5.3 On the Evolution to Equilibrium

In confining our analysis to the equilibrium situation, we have neglected to address the important question of the approach to equilibrium. Ideally, if an equation of the Fokker-Planck type could be set up and solved, the resulting time-dependent density would solve the problem completely. In view of the difficulties in that approach[2], we had bypassed the issue and proceeded to the equilibrium situation straight away. Still, we can qualitatively understand the approach to equilibrium by noting that in each short time interval Δt such that $10^{-16}\text{sec}<\Delta t\ll 10^{-9}\text{sec}$, we can regard the motion to be in a plane. Assuming, again for simplicity, circular orbits of instantaneous radius r, we have

$$\left\langle\frac{dW}{dt}\right\rangle_{\text{damping}}=-\frac{\tau e^4}{\mu r^4} \quad \ldots (66)$$

and

$$\left\langle\frac{dW}{dt}\right\rangle_{\text{ZPF}}=\hbar\tau\Omega^3$$
$$=\frac{\tau e^4}{\mu r^4}\left(\frac{a_0}{r}\right)^{1/2} \quad \ldots (67)$$

When $r=r_0$ the two rates add up to zero. Further, it can be seen that there will be a net decrease in the energy and a shrinking of the orbit size if $r>r_0$ and a net increase in energy and an expansion of the orbit size if $r<r_0$. The orbit size stops changing on an average when $r=r_0$. Thus, during the wobbling motion of the orbital plane under equilibrium conditions, the size of the orbit in its short-time plane does not change.

6 Discussion

The study of a fundamentally nonlinear system like the hydrogen atom subject to the forces of RED cannot be carried out by brute force mathematical techniques such as perturbations on elliptic orbits because the characteristic parameter $\hbar$ of the ZPF plays a decisive role in determining the natural periods of the system.

Our step-by-step analysis provides a physical picture essentially based on classical ideas that is expected of a covering theory of quantum mechanics. For example, the RED analysis differs both from the

Bohr model and the Schrödinger picture as obtained in quantum mechanics in several important respects.

Indeed, it actually provides a bridge between these well-known models, and explains in a manner which is in consonance with classical intuition, the physical basis of both pictures.

The absence of radiation from the ground state is explained quantum mechanically by the statement that there is no lower energy state the atom can go into by emitting a quantum of radiation. But then all the excited states also qualify equally as radiationless stationary states according to the Schrödinger theory, if the atom is not coupled to the vacuum state of the quantized Maxwell fields and some open-system arguments are not brought to bear on the problem. The RED picture envisages an absence of radiation in the net in the ground state and evolution to this state at temperature zero from arbitray initial conditions with the energy less than zero.

The Bohr picture gives the correct energy level and this is sought to be explained in quantum mechanics by the fact that the position probability density $r^2|\psi(r)|^2$ attains a maximum at $r=a_0$. However, the Bohr picture is two-dimensional and the s-state is spherically symmetric.

Our picture based on short- and long-time scales provides a natural reconciliation between the two pictures each of which is based, although in different ways, on the quantum of action. Further, on short-time scales the RED model predicts an arbitrary projection of angular momentum in the range $(0, (\hbar/\sqrt{2}))$ on any direction instantaneously but zero average over times larger than 10^{-9}sec for an individual system, or over an ensemble at any given time. The square of the angular momentum is not zero but has an ensemble average value of $\hbar^2/2$. The quantum mechanical prediction of zero as an eigenvalue of L^2 (and not as ensemble average) makes any classical visualization of the system evolution impossible, because every member of the ensemble, on every measurement, has to yield the precise value of zero, according to our understanding of the eigenstates of the angular momentum operator which can be also chosen as eigenstates of the energy operator. This requires the two particles to be always moving collinearly in a classical picture. Our model does not rule out such motions because the orbits are defined only with a mean-square radius but allows the system to have a nonzero ensemble average value for the square of the angular momentum.

However, the RED picture of the atom is still incomplete. The line spectrum, which is the most important experimental information, has to be accounted for by considerations of equilibrium of the atom with the Planck radiation added to the ZPF. Work in this direction is in progress.

References

1 Sachidanandam S & Raghavacharyulu I V V, *Indian J Pure & Appl Phys*, **21** (1983) 408.
2 Claverie P & Soto F, *J Math Phys* (*USA*), **23** (1982) 753.
3 Landau L & Lifschitz E, *The classical theory of fields* (Addisson-Wesley, Massachusetts, USA) 1951, 226.
4 Sachidanandam S, *Random electrodynamics: A classical foundation for key quantum concepts*, BARC Rep-1115, 1981.
5 Elizier J, *Rev Mod Phys* (*USA*), **19** (1947) 147.
6 Plass G N, *Rev Mod Phys* (*USA*), **33** (1961) 37.
7 Marshall T W, *Proc R Soc, London* (*GB*), **284** (1963) 475.
8 Boyer T H, *Phys Rev* (*USA*), **182** (1969) 1374.
9 Braffort P, Spighel M & Tzara C, *C R Acad Sci Paris* (*France*), **239** (1954) 157.
10 Boyer T H, *Phys Rev D* (*USA*), **11** (1975) 790, 809.
11 Cleaverie P & Diner S, *Int J Quant Chem* (*USA*), **12** (Suppl 1) (1977) 41.
12 de la Pena-Aurbach L & Cetto A M, *J Math Phys* (*USA*), **20** (1979) 469.
13 Rueda A, *Phys Rev A* (*USA*) **23** (1981) 2020.
14 Loudon R, *The quantum theory of light* (*Oxford University Press, Oxford*) 1973, 146.

Indian Journal of Pure & Applied Physics
Vol. 21, December 1983, pp. 716-718

Loading Considerations on the Performance Characteristics of Thin-Film Integrated Circuits

H R SINGH
Central Electronics Engineering Research Institute Extension Centre, CSIR Complex, New Delhi 110012

Received 6 *September* 1982; *accepted* 29 *August* 1983

The influence of various resistive loadings on the performance characteristics of three different subnetworks obtained from a two-port four-terminal three-layer *R-C-KR* microstructure is reported. The structures provide ready and simple physical realization in the thin-film integrated form.

1 Introduction

The concept of microminiaturization is accomplished through the use of distributed multilayer thin-film integrated devices. This approach has already amply demonstrated its capabilities and is well within the range of modern technology. This family of the integrated devices belongs to the category of integrated morphology and are amenable to the mathematical treatment of the distributed parameter networks. Various types of electrical performance characteristics may be obtained from a multiterminal thin-film structure by imposing different sets of constraints on its terminals whereby a complete series of subnetworks can be obtained[1].

In its basic form, a multilayer distributed *R-C-KR* microstructure of length *l*(*l* being much larger than its breadth) may be realized by considering a dielectric layer (*c*) sandwiched between two resistive layers (*R*). A one-dimensional transmission line taken as a mathematical model of the above structure is shown in Fig. 1. The per-unit-length (pul) series impedances of the two resistive layers are $R = R_0 \exp(kx)$ and KR and the per-unit-length shunt capacitance of the dielectric layer is $C = C_0 \exp(-kx)$ where R_0 and C_0 are constants, K being the ratio of the resistivity of the two resistive layers and k the exponential taper constant.

The results of the analysis of the distributed multilayer $R-C-KR$ structure which forms the above mathematical model of the three-layer, four-terminal, thin-film microsystem are available in the literature[2,3]. The special case of uniform $R_0-C_0-KR_0$ structure (for $K=0$) gives the well known uniform *RC* structure, studied exhaustively for its low-pass and high-pass characteristics[4,5]. Realization of frequency-selective or -rejective filters based on distributed parameter $R-C-KR$ microsystems has been in practical implementation for some time[6,7]. Recently, some new subnetworks generated from the fundamental $R-C-KR$ structure have been reported for their band-rejection characteristics[7,8]. Similarly, the band-pass characteristics of other subnetworks of this series, both in uniform and non-uniform configurations have been achieved by suitable combinations of the characterizing parameters of the microsystem structure[9,10]. This paper describes the effects of resistive loading on the performance characteristics of three such subnetworks (Figs. 2-4) which behave as high-pass, band-pass and band-

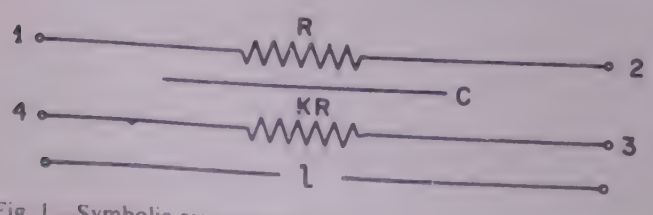

Fig. 1—Symbolic representation of the *R-C-KR* microstructure

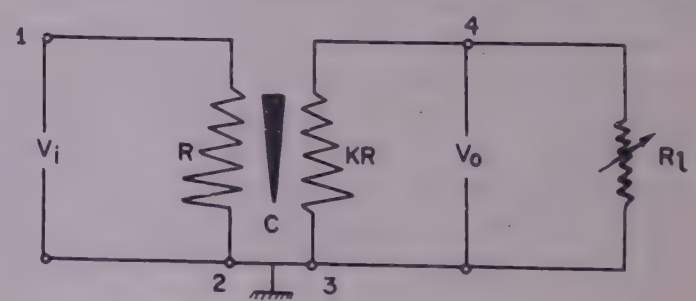

Fig. 2—High-pass filter with load

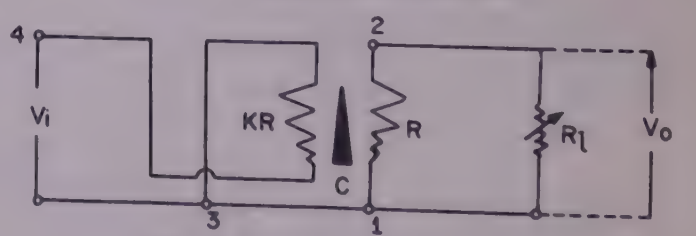

Fig. 3—Loaded band-pass filter

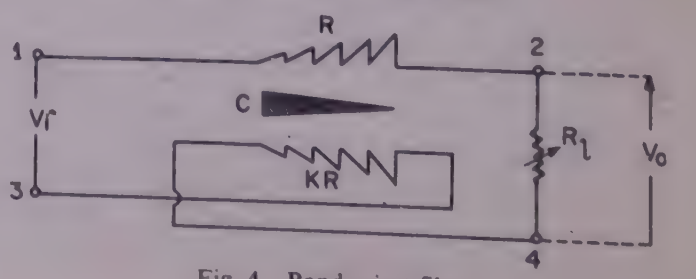

Fig. 4—Band-reject filter

rejection filters for different values of the parameters of the microstructure.

2 Analysis

The loaded voltage ratio transfer functions $|T_{vl}|$ of the three subnetworks considered here for analysis may be stated in terms of the matrix parameter functions (MPFs) of Z-Y-KZ structure[2] as

$$|T_{vl}|_2 = \frac{(1+K)h - y/W}{(1+K)h + (y/W)(1/K) + (1+K)y/R_l} \quad \ldots (1)$$

$$|T_{vl}|_3 = \frac{Y/W - (1+K)a}{(1+K)g + K(y/W) + (1+K)(y/R_l)} \quad \ldots (2)$$

$$\text{and } |T_{vl}|_4 = \frac{a + K(g+h-p) + K^2(a-p)}{g + K(2a+p) + K^2(h+p) + [K(1+K)W_t + (1-K)^2 Y]/R_l} \quad \ldots (3)$$

where the MPF's involved here are found to be[3].

$g = m\cosh(ml) + 0.5k \sinh(ml)$

$a = m \exp(0.5\, kl)$

$h = m \cosh(ml) - 0.5\, k \sinh(ml) \exp(kl)$

$z = j\omega C_0 \sinh(ml)$

and $y = (1+K)R_0 \sinh(ml)$

In Eqs (1)-(3), $W = R_t = \int_0^l R_0 \exp(kx) = R_0 = \frac{e^{Kl} - 1}{K}$

$= R_0 l$ for $k = 0$, i.e. for uniform configuration

$$C_t = \int_0^l C_0 \exp(-kx) = \frac{C_0}{k} = (1 - e^{-kl})$$

$= C_0 l_t$ for uniform configuration

and $m = [(0.5k)^2 + ju(1+K)]^{1/2}$ with $u = \omega R_0 C_0$

$p = zR_t$ and $R_L = R_0/R_l$

where R_l is the resistive loading.

Defining normalized frequency u_t as $u_t = \omega R_t C_t$, the magnitude $|T_v|$ and the phase angle φ of the above three subnetworks have been computed as a function of normalized frequency u_t for variable resistive load in the range $R_0 \le R_l \le 100\, R_0$ for several combinations of the parameters l, k and K. Some of the numerically evaluated results are shown in Figs. 5-9.

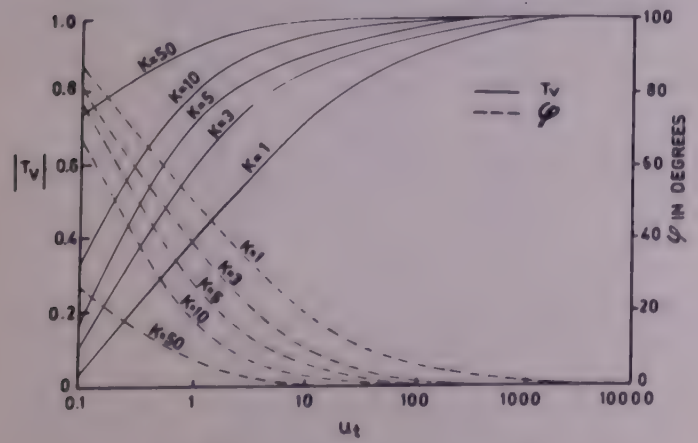

Fig. 5—High-pass characteristics

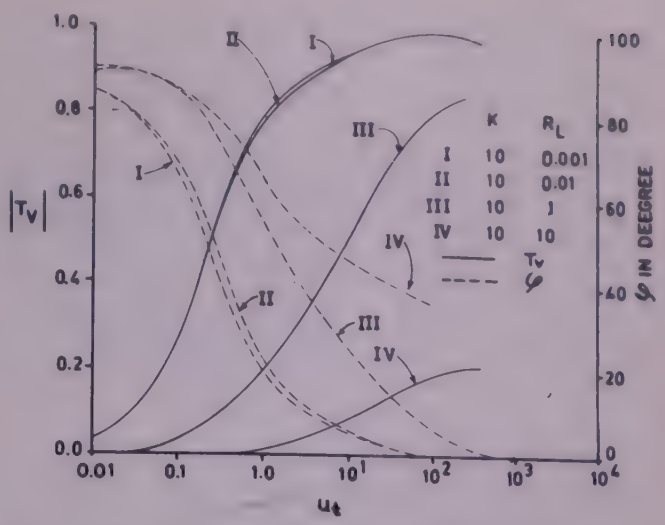

Fig. 6—Effects of load on high-pass characteristics of uniform structure

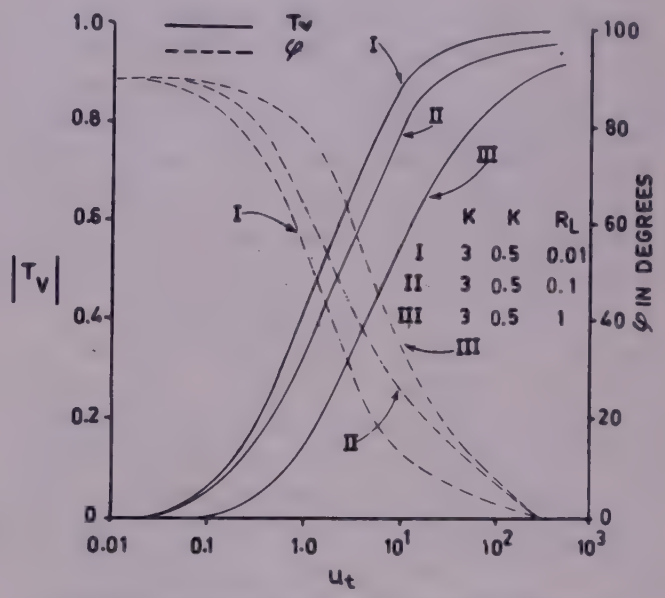

Fig. 7—Loading effects on non-uniform structures

3 Discussion

The subnetwork of Fig. 2 finds wide application for use as a perfect differentiator for all values of K (see Fig. 5). It has been found that the loading effects are more pronounced in uniform configuration to that of non-uniform configuration as shown in Figs. 6 and 7. It is also observed that the subnetwork ceases to behave as a high-pass filter for higher values of R_L, both for uniform and non-uniform configurations. However, for same values of l, K and k in no-load condition, the subnetwork continues to work as a high-pass filter. The change in phase angle φ remains almost same for smaller values of R_L in both the configurations. Loading effects on the band-reject characteristics of the subnetwork of Fig. 4 are depicted in Fig. 8. It is shown that the load fluctuations in the range $10 \le R_l \le 100$ in non-uniform configuration do not make any notice-

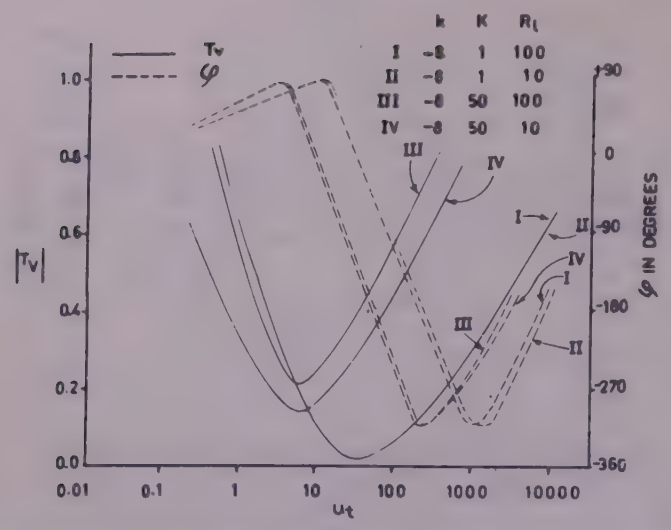

Fig. 8—Band-reject characteristics of the subnetwork under varying resistive loading

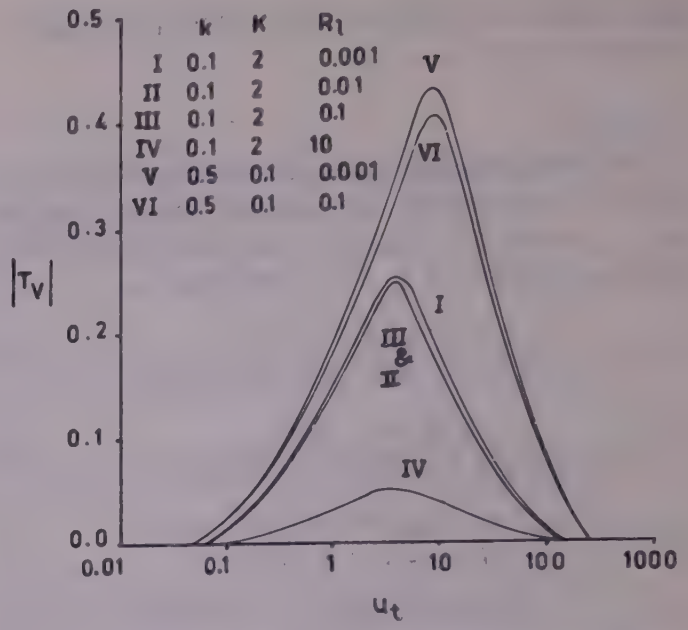

Fig. 9—Band-pass characteristics of the subnetwork with different loads

able effect on the performance characteristics of the subnetwork. However, smaller values of load fluctuation show remarkable changes in the band-reject characteristics. Fig. 9 displays the band-pass characteristics of the subnetwork under varying resistive loading conditions. It is concluded that the centre frequency of the band-pass region remains constant for larger load fluctuations in the range $0.001 \leq R_l \leq 10$. It is also observed that the Q- factor of the structure goes down as the load increases. These results are intended to indicate the possible applications of the distributed *R-C-KR* microstructures whose functional requirements can be controlled by appropriate choice of the parameters k, K, and R_L.

This work may serve as a basis for formulating design data for similar integrated filters. Also, the results evolved may be helpful in formulating a functional device approach for the design of certain ICs by relating terminal properties of the integrated devices to their performance characteristics.

The author, as part of experimental verification of the results so obtained, has fabricated certain *R-C-KR* structures using nichrome as resistive material and SiO or SiO_2, mica and alumina as the dielectric material. The results of the measurements conducted on these structures are to be reported shortly.

Acknowledgement

The author is grateful to Prof. K U Ahmed, Roorkee University, Roorkee, for his help and useful discussion in preparing this paper. Thanks are due to Mr K D Pavate, Deputy Director, CEERI Extension Centre, New Delhi for encouragement.

References

1 Castro P S & Happ W W, *IRE International Rec (USA)*, **10** (Part 2) (Mar) 1962, 3-7.

2 Ahmed K U, *IEEE Trans Circuit Theory (USA)*, **19** (1972) 506.

3 Ahmed K U, *Microelectronics & Reliability J (GB)*, **23** (1983) 795.

4 Smit A B & Cooper G, *Electrical Manufacturing (USA)* (The Gage Publishing Co, New York) (1956) (Nov) 121.

5 Holm C, *Electrical Manufacturing (USA) (CM Tech Pub Corp, New York)*, **65** (1960) (April), 92.

6 Kaufman W M, *Proc IRE (USA)*, **48** (1960), 1540.

7 Ahmed K U & Singh H R, *23rd Midwest Symposium on Circuits and Systems* (Western Periodicals Company, California, USA) 4-5 August, 1980, 191.

8 Singh H R, *Microelectronics & Reliability J (GB)*, **23** (1983), in press.

9 Ahmed K U & Singh H R, *Electronic Lett (GB)*, **16** (1980) (Apr), 277.

10 Singh H R, *Microelectronics & Reliability J (GB)*, **23** (1983), 183.

Indian Journal of Pure & Applied Physics
Vol. 21, December 1983, pp. 719-721

Addition to the Identification of $4p^3 - 4p^2 4d$ Transitions & $4d$ Levels of Nb IX Spectra

A MUSHTAQ & M S Z CHAGHTAI
Department of Physics, Aligarh Muslim University, Aligarh 202001

Received 20 *May* 1983

Further analysis of the Nb IX spectra, recorded using a 3 m normal incidence vacuum spectrograph, has been made and 19 new $4p$-$4d$ transitions have been identified. Two of earlier reported $4d$ levels have been revised and 7 new ones added thus fixing 26 levels of the theoretically predicted 28 levels of this spectrum. Percentage compositions of different levels are also reported.

1 Introduction

The first analysis of Nb IX spectrum was published by Chaghtai[1]. Rahimullah *et al.*[2] followed it with improvements regarding $4p^3 - 4p^2 5s$ transitions. Two years later, Rahimullah *et al.*[3] have added $4p^3 - 4p^2 4d$ transitions. All the ground intervals, the 8 levels of $5s$ and 19 levels of $4d$ were thus worked out. Reader and Acquista[4] have confirmed the $4p^3$, $4p^2 5s$ levels of Rahimullah *et al.*[2] and added, to the existing data, from the analysis of $4s^2 4p^3 - 4s4p^4$ transitions.

On the basis of Nb spectra taken in 1978 using a 3-m normal incidence vacuum spectrograph that uses a

Table 1—$4p^2 4d$ Levels of Nb IX

Energy levels (cm^{-1})		Designation		% Composition†
Exptl	Calc.‡	*LS*	*jj*	
326002	323805	$(^3P)^4F_{3/2}$		$-82-8(^3P)^4D-5(^1S)^2D$
329775	329614	$(^3P)^4F_{5/2}$		$-80-15(^3P)^4D$
336338	337616	$(^3P)^4F_{7/2}$		$-87-11(^3P)^4D$
338606	339433	$(^3P)^2F_{5/2}$		$-27-39(^1D)^2F+22(^3P)^4D-10(^3P)^4F$
340630	340112	$(^3P)^4D_{1/2}$	$(3P_1, 3/2)_{1/2}$	$91-7(^3P_2, 5/2)$
342812	344282	$(^3P)^2F_{7/2}$		$-16+45(^3P)^4D-30(^1D)^2F$
344004**	340049	$(^3P)^4D_{3/2}$		$52+26(^3P)^2P-13(^3P)^4F-6(^1D)^2P$
349720*	349844	$(^3P)^4D_{5/2}$		$-55-17(^1D)^2F-15(^3P)^2F-8(^3P)^4F$
361032	362534	$(^3P)^4D_{7/2}$		$42+22(^1D)^2F+20(^3P)^2F-9(^1D)^2G$
370221*	350323	$(^3P)^2P_{3/2}$		$-49+36(^3P)^4D+11(^1D)^2P$
373924*	374449	$(^1D)^2G_{7/2}$		$-85-11(^1D)^2F$
380568*	373994	$(^3P)^4P_{5/2}$		$78-14(^1D)^2D$
383651*	364462	$(^3P)^2P_{1/2}$	$(^3P_2, 3/2)_{1/2}$	$-80-14(^1D_2, 5/2)$
385291	377810	$(^3P)^4P_{3/2}$		$77-7(^1D)^2D+7(^1D)^2P$
390121*	380552	$(^3P)^4P_{1/2}$	$(^3P_2, 5/2)_{1/2}$	$-84-7(^3P_1, 3/2)+6(^1D_2, 5/2)$
392581*	388509	$(^3P)^2D_{3/2}$		$31+34(^1S)^2D-15(^3P)^4P-10(^1D)^2D$
402326**	391235	$(^3P)^2D_{5/2}$		$-20+54(^1D)^2D+15(^3P)^4P-8(^1S)^2D$
409130*	396800	$(^1D)^2D_{3/2}$		$79+9(^1S)^2D+8(^3P)^2D$
411392	411074	$(^1D)^2D_{5/2}$		$28+49(^1S)^2D+19(^3P)^2D$
415540*	410649	$(^1D)^2P_{1/2}$	$(^1D_2, 3/2)_{1/2}$	93
419914*	423641	$(^1D)^2F_{5/2}$		$-30+35(^3P)^2F+20(^3P)^2D-12(^1S)^2D$
425220**	422268	$(^1D)^2P_{3/2}$		$-71-20(^3P)^2P$
425969*	414962	$(^1D)^2S_{1/2}$	$(^1D_2, 5/2)_{1/2}$	$77-15(^3P_2, 3/2)$
427875*	433479	$(^1D)^2F_{7/2}$		$-36+62(^3P)^2F$
445329*	448140	$(^1S)^2D_{3/2}$		$42-56(^3P)^2D$
446526*	448824	$(^1S)^2D_{5/2}$		$23-39(^3P)^2D+21(^3P)^2F-14(^1D)^2F$

‡ Energy level and purity calculations were performed by R D Cowan (Ref. 5).
† In percentage composition, contributions less than 5% are omitted and only the four largest components are included.
* Rahimullah *et al.* (Ref. 3)
** Rahimullah *et al.* (Ref. 3) value improved.
The assignment of level at 427875 is unaffected as a result of this study.

gold coated grating of 1200 lines/mm, at the Lund University the authors have taken up the analysis of Nb IX again and the results are reported in this paper.

2 Experimental Details

Some of the experimental details followed in the present study are already given in the earlier works[1-3] and hence not repeated here. As the efficiency of the grating used in our present work is, due to the known high reflectance of gold for shorter wavelengths ($\lambda < 700$Å), far superior to those used by us earlier to record the same spectrum, we could detect lines corresponding to some new transitions. Our measurements are estimated to admit errors up to 0.025 Å.

3 Results and Discussion

We observed on our plates, 14 out of 16 $4s^2 4p^3 - 4s4p^4$ transitions which Reader and Acquista[4] have reported, along with 12 additional ones connecting the levels of the two configurations. These spectral lines helped us to verify the ionization affiliation of the lines and we classify these as $4p^3 - 4p^2 4d$ transitions. As stated in our earlier papers[2,3], this is achieved by studying the variation of line intensities as a function of the inductance in the spark circuit.

In the $4p$-$4d$ analysis, we confirm 16 levels of Rahimullah *et al.*[3] with improvement in values of three earlier reporter ones. One of their levels[3] could not be checked, since transitions from it to the ground levels fall at wavelengths shorter than those accessible to us on the newly recorded plates. We have revised values of two of the earlier reported $4d$ levels and have added nine more levels to the remaining 17 (Table 1), bringing the total number of known levels to 26. The two $4d$ levels that remain unknown still ($J = 9/2$) do not combine with the levels of the ground $4p^3$ configuration. The $4d$ levels, as experimentally determined are plotted in Fig. 1, where the theoretically predicted position of the unknown ones is indicated by broken lines. In this study, we have classified 19 new lines as $4p$-$4d$ transitions, some of which replace the earlier reported ones. All the newly classified lines of Nb IX are assembled in Table 2.

It is evident from Table 1, that *LS*-description is adopted for labelling the $4d$ levels. Cowan's calculations[5] reveal that this scheme either dominates over others (*jj*, *jk* and *lk*) or has the same purity as the best of the others. For $J = 1/2$ levels, however, the calculations indicate better purities in the *jj*-scheme. These levels have been given, therefore, in *jj* notations also. For them, the percentage composition is given in *jj*-scheme.

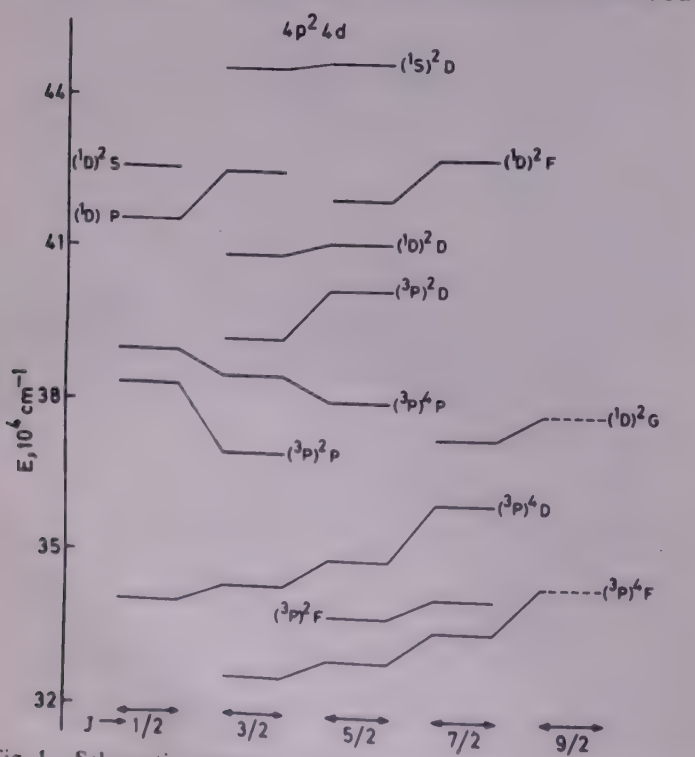

Fig. 1—Schematic energy level diagram of $4p^2 4d$ configuration of Nb IX (Broken lines indicate the theoretically predicted positions of unobserved levels.)

Table 2—Newly Classified Lines of Nb IX

Wavelength (Å)	Intensity (*I*)	Classification
259.546	40	$4p^3\,{}^4S_{3/2} - 4p^2 4d({}^3P)\,{}^4P^{**}_{3/2}$
263.588	15	$4p^3\,{}^2D_{5/2} - 4p^2 4d({}^1D)\,{}^2D^{**}_{5/2}$
266.985[a]	130	$4p^3\,{}^2P_{1/2} - 4p^2 4d({}^1D)\,{}^2P^{**}_{3/2}$
278.970	10	$4p^3\,{}^2P_{1/2} - 4p^2 4d({}^1D_{3/2}$
283.061	20	$4p^3\,{}^2D_{5/2} - 4p^2 4d({}^3P)\,{}^4P_{3/2}$
293.574	30	$4p^3\,{}^4S_{3/2} - 4p^2 4d({}^3P)\,{}^4D_{1/2}$
294.377	20	$4p^3\,{}^2P_{3/2} - 4p^2 4d({}^3P)\,{}^2D^{**}_{5/2}$
303.236	30	$4p^3\,{}^4S_{3/2} - 4p^2 4d({}^3P)\,{}^4F_{5/2}$
303.933	9	$4p^3\,{}^2D_{5/2} - 4p^2 4d\,({}^3P)\,{}^4D_{7/2}$
306.749	15	$4p^3\,{}^4S_{3/2} - 4p^2 4d({}^3P)\,{}^4F_{3/2}$
318.754	20	$4p^3\,{}^2D_{3/2} - 4p^2 4d({}^3P)\,{}^2F_{5/2}$
320.523	20	$4p^3\,{}^2D_{5/2} - 4p^2 4d({}^3P)\,{}^4D^{**}_{3/2}$
321.750	8	$4p^3\,{}^2D_{5/2} - 4p^2 4d({}^3P)\,{}^2F_{7/2}$
328.595	20	$4p^3\,{}^2D_{5/2} - 4p^2 4d({}^3P)\,{}^4F_{7/2}$
332.094	9	$4p^3\,{}^2D_{3/2} - 4p^2 4d({}^3P)\,{}^4F_{3/2}$
340.146[d]	140	$4p^3\,{}^2D_{5/2} - 4p^2 4d({}^3P)\,{}^4F_{3/2}$
342.258[b]	70	$4p^3\,{}^4S_{3/2} - 4s4p^4\,{}^2P_{3/2}$
348.626[b]	130	$4p^3\,{}^2D_{3/2} - 4s4p^4\,{}^2P_{1/2}$
359.713	9	$4p^3\,{}^2P_{3/2} - 4p^2 4d({}^3P)\,{}^4D_{1/2}$
362.349	9	$4p^3\,{}^2P_{3/2} - 4p^2 4d({}^3P)\,{}^2F_{5/2}$
374.331[a]	110	$4p^3\,{}^2P_{3/2} - 4p^2 4d({}^3P)\,{}^4F_{5/2}$
383.079	10	$4p^3\,{}^2P_{1/2} - 4s4p^4\,{}^2P_{1/2}$
388.205[c]	15	$4p^3\,{}^4S_{3/2} - 4s4p^4\,{}^2D_{5/2}$
429.730[a]	15	$4p^3\,{}^2D_{3/2} - 4s4p^4\,{}^2D_{5/2}$
504.938	8	$4p^3\,{}^2D_{3/2} - 4s4p^4\,{}^4P_{1/2}$
515.650[a]	70	$4p^3\,{}^2D_{3/2} - 4s4p^4\,{}^4P_{3/2}$
523.225	9	$4p^3\,{}^2P_{3/2} - 4s4p^4\,{}^2D_{3/2}$
573.420	9	$4p^3\,{}^2D_{5/2} - 4s4p^4\,{}^4P_{5/2}$
580.518	10	$4p^3\,{}^2P_{1/2} - 4s4p^4\,{}^4P_{1/2}$
623.851	9	$4p^3\,{}^2P_{3/2} - 4s4p^4\,{}^4P_{1/2}$
695.574	9	$4p^3\,{}^2P_{3/2} - 4s4p^4\,{}^4P_{5/2}$

** Transition given by Rahimullah *et al.* (Ref. 3) revised.

[a] Blended with an oxygen line.

[b] Blended with a line of lower ionization.

[c] Also classified in Nb VII as $4p^4 5s\ ({}^3P_0)_{1/2} - 4p^4 6p({}^3P)\,{}^2D_{3/2}$.

[d] Also classified in Nb VIII as $4p^4\,{}^3P_1 - 4p^3 4d({}^2D)\,{}^3D_2$.

The mistake in marking the $c^2D_{3\cdot 2,5/2}$ levels detected in Rahimullah *et al.*'s paper[3] has now been rectified by us.

Acknowledgement

The authors acknowledge the collaboration of JO Ekberg in recording the spectra and thank R D Cowan for providing them with the *ab initio* calculations.

References

1 Chaghtai M S Z, *J Opt Soc Am (USA)*, **61** (1971) 1264.

2 Rahimullah K, Chaghtai M S Z & Khatoon S, *Phys Scr (Sweden)*, **14** (1976) 221.

3 Rahimullah K, Chaghtai M S Z & Khatoon S, *Phys Scr (Sweden)*, **18** (1978) 96.

4 Reader J & Acquista N, *J Opt Soc Am (USA)*, **71** (1981) 434.

5 Cowan R D, LASL, Los Alamos, USA, private communication, 1967.

COMMUNICATIONS

Indian Journal of Pure & Applied Physics
Vol. 21, December 1983, pp. 722-724

Calculation of Specific Heat of a Weakly Inhomogeneous Interacting Electron Gas

SURESH G MENON
Department of Physcis, University of Poona, Pune 411 007

Received 27 *July* 1983; *revised received* 14 *November* 1983

Calculation of the free energy and the specific heat of a weakly inhomogeneous, interacting electron gas has been done within the framework of the density functional formalism. The simple temperature-dependent Thomas-Fermi approach has been used to get explicit analytical forms for these quantities.

In this communication, a novel calculation of the free energy and the specific heat at constant volume of a system of interacting electrons moving in an external potential furnished by the ions is presented. This external potential is represented by two parts—one arising from a uniform, positive ionic charge background which exactly neutralizes the part of the electronic charge density which is uniform, as in the jellium model, and the other, a very weak, periodic, slowly varying potential acting as a perturbation. This Hamiltonian is in some way an approximation to that of the motion of conduction electrons in metals[1,2]. Explicitly the Hamiltonian is

$$H=\sum_{i=1}^{N}\frac{\mathbf{p}_i^2}{2m}+\sum_{\substack{i,j=1\\ i\neq j}}^{N}\frac{e^2}{(2|\mathbf{r}_i-\mathbf{r}_j|)}+\sum_{i=1}^{N}v(\mathbf{r}_i)$$

+self energy of uniform, positive charge background. ... (1)

where $\mathbf{p}_i$ denotes the momentum, $\mathbf{r}_i$ and $\mathbf{r}_j$ are the coordinates for the electrons, $v(\mathbf{r}_i)$ is the weak, external ionic potential energy of the ith electron, and N is the total number of particles.

Explicitly,

$$v(\mathbf{r})=\tilde{v}(\mathbf{r})+v_{so}(\mathbf{r}) \quad \ldots (2)$$

where $\tilde{v}(\mathbf{r})$ is the weak, slowly varying periodic potential of the form $\sum_{G=0} V_G\exp(i\mathbf{G}.\mathbf{r})$ and $v_{so}(\mathbf{r})$ is a constant potential arising due to the uniform positive charge distribution given as

$$v_{so}(\mathbf{r})=-e^2n_0\int d^3\mathbf{r}'/|\mathbf{r}-\mathbf{r}'| \quad \ldots (3)$$

which is infinite. However, it is well known that this exactly cancels with the self-energy of uniform, positive charge background together with the part of self-energy arising from uniform electronic density. In Eq. (3), n_0 is a constant, corresponding to the uniform density, i.e. density in the homogeneous system and is independent of $\tilde{v}(\mathbf{r})$.

The calculation is done analytically using the finite temperature Thomas-Fermi (TF) approach[3] and simplified perturbation theory in terms of the external periodic potential. Normally, to obtain the specific heat of the inhomogeneous electron gas, one can directly use the finite temperature many-body perturbation theory[4]. However, it is a complicated formalism, in general. Here, the density functional formalism is resorted to, considering the fact that it is an elegant formalism which takes care of inhomogeneity in the system due to the external potential, as well as the electron-electron interaction at the same time[5]. Since in the TF approximation, exchange and correlation effects are neglected, an alternative approach with the independent-particle Hamiltonian

$$H=\sum_i \mathbf{p}_i^2/2m+\sum_{i,G}V_G\exp(i\mathbf{G}.\mathbf{r}_i)\varepsilon_{\mathbf{G}}$$

$$=\sum_i \mathbf{p}_i^2/2m+\sum_{i,G}V_{\mathbf{G}}(\mathbf{r}_i)/\varepsilon_{\mathbf{G}}$$

could also be used.

It is known[3] that one can define a functional of the density $G[n(\mathbf{r})]$ independent of the external $v(\mathbf{r})$, such that the thermodynamic functional

$$\Omega[n(\mathbf{r})]=\int v(\mathbf{r})n(\mathbf{r})d^3\mathbf{r}+e^2\iint\frac{d^3\mathbf{r}d^3\mathbf{r}'n(\mathbf{r})n(\mathbf{r}')}{(2|\mathbf{r}-\mathbf{r}'|)}+G[n(\mathbf{r})]$$

... (4)

is a minimum and equals the grand potential when $n(\mathbf{r})$ is the equilibrium density in the grand ensemble in presence of $v(\mathbf{r})$. The grand potential is defined as

$$\Omega=F-\mu N=-k_BT\ln Z \quad \ldots (5)$$

where F is the Helmholtz free energy, μ the chemical potential, k_B the Boltzmann constant, T the absolute temperature, and Z the grand partition function.

In the spirit of TF theory, if one neglects exchange and correlation effects and approximates the

contribution of F to G by a form which is locally the free-particle expression, one finds

$$G[n(\mathbf{r})] = (2/(2\pi\hbar)^3)\int d^3\mathbf{r}d^3\mathbf{p} \times \{-\frac{1}{\beta}\ln[1+\exp(-\beta(\mathbf{p}^2/2m)-\tilde{\mu}(\mathbf{r}))] + \tilde{\mu}(\mathbf{r})[1+\exp(\beta((\mathbf{p}^2/2m) - \tilde{\mu}(\mathbf{r})))]^{-1}\} - \mu\int n(\mathbf{r})d^3\mathbf{r} \quad \ldots (6)$$

where $\beta=(k_BT)^{-1}$ and $\tilde{\mu}(\mathbf{r})$ is a local functional of the density, implicitly defined by

$$n(\mathbf{r}) = 2\int d^3\mathbf{p}\frac{\{\exp[\beta((\mathbf{p}^2/2m)-\tilde{\mu}(\mathbf{r}))]+1\}^{-1}}{(2\pi\hbar)^3} \quad \ldots (7)$$

Using the variational principle for $\Omega[n(\mathbf{r})]$, one can write

$$-\mu(\mathbf{r}) = v(\mathbf{r}) + v_i(\mathbf{r}) - \mu \quad \ldots (8)$$

where

$$v_i(\mathbf{r}) = e^2\int d^3\mathbf{r}'n(\mathbf{r}')/|\mathbf{r}-\mathbf{r}'| \quad \ldots (9)$$

Hence

$$F[n(\mathbf{r})] = \int v(\mathbf{r})n(\mathbf{r})d^3\mathbf{r} + e^2\iint\frac{d^3\mathbf{r}d^3\mathbf{r}'n(\mathbf{r})n(\mathbf{r}')}{(2|\mathbf{r}-\mathbf{r}'|)} + \frac{2}{(2\pi\hbar)^3}\int d^3\mathbf{r}d^3\mathbf{p}\Big\{-\frac{1}{\beta}\ln[1+\exp(-\beta(p^2/2m + v(\mathbf{r})+v_i(\mathbf{r})-\mu))] + (\mu - v(\mathbf{r}) - v_i(\mathbf{r})) \times [\exp(\beta((\mathbf{p}^2/2m)+v(\mathbf{r})+v_i(\mathbf{r})-\mu))+1]^{-1}\Big\} \quad \ldots (10)$$

and

$$n(\mathbf{r}) = 2\int d^3\mathbf{p}\{\exp[\beta((\mathbf{p}^2/2m) + v(\mathbf{r})+v_i(\mathbf{r})-\mu)]+1\}^{-1}/(2\pi\hbar)^3 \quad \ldots (11)$$

Eqs (10) and (11) form the starting point for the calculation of specific heat. Coupling Eq. (11) with the Poisson equation gives the temperature-dependent TF equation.

Since $\tilde{v}(\mathbf{r})$ is assumed to be weak, a perturbation scheme could be used. Let

$$n(\mathbf{r}) = n_0 + n_1(\mathbf{r}) + n_2(\mathbf{r}) + \ldots$$
$$\mu \quad = \mu_0 + \mu_1 + \mu_2 + \ldots \quad \ldots (12)$$

where $n_1(\mathbf{r})$ and μ_1 are of the first order in $\tilde{v}(\mathbf{r})$, etc.

Also

$$v_i(\mathbf{r}) = v_{i0}(\mathbf{r}) + v_{i1}(\mathbf{r}) + v_{i2}(\mathbf{r}) + \ldots \quad \ldots (13)$$

where

$$v_{i0}(\mathbf{r}) = e^2n_0\int d^3\mathbf{r}'/|\mathbf{r}-\mathbf{r}'| = -v_{s0}(\mathbf{r}) \quad \ldots (14)$$

Therefore

$$v(\mathbf{r}) + v_i(\mathbf{r}) = \tilde{v}(\mathbf{r}) + v_{i1}(\mathbf{r}) + v_{i2}(\mathbf{r}) \quad \ldots (15)$$

Eq. (11) becomes

$$n_0 + n_1(\mathbf{r}) + n_2(\mathbf{r}) = 2\int d^3\mathbf{p}\{\exp[\beta((\mathbf{p}^2/2m) + \tilde{v}(\mathbf{r}) + v_{i1}(\mathbf{r}) + v_{i2}(\mathbf{r}) - \mu_0 - \mu_1 - \mu_2)] + 1\}^{-1}/(2\pi\hbar)^3 \quad \ldots (16)$$

Equating powers of the same order, expressions for n_0, $n_1(\mathbf{r})$ and $n_2(\mathbf{r})$ are determined. Evaluation of n_0, $n_1(\mathbf{r})$ and $n_2(\mathbf{r})$ is done in $k_BT \ll \mu_0$ limit. Using the fact that

$$n_0 = \int d^3\mathbf{r} = N \quad \ldots (17)$$

implying, $n_0 = N/V$ and

$$\int n_1(\mathbf{r})d^3\mathbf{r} = 0 = \int n_2(\mathbf{r})d^3\mathbf{r} \quad \ldots (18)$$

expressions for μ_0, μ_1 and μ_2 are obtained. One finds

$$\mu_0 = E_{F_0}[1-(\pi^2/12)(k_BT/E_{F_0})^2] \quad \ldots (19)$$

where $E_{F_0} = h^2(3\pi^2n_0)^{2/3}/2m$ is the Fermi energy at $T = 0$K. Also μ_1 is identically zero because it is related to spatial integrals over $\tilde{v}(\mathbf{r})$ and $v_{i1}(\mathbf{r})$, each of which is zero.

$$n_1(\mathbf{r}) = \sum_{G\neq 0} V_G\exp(i\mathbf{G}.\mathbf{r})\{[-3n_0/(2E_{F_0}\varepsilon_{TF}(\mathbf{G},0))] + T^2n_0\pi^2k_B^2/(8E_{F_0}^3\varepsilon_{TF}^2(\mathbf{G},0))\} \quad \ldots (20)$$

Similarly, one finds

$$\mu_2 = -\sum_{G\neq 0}(|V_G|^2/4E_{F_0})\Big\{\varepsilon_{TF}^{-2}(\mathbf{G},0) - [(2-5\varepsilon_{TF}(\mathbf{G},0)\pi^2k_B^2T^2/(12E_{F_0}^2\varepsilon_{TF}^3(\mathbf{G},0)]\} \quad \ldots (21)$$

where $\varepsilon_{TF}(\mathbf{G},0) = 1 + q_{FT}^2/G^2$ is the TF dielectric function and $q_{FT} = [(6\pi e^2n_0/E_{F_0})^{1/2}]$ is the TF wave vector.

Expanding Eq. (10) up to second order in $\tilde{V}(\mathbf{r})$ gives the expression for free energy, as

$$F = \left(\frac{3NE_{F_0}}{5}\right) - \left(\frac{3N}{4E_{F_0}}\right)\sum_{G\neq 0}\frac{|V_G|^2}{\varepsilon_{TF}(\mathbf{G},0)} - T^2\left\{\left(\frac{N\pi^2k_B^2}{4E_{F_0}}\right)\left[1-\left(\frac{1}{4E_{F_0}^2}\right)\sum_{G\neq 0}\frac{|V_G|^2}{\varepsilon_{TF}^2(\mathbf{G},0)}\right]\right\} \quad \ldots (22)$$

The specific heat at constant volume is

$$C_v = -T(\partial^2 F/\partial T^2)_V$$
$$= \left(\frac{N\pi^2 k_B^2 T}{2E_{F_0}}\right)\left[1-\left(\frac{1}{4E_{F^0}^3}\right)\sum_{G\neq 0}\frac{|V_G|^2}{\varepsilon_{TF}^2(\mathbf{G},0)}\right] \quad \ldots (24)$$

Results and discussion—The first term on the right hand side of Eq. (24) is exactly the specific heat expression for a system of free electrons[6]. The second term is what one intuitively expects on the basis of perturbation to the single electron energy, brought by the screened external potential, the screening being caused by the electron-electron interaction. If we take $V_G \sim 3$eV and $E_{F_0}=7$eV for Cu[6], since $G \sim q_{FT}$ in metals, it is seen that a 1% correction to the specific heat is obtained. If however, $V_G=0$ for all **G**, then of course, the gas behaves like a free-electron gas (Hartree term is absent in the jellium model).

In metals, the magnitude of the reciprocal lattice vector $G \sim q_{TF}$. It is, however, known that the *TF* approximation is good only for $G \ll q_{TF}$, i.e. for a gas of slowly varying density. Thus for usual metals, this result cannot be exact and one has to go beyond the *TF* approximation since the inhomogeneity introduced is large. Nevertheless, this simple approach gives a good order-of-magnitude estimate for the deviation of the results from the completely free-electron approximation. A simple way to improve these results is to replace the *TF* dielectric function $\varepsilon_{TF}(\mathbf{G},0)$ in the expressions for free energy and specific heat, viz. Eqs (23) and (24) by the exact[2] dielectric function $\varepsilon(\mathbf{G},0)$ of the interacting but homogeneous electron gas, which includes exchange and correlation. The results can be improved by taking into account the gradient corrections[5] and exchange-correlation effects simultaneously.

The author thanks Prof. Sudhanshu S Jha for suggesting this problem while he was a participant in the Visiting Student Research Programme at the Tata Institute of Fundamental Research, Bombay. He is also thankful to Shri Ranjan Chaudhury and Shri Tanmoy Bhattacharya for the critical discussions with them.

References

1 Mahan G D, *Many-particle physics* (Plenum Press, New York), 1981, Chap 6.
2 Pines D, *Elementary excitations in solids* (Benjamin, New York), 1963, Chaps 3 & 4.
3 Mermin N D, *Phys Rev A (USA)*, **137** (1965) 1441.
4 Fetter A L & Walecka J D, *Quantum theory of many-particle systems* (McGraw Hill, New York), 1971, Chaps 7 & 8.
5 Hohenberg P & Kohn W, *Phys Rev B (USA)*, **136** (1964) 864.
6 Kittel C, *Introduction to solid state physics* (John Wiley, New York), 3rd Edn, 1968, 208-211.

NOTES

Indian Journal of Pure & Applied Physics
Vol. 21, December 1983, pp. 725-726

Pseudopotential Dependence of Superconducting State Parameters of Al

RENU SHARMA & K S SHARMA
Department of Physics, M S J College, Bharatpur 321 001

Received 3 *March* 1983; *revised received* 17 *August* 1983

Superconducting state parameters, i.e. the electron-phonon coupling strength (λ), the Coulomb pseudopotential (μ^*), transition temperature (T_c), isotope effect exponent (α), and the effective interaction strength (N_0V) have been evaluated for Al by employing six different forms of pseudopotential functions in conjunction with RPA screening. It is observed that Heine-Abarenkov as well as Harrison's potentials provide the best explanation of almost all parameters.

It has now become possible[1] to predict theoretically the transition temperature (T_c) and the isotope effect exponent (α) of superconductors from the Eliasberg gap equations[2] in terms of the interaction strength parameter (λ) and the Coulomb pseudopotential (μ^*). The essential ingredients needed for the evaluation of λ and μ^* are the electron-ion pseudopotential (EIP), dielectric screening function [$\varepsilon(x)$], and the phonon spectra of the metal. (The last term is usually characterized[3] by a single average square frequency [$\langle\omega\rangle$] for the sake of simplicity.)The dependence of the superconducting state parameters (T_c, α, λ, μ^*) on $\varepsilon(x)$ has been studied by Jain and Rajput[4] and Jain and Kachhawa[5], but their dependence on the electron-ion pseudopotential has not been studied till now. Hence we have taken up this study, as it would help us in selecting a potential, which along with a particular screening may provide an explanation for the superconductivity in a metal.

In the present study dealing with Al metal, six different forms of electron-ion pseudopotential have been used in conjunction with the RPA form[6] of dielectric screening. The above 6 pseudopotentials taken from Refs 7-12 are V_{HA}, V_{HR}, V_{AS}, V_{KN}, V_{LR} and V_{SW}. The expressions employed for the evaluation of the parameters are given by[13]:

$$\lambda = \frac{12m^*Z}{M\langle\omega^2\rangle}\int_0^1 dx\, x^3 |V_s(x)|^2 \qquad \ldots (1)$$

$$\mu^* = \frac{\frac{1}{\pi k_F}\int_0^1 \frac{dx}{x\varepsilon(x)}}{1+\frac{1}{\pi k_F}\ln\left(\frac{k_F^2}{100_D}\right)\int_0^1 \frac{dx}{x\varepsilon(x)}} \qquad \ldots (2)$$

$$T_c = \frac{\theta_D}{1.45}\exp\left[\frac{-1.04(1+\lambda)}{\lambda-\mu^*(1+0.62\lambda)}\right] \qquad \ldots (3)$$

and

$$\alpha = \frac{1}{2}\left[1-\left(\mu^*\ln\frac{\theta_D}{1.45T_c}\right)^2\frac{1+0.62\lambda}{1.04(1+\lambda)}\right] \qquad \ldots (4)$$

$V_s(x)$ in Eq. (1) represents the screened pseudopotential form factors at the Fermi surface, and

$$x\langle\omega^2\rangle^{1,2} = \frac{\omega_L+\omega_T}{2} \qquad \ldots (5)$$

ω_L and ω_T being the most representative maximum frequencies of the longitudinal and transverse modes of the phonon spectra, as measured by neutron inelastic scattering experiment. In Eq. (2), $\varepsilon(x)$ represents the dielectic screening function, k_F the Fermi momentum, and θ_D the Debye temperature of the metal under consideration.

Finally we have[14]:

$$N_0V = \frac{\lambda-\mu^*}{\left(1+\frac{10\lambda}{11}\right)} \qquad \ldots (6)$$

for the computation of the effective interaction strength of the superconductor.

The results obtained for the parameters λ, μ^*, T_c, α and N_0V for Al using the six forms of the pseudopotential form factors are presented in Table 1, along with the experimental data. Table 1 also includes the results of other workers[3,13-15] for the sake of comparison. The input data $m^*=1.49$, $\theta_D=420$ K, $\omega_L=14.296\times10^{-4}$ a.u. and $\omega_T=10.364\times10^{-4}$ a.u. are taken from Allen and Cohen[3], whereas $k_F=0.9276$ a.u. for Fermi momentum is taken from Cohen and Heine[16].

It may be observed (Table 1) that the values of T_c obtained from the Heine and Abarenkov (HA) and Harrison potentials are in good agreement with the experimental value of 1.196 (Ref. 13), whereas those obtained with other potentials differ considerably, the linear potential (V_{LR}) predicting the superconductivity to occur at 2.26 K. It may also be observed that the present value of T_c using the HA potential is now in better agreement with the experimental value as compared to the values given by Allen and Cohen[3], and Rajput and Gupta[14] using the point-ion model of Harrison, and Jain and Kachhawa[5] using the Veljkovic and Slavic pseudopotential.

Another important parameter of superconductors is the isotopic effect exponent α. Since experimental data are not available for α, we compare the presently computed values of α with the theoretical values reported by Swihart[17], Garland[18], Morel and Anderson[15] and Jain-Kachhawa[13].

Table 1—Comparison of Values of Superconducting State Parameters Obtained Using Different Potentials

Potential used	λ a.u.	μ^* a.u.	T_c K	α	N_0V
Presently computed values on:					
V_{HA}	0.42	0.12	1.190	0.314	0.203
$V_{HR(x)}$	0.41	0.12	1.020	0.304	0.211
$V_{AS(x)}$	0.34	0.12	0.232	0.182	0.169
$V_{KN(x)}$	0.31	0.12	0.089	0.088	0.148
$V_{LR(x)}$	0.47	0.12	2.260	0.357	0.345
V_{SW}	0.36	0.12	0.337	0.215	0.178
Experimental data			1.196[a]	0.3[b]	0.175[d]
					0.19[e]
				0.37±0.025[c]	
Morel & Anderson values	0.33	0.10	—	0.34	0.14
Allen and Cohen values on:					
V_{HA}	0.53	0.14	3.00		
V_{AS}	0.52	0.14	2.60		
Rajput-Gupta values on:					
V_{PI}[g]	0.43	0.13	0.10	—	0.18
Jain-Kachhawa values on:					
V_{VS}[f]	0.45	0.12	1.75	0.391	—

[a] Exptl[13]
[b] Due to Swihart[17]
[c] Due to Garland[18]
[d] Exptl[19]
[e] BCS parameter[14]
[f] Veljkovic and Salvic pseudopotential, values reported by Jain and Kachhawa[13]
[g] Point-ion model of Harrison, values reported by Rajput and Gupta[14].

It may be observed that the HA, Harrison and linear potentials provide α values which are in good agreement with all these values. The HA and Harrison results are in close agreement with the result of Swihart[17], whereas the linear potential result of $\alpha = 0.357$ is quite close to the values obtained by Garland[18] as well as by Morel and Anderson[15], while the value reported by Jain-Kachhawa[13] is slightly higher. Ashcroft[9], Khanna[10] and Shaw[12] potentials provide us low values of α.

A further test to the pseudopotentials is provided through the calculation of the effective interaction strength N_0V. It may be emphasized that the N_0V value obtained with Shaw potential has the best agreement with the experimental value[19] of 0.175. A comparison of this value with the values obtained with the BCS parameter (0.19), Morel-Anderson potential (0.14) and on the point-ion model by Rajput and Gupta (0.18) suggests that the results obtained from HA, Harrison, Ashcroft, Khanna and Shaw potentials are all satisfactory. Only the linear potential provides a higher value for this parameter.

Thus, it is concluded that the HA potential provides the best explanation of the superconducting state in Al. Harrison potential could also be considered quite satisfactory. The higher results obtained from the linear potential suggest that the potential parameter as determined from the phonon frequency data is not appropriate for the explanation of superconducting state, for which form factors only up to $q = 2k_F$ are required. Thus for making the potential suitable for explaining the superconductivity, the potential parameter should be determined from the low-q form factors or from a low-q-dependent property like liquid metal resistivity. The Shaw potential underestimates the electron-phonon interaction (EPI), and needs improvement, so as to suit the correlation of superconducting state parameters of Al. Same is the case with the Ashcroft and Khanna potentials. Until such an attempt is made, we may recommend the use of HA and Harrison potentials for the calculation of superconducting state parameters and for appropriate representation of DPI in Al.

The authors acknowledge gratefully the departmental facilities extended for this work by the Principal, M S J College, Bharatpur. They are also thankful to Dr C M Kachawa, University of Rajasthan, Jaipur, for his keen interest in the work and for the encouragement provided by him from time to time. One of the authors (R S) thanks the University Grants Commission, New Delhi, for providing her financial assistance.

References

1 Mc Millan W L, *Phys Rev (USA)*, **167** (1968) 331.
2 Eliasberg G M, *Sov Phys JETP (USA)*, **11** (1960) 696; **12** (1961) 1000.
3 Allen P B & Cohen M L, *Phys Rev (USA)*, **187** (1969) 525.
4 Jain L K & Rajput J S, *Indian J Pure & Appl Phys*, **14** (1976) 533.
5 Jain S C & Kachhawa C M, *Indian J Pure & Appl Phys*, **18** (1980) 489.
6 Gallmann M & Brueckner K A, *Phys Rev (USA)*, **106** (1958) 364.
7 Heine V & Abarenkov I, *Philos Mag (GB)*, **9** (1961) 451.
8 Harrison W A, *Pseudopotentials in the theory of metals* (Benjamin, New York), 1966, 299.
9 Ashcroft N W, *Phys Lett (Netherlands)*, **23** (1966) 48.
10 Khanna K N, *Indian J Phys A*, **52** (1978) 552.
11 Sharma K S & Kachhawa C M, *Indian J Pure & Appl Phys*, **18** (1980) 536.
12 Shaw R W, *Phys Rev (USA)*, **174** (1968) 769.
13 Jain S C & Kachhawa C M, *Phys Status Solidi b (Germany)*, **101** (1980) 619.
14 Rajput J S & Gupta A K, *Phys Rev (USA)*, **181** (1969) 743.
15 Morel P & Anderson P W, *Phys Rev (USA)*, **126** (1962) 1263.
16 Cohen M L & Heine V, in *Solid state physics* (Academic Press, New York), **24** (1970) 196.
17 Swihart J C, *IBM J Res & Dev (USA)*, **6** (1962) 14.
18 Garland G W (Jr), *Phys Rev (USA)*, **153** (1967) 460.
19 Morel P, *J Phys & Chem Solids (GB)*, **10** (1959) 217.

Indian Journal of Pure & Applied Physics
Vol. 21, December 1983, pp. 727-728

A Note on the Spherically Averaged Effective-Mass

K NAVANEETHAKRISHNAN
School of Physics, Madurai Kamaraj University, Madurai 625 021
and
T THENAPPAN
Physics Department, Alagappa College, Karaikudi 623 003

Received 12 *January* 1982; *accepted* 3 *October* 1983

A geometrical representation of different effective-masses (m^*) is given. It is shown that only three effective-masses are possible in approximating the mass ellipsoid to a sphere. While two of our results for m^* are the well known optical and density averages, the third is a new result which has not been used so far in the study of any physical property of a many-valley semiconductor. The validity of using any other m^* in the study of impurity states in semiconductors is critically examined.

Many semiconductors, including Si and Ge, exhibit a multivalley structure in the conduction band[1]. As a consequence, the constant energy surfaces near the conduction band minima are ellipsoids of revolution. The effective-mass tensor, in the body-fixed frame of reference, is given by two transverse masses (m_{t_1} and m_{t_2}) and a longitudinal mass (m_l). In many semiconductors (e.g. Si and Ge), the two transverse masses are equal. The degree of anisotropy (γ) is given by $\gamma = m_t/m_l$.

In the computation of any physical property of a many-valley semiconductor, one normally makes a spherical band approximation (SBA) in which a single mass (m^*) is used in place of m_t and m_l. The m^* value is usually taken as a suitable average of m_t and m_l[2,3]. In the study of impurity states in Si and Ge, to reduce the labour of evaluating several numerical integrals, several authors have preferred using the SBA[4-7]. These authors, following the suggestion by Kohn[8], have used an m^* value obtained by equating the hydrogenic energy expression, for the ground state of the donor, to the accurately evaluated ground state energy of Faulkner[9] in the one-valley model (we call this m^* value as the energy average). Many of these authors have used the same m^* value for several excited states also. However, if the energies are equated for the excited states, one gets different effective-masses for different states[6]. Shindo and Nara[7] have used an m^* obtained from the experimental ionization energy of the P donor, in their many-valley effective-mass theory (MVEMT) for Si. Thus one has different sets of m^* values for different impurities in a particular semiconductor, since the donor spectra, especially the ground states are strongly impurity-dependent[8]. Recently, some authors[10] have tried to handle the anisotropic effective-mass hamiltonian without making the SBA. In a MVEMT, even for the donor ground state in Si $\{1s(A_1)$ symmetry$\}$ the longitudinal and transverse intervalley terms have to be evaluated either numerically or approximately. In addition, several papers have recently appeared on the proper use of the intervalley terms in the kinetic and potential energy terms[7,11,12]. In these works, the Bloch functions of the conduction band minima appear explicitly, making the calculations more involved numerically. Hence the SBA, we hope, will continue to exist for some more time. In the present work, we demonstrate that there are three ways of choosing m^* as averages of m_t and m_l. The energy average is artificial, and, if used, will lead to complications as explained above. Our m^* values will be independent of the donors' state and the nature of the impurity, as these are based on a geometrical representation of the mass ellipsoid of the host semiconductor.

The components of the effective-mass tensor are defined by $(1/m)_{ij} = \partial^2 E/(\partial k_i \partial k_j)$. A transformation from laboratory-fixed coordinate system to the body coordinate system (usually an orthogonal transformation) brings the above ellipsoid to a diagonal form as:

$$M_{DL} = \begin{pmatrix} 1/m_t & 0 & 0 \\ 0 & 1/m_t & 0 \\ 0 & 0 & 1/m_l \end{pmatrix} \quad \ldots (1)$$

Thus the quadratic surface in the body fixed frame of reference is given by

$$\frac{x^2}{(\varepsilon_0/m_t)^2} + \frac{y^2}{(\varepsilon_0/m_t)^2} + \frac{z^2}{(\varepsilon_0/m_l)^2} = 1 \quad \ldots (2)$$

with (ε_0/m_t) and (ε_0/m_l) as the semimajor and semiminor axes respectively. ε_0 is the static dielectric constant of the host semiconductor. The SBA leads Eq. (2) to a form

$$x\frac{x^{1^2}}{(\varepsilon_0/m^*)^2} + \frac{y^{1^2}}{(\varepsilon_0/m^*)^2} + \frac{z^{1^2}}{(\varepsilon_0/m^*)^2} = 1 \quad \ldots (3)$$

which is the equation to a sphere in the normal form. The two sets of coordinates are related by $x^1 = (m_t/m^*)x$, $y^1 = (m_t/m^*)y$ and $z^1 = (m_l/m^*)z$. The matrix associated with Eq. (3) is

$$M_{SPL} = \begin{pmatrix} 1/m^* & 0 & 0 \\ 0 & 1/m^* & 0 \\ 0 & 0 & 1/m^* \end{pmatrix} \quad \ldots (4)$$

It can be easily seen that $M_{SPL}=T^{-1}M_{SDL}$, where T is a diagonal matrix that relates (x^1, y^1, z^1) to (x, y, z). Physically, M_{SPL} can be thought of as obtainable from the original mass ellipsoid M, by first performing a rotation so that $M\rightarrow M_{SDL}$, and then a transformation that either elongates and/or contracts the axes of the ellipsoid to obtain M_{SPL}. Since M_{SPL} and M_{SDL} are not related by a similarity transformation, the norm of a vector (the position vector of a point on the ellipsoid with reference to an arbitrary origin) is not preserved. Hence, there are different ways of mapping an ellipsoid into a sphere.

The characteristic equation of a 3×3 matrix is of the form $\lambda^3-a\lambda^2+b\lambda+c=0$, where a, b and c are constants. Writing down the characteristic equations of M_{SDL} and M_{SPL} and equating the coefficients of different powers of λ, we get

$$(1/m^*)=(1/3)(2/m_t+1/m_l) \quad \text{(coeff. of } \lambda^2) \qquad \ldots (5)$$

$$(1/m^*)=\left\{\frac{1}{3}\left(\frac{1}{m_t^2}+\frac{1}{m_t m_l}\right)\right\}^{1/2} \quad \text{(coeff. of } \lambda) \qquad \ldots (6)$$

$$\text{and} \quad m^*=(m_t^2 m_l)^{1/3} \quad \text{(coeff. of } \lambda^0) \qquad \ldots (7)$$

Eqs. (5) and(7) can be recognized as the optical and density averages respectively. Eq. (6) is a new result which has not been used previously. It is interesting to note that Eq. (5) is obtained by equating the 'lengths' (sum of major and minor axes equal to 3 times the radius of the sphere), Eq. (6) is obtained by equating the 'surface areas' and Eq. (7) follows from equating the volumes. For Si, as an example, $\gamma=0.2079$, m^* (optical average) $=0.2588$, m^* (areal average) $=0.28$, m^* (density average) $=0.3216$ and m^* (energy average) $=0.2982$ (Ref. 8).

The optical average value of m^* has been used by Schechter[2] and Tefft *et al.*[13] This value is a little lower and gives a poor value for the donor ionization energy, which differs from the value of Faulkner[9] by about 14% for Si. Both the areal and density averages differ from the energy average value of m^* by about 7%. The density average is also obtainable from equating the probability densities ($|\psi(0)|^2$) of finding the donor electron at the donor site in the SBA and in the spheroidal model[8] for the ground state. In the one-valley model, except for the $l=0$ states ($1s$, $2s$ etc.) $\psi(\bar{\gamma})$ vanishes at $\bar{\gamma}=0$. In the MVEMT also, except the $1s(A_1)$, $2s(A_1)$ etc. states, the wavefunctions vanish at the donor site for $1s(E)$, $1s(T_2)$ and all other excited states. Hence the use of the density-averaged effective-mass is more justified.

References

1 Kittel C, *Introduction to solid state physics* (University Edition) (Wiley Eastern, New Delhi), 5th Edn, 1979, 205.

2 Schetchter D, *Surface Sci (Netherlands)*, **11** (1968) 352.

3 Kireev P S, *Semiconductor physics* (Mir Publishers, Moscow) 1975, 180.

4 Ning T H & Sah C T, *Phys Rev B (USA)*, **4** (1971) 3468.

5 Pantelides S T & Sah C T, *Phys Rev B (USA)*, **10** (1974) 621.

6 Palaniyandi E & Balasubramanian S, *Indian J Pure & Appl Phys*, **14** (1976) 17.

7 Shindo K & Nara H, *J Phys Soc Jpn (Japan)*, **40** (1976) 1640.

8 Kohn W, *Solid state physics*, Vol 5, edited by F Seitz and D Turnbull (Academic Press, New York), 1957, 257.

9 Faulkner R A, *Phys Rev (USA)*, **184** (1969) 713.

10 Sarkar A Q, *J Phys C (GB)*, **10** (1979) 215.

11 Resca L & Resta R, *Solid State Commun (GB)*, **29** (1979) 275.

12 Altarelli M, *Phys Rev Lett (USA)*, **46** (1981) 205.

13 Tefft N E, Bell R T & Romero H V, *Phys Rev (USA)*, **177** (1969) 1194.

Indian Journal of Pure & Applied Physics
Vol. 21, December 1983, pp. 729-730

On Low Frequency Dielectric Behaviour of GaP under Illumination

V K FARKYA & N L PORWAL
Physics Department, Jabalpur University, Jabalpur 482001

Received 26 *August* 1982; *revised received* 3 *May* 1983

The variation, with frequency, of dielectric loss of positively doped GaP, illuminated with different mercury wavelengths, has been investigated in the low frequency region 100 Hz-10 kHz and at a temperature of 300 K. The real and imaginary components of the complex permittivity have been explained on the basis of Debye's dispersion relations.

Gallium phosphide (GaP) is a compound semiconductor belonging to IIIrd-Vth group and has got much importance on account of its specific behaviour on illumination and uses in electro-optical devices. In the present investigation, a GaP wafer [$A=7$ sq.mm, $d=0.36$ mm, $\rho=50$ ohm.cm, $n=10^{17}$/cc] obtained from its single crystal was used. This thin wafer of GaP was sandwiched between two conducting glass plates prepared by a special technique[1], and forms the imperfect capacitor. This was connected to the fourth arm of a Schering bridge[2] (Systronics type 921). The ohmic contacts of the sample with the glass electrodes were ensured before the start of the experiment. The sample was placed in dark for sufficient period and the capacitance and the loss factor were measured by varying the frequency in regular small steps in the range 100 Hz-10 kHz at a temperature of 300 K. The sample was then illuminated by light of wavelength $\lambda=545$ nm, using calibrated filter and a 100 W mercury vapour lamp and the capacitance and loss factor were measured in the frequency range 100 Hz-10 kHz. The observations were repeated by illuminating the sample with light of wavelengths 405 and 365 nm separately. The values of ε' and ε'' for GaP sample were computed as described in an earlier work on compound semiconductors[3]. The curves for $C_0\varepsilon'$ and $C_0\varepsilon''$ versus frequency for different mercury wavelengths are shown in Figs 1 & 2 respectively. The change in real and imaginary components of the complex permittivity of the sample may be attributed to the increase in dipoles on illumination as compared to dark, as done by Uchida[4] in the case of ZnS (Cu:Cl). This change may also be explained as due to the excitation of the crystal "defects" on account of doping. But the defect concentration may be of the order of 1 in 10^{18} atoms and hence very small to permit large variations of ε'[5,6].

In general, the curves (Figs 1 & 2) follow Debye's dispersion relations, given by[7]

$$\varepsilon'-\varepsilon'(\infty)=\frac{\varepsilon'(0)-\varepsilon'(\infty)}{1+\omega^2\tau^2}$$

and

$$\varepsilon''=\frac{[\varepsilon'(0)-\varepsilon'(\infty)]\omega\tau}{1+(\omega\tau)^2}$$

where $\varepsilon'(0)$ and $\varepsilon'(\infty)$ are the static and high frequency values of the dielectric constant, τ the relaxation time and ω the angular frequency ($=2\pi f$). It is also observed that with the illumination of the sample with

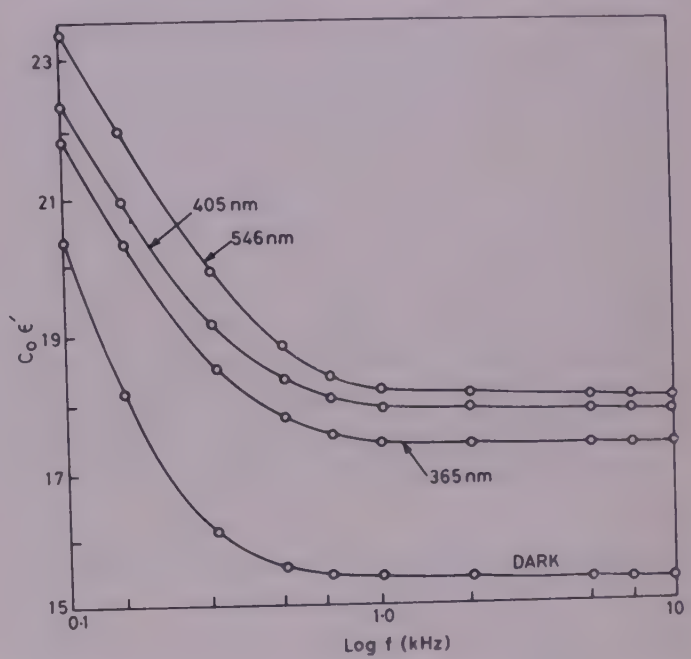

Fig. 1—Variation of $C_0\varepsilon'$ with frequency for dark and illumination

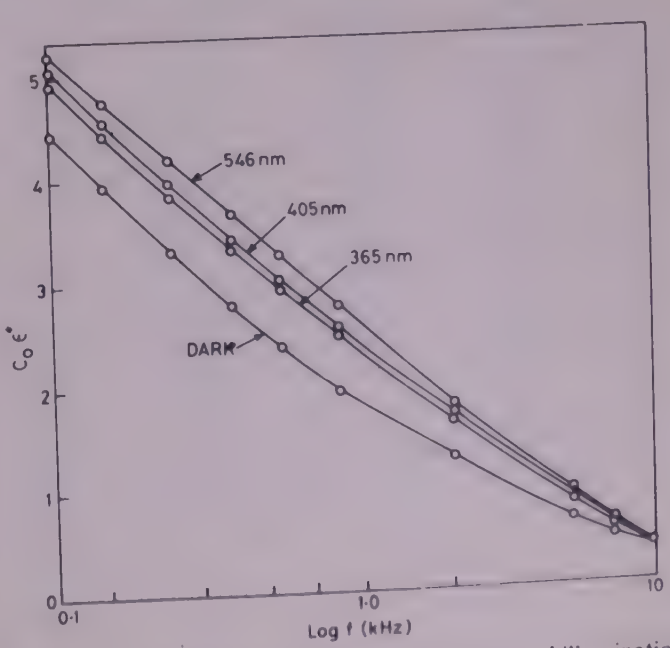

Fig. 2—Variation of $C_0\varepsilon''$ with frequency for dark and illumination

longer wavelengths, the values of both $C_0\varepsilon''$ and $C_0\varepsilon''$ are higher on the left, but have a little difference on the extreme right as per provisions of the theory.

Thus, it is concluded that the dielectric properties of GaP follow Debye's dispersion relations in the low frequency region on illumination with light of different wavelengths.

We are grateful to Prof T S Murty, Head of the Department of Physics (presently, Director, Council of Science and Technology, Madhya Pradesh), for providing facilities for carrying out this work.

References

1 Farkya V K, *Dielectric investigation of plasma*, Ph.D. thesis, University of Indore, Indore, 1972.

2 Owen D, *Alternating current measurements* (Methuen & Co., London), 1953, 51.

3 Farkya V K, Bandopadhyaya T K & Das Gupta S M, *Indian J Pure & Appl Phys*, **12** (1974) 465.

4 Uchida I, *Jpn J Appl Phys (Japan)*, **1** (1962) 71.

5 Bandopadhyaya T K, *Indian J Pure & Appl Phys*, **6** (1966) 289.

6 Roux J, *L' Effect Photodielectrique dans Sulphur et oxide de zinc*, D. Phil thesis, University of Paris, Paris, 1956.

7 Dekker A J, *Solid state physics* (Macmillan & Co., London), 1970, 151.

Indian Journal of Pure & Applied Physics
Vol. 21, December 1983, pp. 731-732

On the Application of Perturbation Theory for the Calculation of Molecular Constants from Isotopic Frequency Shifts

N SUBRAMANIAN & R SRINIVASAMOORTHY

Department of Physics, St. Joseph's College (Autonomous), Tiruchirapalli 620002

and

R JAGANNATHAN

Matscience, The Institute of Mathematical Sciences, Madras 600113

Received 5 *July* 1982; *accepted* 10 *October* 1983

The first-order perturbation theory is used to obtain directly the L-matrix in the 2×2 case from data on isotopic frequency shifts. Out of the two resulting solutions for the L-matrix one always has that $L_{12}=0$ is in agreement with the principle of the L approximation method. The improved approximate L-matrix so obtained leads to good prediction of the molecular constants. The case of some symmetric nonlinear XY_2 molecules is considered in detail to demonstrate the application of the theory.

Muller and his coworkers have established that the first-order perturbation theory is useful in predicting the isotopic frequency shifts due to small mass changes. They have also pointed out that a direct determination of L_0 from the observed isotopic frequency shifts leads to poor estimates of the force constants (Refs 1 and 2). We are concerned mainly with this problem here.

Method and calculations from the fundamental relations

$$GFL = L\lambda \qquad \ldots (1)$$

and $$G = L\tilde{L} \qquad \ldots (2)$$

we get, using the first-order perturbation theory and assumption $\Delta F=0$ under isotopic substitution,

$$\tilde{L}_0^{-1}\Delta G L_0^{-1} = \begin{bmatrix} \Delta\lambda_1/\lambda_1^0 & x \\ x & \Delta\lambda_2/\lambda_2^0 \end{bmatrix} \qquad \ldots (3)$$

(Here the subscript 0 stands for the parent molecule.) Without loss of generality, we take

$$L_0^{-1} = \Gamma L_{0a}^{-1} = \begin{pmatrix} \cos\theta & -\sin\theta \\ \sin\theta & \cos\theta \end{pmatrix}(L_{0a}^{-1}) \qquad \ldots (4)$$

with

$$L_{0a}^{-1} = \begin{bmatrix} 1/\sqrt{G_{11}} & 0 \\ -G_{12}/\sqrt{G_{11}\det G} & \sqrt{G_{11}/\det G} \end{bmatrix} \qquad \ldots (5)$$

such that

$$\tilde{L}_0^{-1}L_0^{-1} = \tilde{L}_{0a}^{-1}L_{0a}^{-1} = G^{-1} \qquad \ldots (6)$$

Taking $L_{0a}^{-1}\Delta G L_{0a}^{-1} = Z$ we will get

$$\begin{pmatrix} \cos\theta & -\sin\theta \\ \sin\theta & \cos\theta \end{pmatrix}\begin{pmatrix} Z_{11} & Z_{12} \\ Z_{12} & Z_{22} \end{pmatrix}\begin{pmatrix} \cos\theta & \sin\theta \\ -\sin\theta & \cos\theta \end{pmatrix}$$

$$= \begin{pmatrix} \Delta\lambda_1/\lambda_1 & x \\ x & \Delta\lambda_2/\lambda_2 \end{pmatrix} = \begin{pmatrix} \delta_1 & x \\ x & \delta_2 \end{pmatrix} \qquad \ldots (7)$$

From the above relations we get

$$(Z_{22}-\delta_1)\tan^2\theta - 2Z_{12}\tan\theta + (Z_{11}-\delta_1) = 0 \qquad \ldots (8a)$$

$$(\delta_2 - Z_{11})\tan^2\theta - 2Z_{12}\tan\theta + (\delta_2 - Z_{22}) = 0 \qquad \ldots (8b)$$

We have the sum rule $$Z_{11}+Z_{22} = \delta_1+\delta_2 \qquad \ldots (9)$$

Combining Eqs (8a) and (8b) we get two values of θ, θ_L and θ_h with $\theta_L<\theta_h$. The apparent success of L-approximation method ($\theta=0$) makes us to choose θ_L as correct values of θ. We write

$$L_j = L_{0a}\begin{pmatrix} \cos\theta_L & \sin\theta_L \\ -\sin\theta_L & \cos\theta_L \end{pmatrix} \qquad \ldots (10)$$

With such improved approximate L_f, we have calculated the force constants and other molecular constants. The force constants are reported in Table 1 and compared with already available values (given in brackets). The Coriolis coupling constants (ζ) are reported in Table 2 and the centrifugal distortion

Table 1—Force Constants (in mdyn/Å) for Nonlinear Symmetrical XY_2 Molecules

Molecule	F_{11}	F_{12}	F_{22}	Ref.
H_2O	8.3550 (8.354 ± 0.005)	0.3557 (0.334 ±0.049)	0.7631 (0.760 ±0.004)	8
D_2O	8.3572 (8.355)	0.3501 (0.345)	0.7623 (0.761)	8
H_2S	4.2731 (4.2731 ±0.0008)	0.0522 (0.064 ±0.01)	0.4248 (0.42 ±0.0002)	4
SO_2	10.2633 (10.34 ±0.2)	0.4946 (0.25 ±0.21)	0.7939 (0.816 ±0.007)	5
NO_2	12.9799 (12.9746)	0.5605 (0.5529)	1.1240 (1.1252)	6
ClO_2	7.0978 (7.1508)	0.5557 (0.2557)	0.6726 (0.6324)	6

Table 2—ζ-Values of Nonlinear Symmetrical XY_2 Molecules Calculated Using Isotopic Frequencies

Molecule	Present work	Ref & experimental value
$^{16}O_3$	−0.58	−0.60 (Ref. 7)
$^{32}S^{16}O_2$	−0.28	−0.31 (Ref. 3)
$^{35}Cl^{16}O_2$	−0.22	−0.26 (Ref. 9)

Table 3 — Centrifugal Distortion Constants (in MHz) of Nonlinear Symmetrical XY_2 Molecules

Molecule	$-\tau_{xxxx}$	$-\tau_{yyyy}$	$+\tau_{xxyy}$	$-\tau_{xyxy}$	Ref.
H_2O	2601(2801)	254.8(360)	544.5(608.55)	117.2(150.53)	10
H_2S	230.1	145.1	—	30.0	4
	(247.56 ± 0.16)	(151.25 ± 0.16)		(27.2)	
D_2S	64.92	36.34	—	7.95	4
	(67.963 ± 0.012)	(36.647 ± 0.012)		(7.9)	
$^{14}NO_2$	289.75(299.4)	0.0431(0.0414)	1.8562(1.843)	0.246(0.2453)	11
$^{15}NO_2$	260.70(273.4)	0.0437(0.0414)	1.774(1.761)	0.2447(0.2445)	11
$^{16}O_3$	25.44(23.92)	0.0681(0.0712)	0.4933(0.52046)	0.2729(0.25773)	12
$^{18}O^{16}O_2$	20.99(20.92)	0.0689(0.0715)	0.4823(0.4705)	0.2681(0.2713)	12
$^{16}O^{18}O_2$	22.73(23.34)	0.0554(0.05622)	—	0.2194	12
$^{32}SO_2$	9.8344(9.8098)	0.0370(0.0397)	0.4850(0.4117)	0.0558(0.0532)	6

constants in Table 3. The experimentally observed values are also noted in brackets for comparison. The agreement between our values and literature values is very satisfactory.

Conclusion—Thus in conclusion it may be pointed out that the first-order perturbation theory as detailed above can be used reliably to evaluate the molecular constants of molecules involving the 2×2 matrix problem from data on isotopic frequency shifts. This looks contrary to what Muller[1] has observed that this method, "leads to poor estimates of force constants". This may be because of taking the off diagonal elements in Eq. (3) as zeroes in their methods. The extension of this method to 3×3 case is under progress.

We thank Rev Fr G A Savari Raj, P.G. Professor and Head of the Dept of Physics, St. Joseph's College (Autonomous) for his encouragement and the authorities of St. Joseph's College for making the facilities available to us.

References

1 Muller A, Schmidt K H & Mohan N, *J Chem Phys (USA)*, **57** (1972) 1752.
2 Chalmers A A & Mechean D C, *Spectrochim Acta (GB)*, **22** (1966) 251.
3 Nakanega T, Kondo S & Saiki S, *J Mol Spectrosc (USA)*, **81** (1980) 413.
4 Cook R L, DeLucia F C & Helminger P, *J Mol Struct (Netherlands)*, **28** (1975) 237.
5 Saito S, *J Mol Spectrosc (USA)*, **30** (1969) 14.
6 Chinnappan V A, *Isotopic invariants of some polyatomic molecules*, Ph D thesis, Madras University, 1981.
7 Barbe A, Secrown C & Jouve P, *J Mol Spectrosc (USA)*, **49** (1974) 171.
8 Cook R L, DeLucia F C & Helminger P, *J Mol Spectrosc (USA)*, **53** (1974) 62.
9 Brand J C D, Redding R W & Richardson A W, *J Mol Spectrosc (USA)*, **34** (1970) 399.
10 Hall R T & Dowling J M, *J Chem Phys (USA)*, **47** (1967) 2454.
11 Bird G R, Baird J C, Jache A W, *et al.*, *J Chem Phys (USA)*, **40** (1964) 3378.
12 Depannemeecker J C & Bellet J, *J Mol Spectrosc (USA)*, **66** (1977) 106.

Indian Journal of Pure & Applied Physics
Vol. 21, December 1983, p. 733

e^--He Elastic Scattering in the Two-Potential HHOB Approximation

C N CHANDRA PRABHA & H S DESAI
Department of Physics, M S University, Baroda 390 002

Received 18 *October* 1982; *revised received* 17 *May* 1983

The two-potential formulation in the high energy higher order Born approximation (HHOB) is applied to the case of elastic scattering of electrons by helium atom, at intermediate energies. The calculated scattering parameters are found to be in good agreement with other theoretical and experimental data.

The two-potential formulation in HHOB[1] is developed along the same lines as the two-potential eikonal approximation[2]. The basic idea in this formulation is to pull out from the interaction potential V an arbitrary potential V_1 such that the rest of the interaction $V_0 = V - V_1$ satisfies semiclassical conditions. For the scattering of an electron from the helium atom, the interaction potential is given by

$$V(r_0, r_1, r_2) = \frac{-2}{r_0} + \sum_{j=1}^{2} \frac{1}{|r_0 - r_j|}$$

where r_0, r_1, and r_2 are the position vectors of the incident and target electrons. For V_1, we have chosen the static potential V_{st} given by Bonham and Strand[3]. Hence $V_0 = V - V_{st}$ is slowly varying and $|V_0| \ll E$ for all r_0.

Now the contribution of V_0 to the scattering amplitude can be obtained in the HHOB approximation and that of V_{st} by partial wave analysis (PWA). The transition amplitude from the target state $|i>$ to be state $|f>$ is given as

$$F_{fi}(\theta) = F_{HHOB} + F_{PW}$$

where $F_{HHOB} = f^{(1)}_{i \to f} + f^{(2)}_{i \to f} + \ldots$

as given by Yates for the potential $V_0 = V - V_{st}$ and F_{PW} is the scattering amplitude in the PWA.

For the ground state of helium, we have used the Hartree-Fock orbitals φ_{1s} of Byron and Joachain[4]. The first and second Born amplitudes in HHOB are obtained in the closed form[1,5]. Similarly F_{HHOB} is calculated for the potential V_0. The procedure for the summation of the partial waves is similar to that given by Jhanwar *et al.*[6] Knowing the scattering amplitudes, the differential cross-section (DCS) can be obtained through $O(1/k_i^2)$.

The total cross-section is calculated using the formula

$$\sigma^{\text{total}} = \frac{4\pi}{k_i} \operatorname{Im} F(\theta = 0)$$

The DCS curve obtained in the present analysis at 200 eV is shown in Fig. 1. As expected, the present

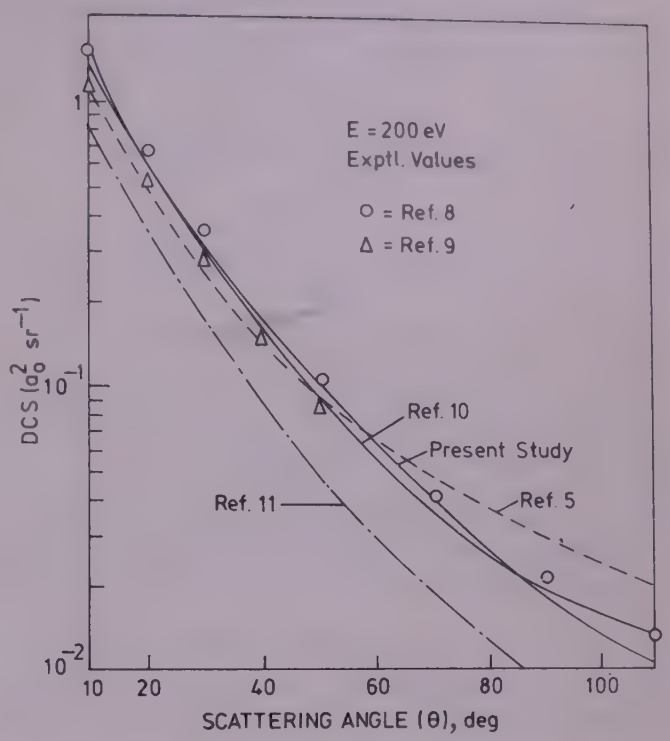

Fig. 1—DCS for electron-helium elastic scattering at 200 eV

Table 1—Comparison of the Total Cross-sections (in units of a_0^2) for e^--He Scattering from Different Sources

Energy eV	Present study	Ref. 5 (HHOB)	Ref. 10		
			Winters *et al.*	Byron & Joachain	EBS
200	3.58	2.93	3.55	3.37	2.92
400	2.08	1.69	2.00	1.86	1.71

results agree well with other available data: both experimental[7-9] and theoretical[5,10,11]. It may be noted that the two-potential formulation in HHOB approximation yields better results than the simple HHOB approximation, especially at large angles. The total cross-section (TCS) results shown in Table 1 are also encouraging.

References

1 Yates A C, *Phys Rev A (USA)*, **19** (1979) 1550.
2 Ishihara T & Chen J C Y, *Phys Rev A (USA)*, **12** (1975) 370.
3 Bonham R A & Strand T G, *J Chem Phys (USA)*, **39** (1963) 3300.
4 Byron F W (Jr) & Joachain C J, *Phys Rev (USA)*, **146** (1966) 1.
5 Rao N S & Desai H S, *Pramana (India)*, **17** (1981) 309.
6 Jhanwar B L, Khare S P & Kumar A, *J Phys B (GB)*, **11** (1978) 887.
7 Bromberg J P, *J Chem Phys (USA)*, **61** (1974) 963.
8 Jansen R H J, Deheer F J, Luyken H J *et al.*, *J Phys B (GB)*, **9** (1976) 185.
9 Register D F, Trajmar S & Srivastava S K, *Phys Rev A (USA)*, **21** (1980) 1134.
10 Byron F W (Jr) & Joachain C J, *J Phys B (GB)*, **10** (1977) 207
11 Singh S N & Tripathi A N, *Phys Rev A (USA)*, **21** (1980) 105.

Indian Journal of Pure & Applied Physics
Vol. 21, December 1983, pp. 734-735

Potential Energy Function for Diatomic Molecules

S V BIRAJDAR
S B College of Science, Aurangabad 431 001
and
S H BEHERE
Department of Physics, Marathwada University, Aurangabad 431 004

Received 16 *August* 1982; *revised received* 16 *September* 1983

The potential function for diatomic molecules suggested by Raghuwanshi and Sharma [*Indian J Pure & Appl Phys*, **16** (1978) 1071] is investigated further. The expressions for α_e and $\omega_e x_e$ are derived in terms of a parameter defined as $\Delta = a^2 r_e^2 + 1$. The $\omega_e x_e$ values for a few diatomic molecules are calculated using this function and are compared with experimental values. The results indicate that the potential is a good approximation for diatomic molecules.

The potential function suggested by Raghuwanshi and Sharma[1] is a combination of Morse[2] and Kratzer[3] potential functions, hereafter we will refer to it merely as MK potential and is of the form

$$U(r) = D_e[1-\exp(-a\rho)]^2 + \frac{D_e\rho^2}{r^2} - 2D_e \qquad \ldots (1)$$

At $r = r_e$, $U(r_e)$ is $-2D_e$ in the above function. In order to make $U(r_e) = 0$, the last term can be omitted without affecting the derivations of α_e and $\omega_e x_e$. This function satisfies all the criteria required for a suitable potential function. The derivatives are

$$U^{II}(r_e) = 2D_e\left(a^2 + \frac{1}{r_e^2}\right)$$

$$U^{III}(r_e) = -6D_e\left(a^3 + \frac{2}{r_e^3}\right)$$

$$U^{IV}(r_e) = 2D_e\left(7a^4 + \frac{36}{r_e^4}\right)$$

Following Varshini[4],

$$\alpha_e = -\left[\frac{Xr_e}{3} + 1\right]\frac{6B_e^2}{\omega_e}$$

where $X = \dfrac{U^{III}(r_e)}{U^{II}(r_e)}$

and anharmonicity constant

$$\omega_e x_e = \left[\frac{5}{3}X^2 - Y\right]\frac{W}{\mu_A} \quad \text{where} \quad Y = \frac{U^{IV}(r_e)}{U^{II}(r_e)} \qquad \ldots (2)$$

and $W = 2.1078 \times 10^{16}$.

The values of X and Y are

$$X = \frac{-3}{r_e}\left(\frac{a^3r_e^3+2}{a^2r_e^2+1}\right) \quad \text{and} \quad Y = \frac{7a^4r_e^4+36}{(a^2r_e^2+1)r_e^2}$$

The second derivative at $r = r_e$ must be equal to a force constant k_e which gives $\Delta = a^2r_e^2 + 1$ or $ar_e = (\Delta-1)^{\frac{1}{2}}$; $a^2r_e^2 = (\Delta - 1)$ etc.

By putting the values of X^2 and Y in Eq. (2), we get

$$\omega_e x_e = \left\{\frac{15(a^3r_e^3+2)^2}{(a^2r_e^2+1)^2 r_e^2} - \frac{7a^4r_e^4+36}{(a^2r_e^2+1)r_e^2}\right\}\frac{W}{\mu_A}$$

Substituting x for ar_e for simplicity, we get

$$\omega_e x_e = \left\{\frac{8x^6 - 7x^4 + 60x^3 - 36x^2 + 24}{(x^2+1)^2}\right\}\frac{W}{\mu_A r_e^2}$$

Using $\Delta = x^2 + 1$, we get

$$\omega_e x_e = \{8\Delta^3 - 31\Delta^2 + 2\Delta + 45 + 60(\Delta-1)^{\frac{3}{2}}\}\frac{W}{\mu_A r_e^2 \Delta^2}$$

or

$$\omega_e x_e = \left\{8\Delta - 31 + \frac{2}{\Delta} + \frac{45}{\Delta^2} + \frac{60(\Delta-1)^{3/2}}{\Delta^2}\right\}\frac{W}{\mu_A r_e^2} \qquad \ldots (3)$$

The values of $\omega_e x_e$ calculated using Eq. (3) are presented in Table 1. For this purpose the constants were taken from the bibliography of Huber and Herzberg[5]. The average % error in $\omega_e x_e$ of those randomly selected molecules, using the present

Table 1—Anharmonicity Constants

Molecule*	$\omega_e x_e$ (Exptl)	$\omega_e x_e$ (Calc.)	% error
Br_2	1.0774	1.458	+35.33
CH	63.0	53.28	−15.42
Cl_2	2.67	3.24	+21.30
CO	13.2883	10.2122	−23.15
CdH	46.3	62.1	+34.07
H_2	121.336	95.49	−21.30
HBr	45.21	43.42	−3.97
HCl	52.82	46.24	−12.45
HF	89.88	81.23	−31.87
HI	39.64	41.61	+4.96
HgH^+	40.9	31.82	−22.20
I_2	0.614	0.825	+34.44
ICl	1.501	1.847	+23.04
Li_2	2.610	2.760	+5.74
K_2	0.2829	0.4100	+44.93
N_2	14.324	14.095	−1.59
NO	14.075	13.978	−0.69
Na_2	0.7254	0.8478	+16.87
OH	84.88	71.09	−16.25
O_2	11.98	12.26	+2.3
P_2	2.835	2.165	−28.81
SO	5.63	6.26	−3.91
ZnH	55.14	71.28	+29.26
AuAl	1.163	0.818	−28.78
GeSe	1.36	0.858	−36.89
He_2^+	35.3	27.52	−22.20
Si_2	2.02	1.88	−6.93

*Ground states

potential function, is ± 20.69 which is much less compared to that from the Morse function, viz. $\pm 26.82\%$. This clearly indicates that the MK potential is a good approximation to a potential of diatomic molecules.

The authors are thankful to Dr P L Sardesai for helpful discussions.

References

1 Raghuwanshi S S & Sharma L K, *Indian J Pure & Appl Phys*, **16** (1978) 1071.
2 Morse P M, *Phys Rev (USA)*, **34** (1929) 57.
3 Kratzer A, *Z Phys (Germany)*, **3** (1920) 289.
4 Varshini Y P, *Rev Mod Phys (USA)*, **29** (1957) 664.
5 Huber K P & Herzberg G, *Constants of diatomic molecules (Van Nostrand & Reinhold Co, New York)*, 1979.

Indian Journal of Pure & Applied Physics
Vol. 21, December 1983, pp. 736-737

Comparative Study of Spectral & Magnetic Characteristics of Some Mn(II) & Co(II) Complexes

R K JAIN & SUDHINDRA N MISRA
Department of Chemistry, University of Jodhpur, Jodhpur
and
G K JOSHI
Department of Chemistry, Government Post Graduate College, Nagaur (Rajasthan) 341 001

Received 22 *October* 1982; *accepted* 17 *May* 1983

Synthesis of Mn(II) and Co(II) complexes having the molecular formula $[M(L)_2(H_2O)_2]X$, where L stands for ethylenediamine or propylenediamine or diethylenetriamine and X stands for $(BeF_4)^{2-}$ or $(BF_4)_2^{2-}$ or $(TiF_6)^{2-}$ or $(SiF_6)^{2-}$ has been described. The complexes have been characterized by infrared, magnetic moment, crystal field splitting energy and nephelauxetic ratio data. The results show that the orbital overlapping in the metal-ligand bond in Mn(II) complexes is comparatively more as compared to that in Co(II) complexes.

The ligand field theory, involving the electronic spectral parameters[1-5] such as Slater-Condon, F_K (interelectronic repulsion parameters), Racah, B and C (which are linear combinations of F_K parameters), crystal field splitting energy parameter, $10\,D_q$, and spin-orbit coupling constant, λ, is still studied in comparison to molecular orbital theory for transition metal complexes. This is because of the fact that the former has relatively a straightforward and simple approach. In the present note, a comparative study of spectral and magnetic characteristics of some Mn(II) and Co(II) complexes synthesized in our laboratory has been made.

Synthesis—The BDH chemicals were used in the synthesis of the present complexes. The synthesis of these complexes was carried out in two steps. In the first step, the metal fluoro salts were prepared by treating the respective metal carbonate with slight excess of different fluoro acids, viz. hydrofluoro beryllic acid, hydrofluoroboric acid, hydrofluorotitanic acid and hydrofluoro silicic acid. The reactions were carried out in a polytheneware assembly. The fluoro salts of Mn(II) and Co(II) were obtained from filtrate by slow crystallization. The crystals were washed with ethanol followed by ether and dried in vacuum.

In the second step, the fluoro salts so prepared were then mixed with different amine ligands in ethanol in the molar ratio 1 : 2. The different mixtures were kept at a temperature between 60 and 80 C for 1 hr. The dark brown crystals were separated out. These were washed with ethanol followed by ether and dried in vacuum. The yield was 80-90%. The analytical data suggest that the complexes have the following chemical formula.

$$[M(L)_2(H_2O)]X$$

where L = ethylenediamine or propylenediamine or diethylenetriamine and $X = (BeF_4)^{2-}$ or $(BF_4)^{2-}$ or $(TiF_6)^{2-}$ or $(SiF_6)^{2-}$.

Absorption spectra—The absorption spectra of the complexes in dimethylformamide (DMF) solution were recorded in Carl-Zeiss VSV-2 spectrophotometer in the region 350 to 950 nm.

Magnetic measurements—A Gouy-type magnetic balance was used to determine the magnetic moment data for the complexes in DMF solution. The room temperature was kept at 300 K.

Infrared spectra—The infrared spectra of the complexes in KBr pellets in the region 4000-400 cm^{-1} were obtained from ATIRA, Ahmedabad and CDRI, Lucknow.

Infrared data supporting the chemical formula—In the infrared spectra, the strong bands appearing between 415 cm^{-1} and 460 cm^{-1}, 1500 cm^{-1} and 1525 cm^{-1} and 1010 cm^{-1} and 1015 cm^{-1} have been assigned the group frequencies[6-8] as ν_{M-N}, $\nu_{S(C-N)}$ and $\nu_{S(C-N+\text{coord water})}$ respectively. This shows that the metal ion is coordinated with nitrogens of the amine ligand and water is present in the form of coordinated water. In this way the infrared data support the chemical formula given earlier.

Electronic spectral and magnetic characteristics—The values of $10\,D_q$ in case of Mn(II) complexes were computed by using the Orgel diagram[4]. In the Orgel diagram the energy level curve due to ν_1 transition $(6_{A1g} \rightarrow 4_{T1g})$ was used. In case of Co(II) complexes the values of $10\,D_q$ were computed by using the relation[2,3] as follows:

$$10\,D_q = \nu_2 - \nu_1$$

The computed values of μ_{eff} (in Bohr Magneton) at 300 K and $10\,D_q$ (in cm^{-1}) are presented in Table 1. The values of β (nephelauxetic ratio) and hx (nephelauxetic parameter for the ligand) were also computed by using the methods reported earlier[1,5] and are given in Table 1.

The reported value of $10\,D_q$ shows that the Mn(II) complexes have a better orbital overlap in the metal

Table 1—Computed Values of μ_{eff}, $10D_q$, β & hx for Some Mn(II) & Co(II) Complexes

Metal complex*	Mn(II) complexes				Co(II) complexes			
	μ_{eff}	$10D_q$	β	hx	μ_{eff}	$10D_q$	β	hx
$[M(L_1)_2(H_2O)_2]X_1$	5.33	10720	0.79	3.00	6.00	9761.0	0.86	0.58
$[M(L_2)_2(H_2O)_2]X_1$	5.82	10830	0.79	3.00	5.95	9541.7	0.87	0.54
$[M(L_3)_2(H_2O)_2]X_1$	6.01	10860	0.78	3.14	5.95	9568.2	0.85	0.50
$[M(L_1)_2(H_2O)_2]X_2$	6.20	10660	0.81	2.71	6.15	9323.2	0.84	0.66
$[M(L_2)_2(H_2O)_2]X_2$	5.91	10640	0.75	3.57	5.18	9596.3	0.85	0.62
$[M(L_3)_2(H_2O)_2]X_2$	5.96	10780	0.77	3.28	6.20	9485.2	0.91	0.37
$[M(L_1)_2(H_2O)_2]X_3$	5.62	10530	0.77	3.28	6.15	9385.2	0.85	0.62
$[M(L_2)_2(H_2O)_2]X_3$	6.20	10580	0.75	3.57	6.05	9426.1	0.92	0.33
$[M(L_3)_2(H_2O)_2]X_3$	5.61	10620	0.74	3.71	5.90	9448.3	0.93	0.29
$[M(L_1)_2(H_2O)_2]X_4$	6.28	10450	0.78	3.14	6.05	9755.2	0.86	0.58
$[M(L_2)_2(H_2O)_2]X_4$	6.30	10660	0.76	3.43	5.95	9822.3	0.88	0.50
$[M(L_3)_2(H_2O)_2]X_4$	5.64	10580	0.75	3.57	5.45	9803.1	0.89	0.45

*L_1, L_2 and L_3 are ethylenediamine, propylenediamine and diethylenetriamine while X_1, X_2, X_3 and X_4 are $(BeF_4)^{2-}$, $(BeF_4)_2^{2-}$ $(TiF_6)^{2-}$ and $(SiF_6)^{2-}$ ions respectively.

ligand bonding as compared to Co(II) complexes under the present study. This has been further supported by the values computed for β and hx (Table 1). In this way the applicability of the ligand field theory has been established.

The authors are highly thankful to Prof. R C Kapoor, Department of Chemistry, University of Jodhpur, Jodhpur for his continued interest in the work. One of them (GKJ) is also grateful to Prof. S N Mehra, Principal, Government Post Graduate College, Nagaur for his inspiration and help throughout the work.

References

1 Konig E, *Struct & Bonding (Germany)*, **9** (1971) 175.
2 Rastogi D K, *J Inorg & Nucl Chem (GB)*, **37** (1975) 685.
3 Jain R K, Joshi G K & Misra Sudhindra N, *Curr Sci (India)*, **48** (1979) 901.
4 Sankhla D S & Misra Sudhindra N, *J Indian Chem Soc*, **57** (1980) 300.
5 Allen G C & Warren K D, *Struct & Bonding (Germany)*, **9** (1971) 49.
6 Colthup N B, Daly L H & Wiberley S E, *Introduction to IR and Raman spectroscopy* (Academic Press, New York) 1975.
7 Ansari M Shameem & Ahmad N A, *J Inorg & Nucl Chem (GB)*, **38** (1976) 1232.
8 Joshi G K, Bhutra M P & Misra Sudhindra N, *J Inorg & Nucl Chem (GB)*, **43** (1981) 585.

Indian Journal of Pure & Applied Physics
Vol. 21, December 1983, pp. 738-740

Proton Magnetic Resonance and Molecular Ordering in Liquid Crystals

J SHASHIDHARA PRASAD & N C SHIVAPRAKASH
Department of Physics, University of Mysore,
Mysore 570006

Received 4 *October* 1982; *revised received* 28 *January* 1983

A study of the proton magnetic resonance of liquid crystalline materials *p*-(*p*-ethoxyphenylazo)phenyl heptanoate and cholesteryl cinnamate is reported in this note. By studying the dipolar splittings, order parameters have been estimated, the values of which are in good agreement with those obtained by optical studies.

The study of liquid crystal forming materials has gained immense importance in recent years due to a wide variety of applications. One of the principal structural characteristics of liquid crystals is the degree of molecular order $S=(3\cos^2\theta-1)/2$, where θ is the angle between the long axes of the molecules and the direction of the axis of preferential orientation (the director). The molecular ordering in the mesophase has been investigated by refractive index, optical circular dichroism, optical rotatory dispersion, proton magnetic resonance (PMR), electron spin resonance (ESR), magnetic compliance and IR and UV light absorption studies[1-3]. Presently, we have evaluated the order parameters of *p*-(*p*-ethoxyphenylazo)phenyl heptanoate (EPPH) and cholesteryl cinnamate (CC) by studying the dipole-diple splittings in the wide line PMR spectra. The order parameters obtained by the wide line PMR studies are compared with those obtained by the optical studies.

Order parameter—The molecular packing coefficient studies of the homologous series of cholesteric and nematic liquid crystals show that these two types of liquid crystals are thermodynamically exactly similar and show similar trends in exhibiting additional smectic phases when the alkyl chain is lengthened[4,5]. Further, we see from these studies that odd-even phenomena of several physical properties within a given homologous series, and the micro variations in *S*-factors are functions of asymmetry or symmetry of the end alkyl groups, and are independent of the central rigid core. These results have also been confirmed theoretically[6-8]. We can therefore treat the cholesteric phase as a twisted nematic phase with a molecular ordering very similar to that of the nematic ordering. Hence there is justification in treating the cholesteric and nematic ordering in the same way.

The doublet splitting δH arising from the dipole-dipole interaction of the adjacent ring protons was used to calculate the order parameter S by means of the equation[3]

$$\delta H = 4\alpha(\tfrac{3}{2}\cos^2\varphi - \tfrac{1}{2})S$$

The dipolar spectrum shows good agreement with the results calculated foe dipole interaction of *ortho* protons of the phenyl ring. For proton dipole-dipole interaction, $\alpha=\frac{3}{2}\mu_H r_{H\text{-}H}^{-3}$, where μ_H is the proton nuclear moment and $r_{H\text{-}H}$ is the distance between the two interacting protons. For EPPH, we assumed $r_{H\text{-}H}=2.45$ Å and $\varphi=10°$, so that $\delta H=5.50\,S$ (in G). In the case of CC, the *ortho* protons of the phenyl ring system[3] are responsible for the dipolar splitting in the wide line PMR spectra. The values of $r_{H\text{-}H}$ and φ are taken to be 2.90 Å and 10° respectively[3]. The doublet splitting $\delta H=3.33\,S$.

Experimental details—The commercially available compounds EPPH (supplied by Eastman Kodak, USA), and CC (supplied by Varilight Corporation, USA) were purified by successive recrystallization. The wide line PMR spectra were recorded at different temperatures using Varian Associates V4200 NMR spectrometer. The experimental details are already described in an earlier paper[3]. The sweep rate was 6.24 G/min.

Results and discussion—Fig. 1 gives the representative PMR spectra for the two samples, each at two different temperatures. We notice that there is no overlap of the central and side PMR peaks, avoiding the necessity of second moment calculations. Most of the reported NMR spectra for various compounds show two- or three-component spectra. Also, it is clear that the two broad components arise due to the high modulation amplitude[9]. The central peak which is prominent in EPPH may be assigned to the alkyl protons. Figs. 2 and 3 give the doublet separations (δH) and the order parameters for EPPH and CC respectively. The S values of EPPH obtained by refractive index measurements are also given for comparison[10]. There is good agreement between the two sets of values, but the values of S obtained by birefringence data are slightly smaller than those obtained from PMR data. This feature has been observed for all other liquid crystalline materials and has been explained earlier[11-13]. The temperature dependence of *S*-factor of EPPH is in good agreement with the results obtained for other compounds of the homologous series[10].

We have also determined the *S*-factor for CC at only one temperature ($S=0.42$ at 95.5°C) as mesomorphic range is extended over just one degree (95-96°C). The *S*-

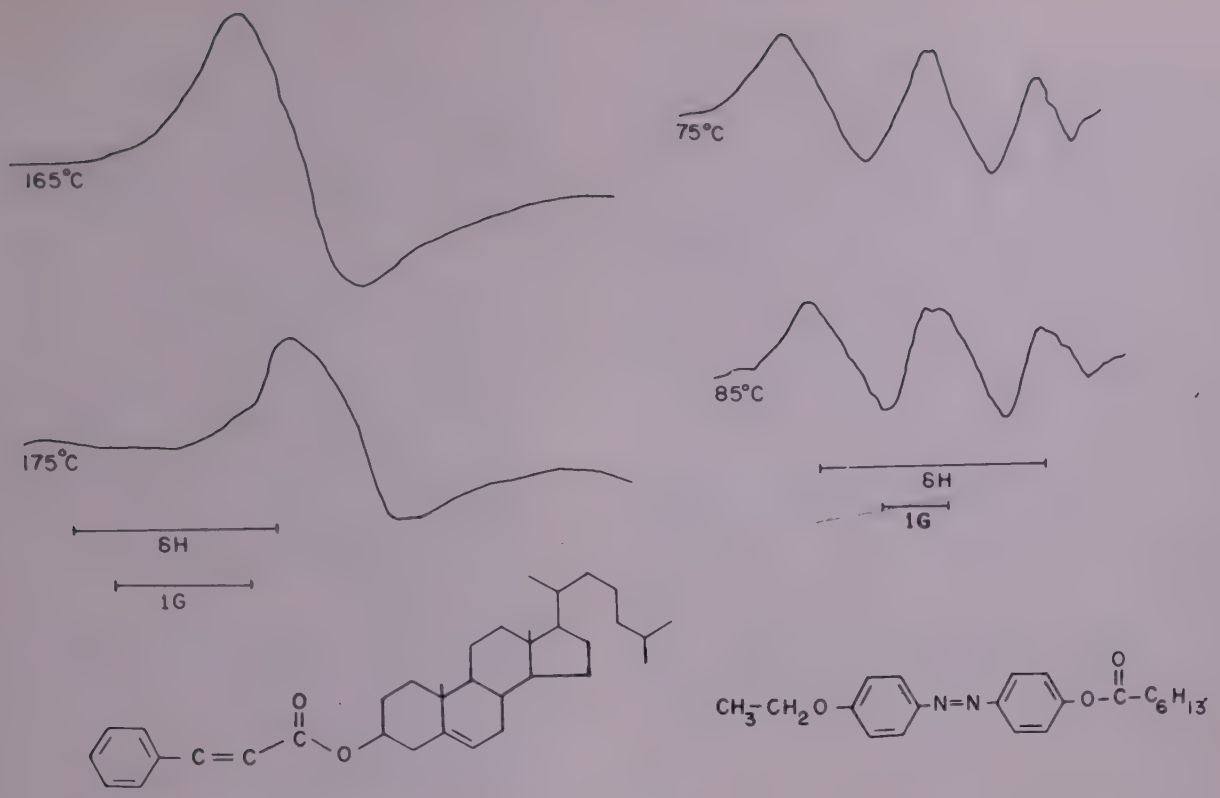

Fig. 1—Representative PMR spectra (along with their structures) for: (a) *p*-(*p*-ethoxyphenylazo)phenyl heptanoate (solid $\overset{161°C}{\longleftrightarrow}$ cholesteric $\overset{214°C}{\longleftrightarrow}$ isotropic) and (b) cholesteryl cinnamate (solid $\overset{60°C}{\longleftrightarrow}$ nematic $\overset{120°C}{\longleftrightarrow}$ isotropic) at two different temperatures

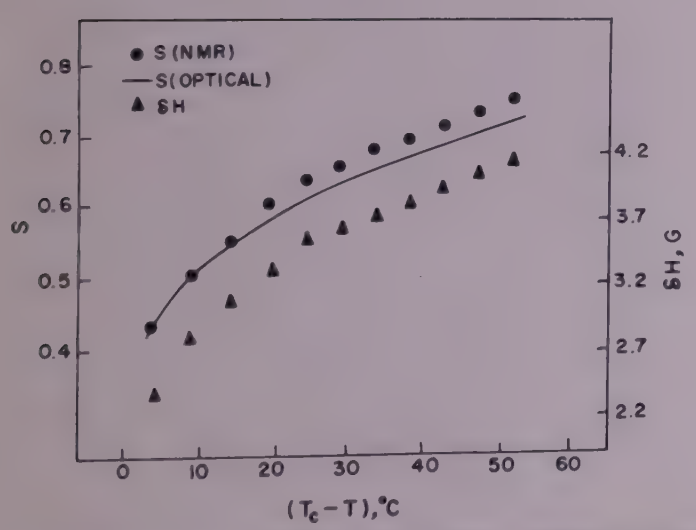

Fig. 2—Dipole-dipole splittings and order parameter versus temperature for *p*-(*p*-ethoxyphenylazo)phenyl heptanoate

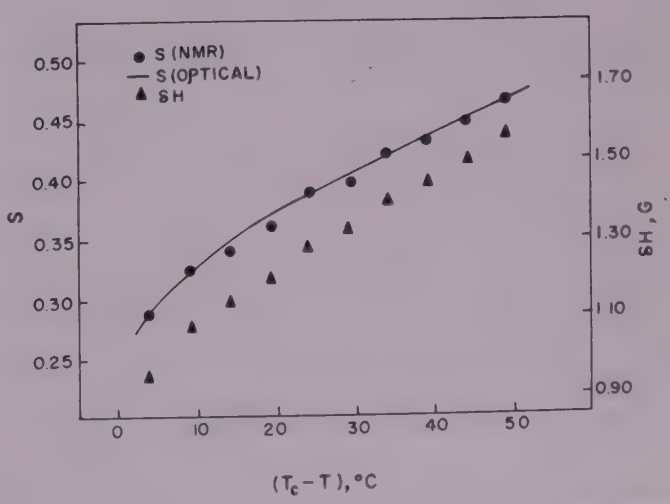

Fig. 3—Dipole-dipole splittings and order parameter versus temperature for cholesteryl cinnamate

factor is comparable with those of other cholesteric liquid crystals.

The order parameter of CC (cholesteric liquid crystal) is lower compared to EPPH (nematic liquid crystal). This feature can be explained as follows. From the macroscopic point of view cholesteric liquid crystals (CC) can be comprehended as spontaneously twisted nematics. As such it is quite possible to characterize the average orientation of molecules in a cholesteric phase with the same set of order parameters as in nematics. It is known[14,15] that dispersion forces in aromatic molecules are larger and more anisotropic than in aliphatic molecules. The sterol groups which form the rigid part of cholesteric-forming molecules are nonaromatic and have smaller dispersion forces, whereas typical nematogenic compounds contain aromatic rings linked by double or triple bonds. Since the dispersion forces are responsible for orientational

order in liquid crystals, the values of the orientational order parameter at the isotropic transition and the dependence of this order on external parameters like temperature in cholesterics will be different from nematics. Also, the interaction between molecules of cholesteric liquid crystal differs from that between molecules of nematic liquid crystal. The above study shows how wide line PMR spectra can be utilized for the determination of the order parameter for both cholesteric and nematic liquid crystals and confirms earlier theoretical and experimental studies on ordering in liquid crystals[6-8].

The authors wish to thank Prof R Vijayaraghavan, Tata Institute of Fundamental Research, Bombay for providing experimental facilities. One of us (JSP) would like to thank the University Grants Commission (UGC), New Delhi for the grant of a Career Award. The award of a post-doctoral fellowship to the other (NCS) by the UGC, is gratefully acknowledged.

References

1 Chandrasekhar S, *Liquid crystals* (Cambridge University Press, Cambridge, England), 1977.

2 Aver'yanov E M & Shabanov V F, *Sov Phys-Crystallogr (USA)*, **24** (1979) 107; **24** (1979) 567.

3 Shivaprakash N C & Shashidhara Prasad J, *J Chem Phys (USA)*, **76** (1982) 866.

4 Shivaprakash N C, Rajalakshmi P K & Shashidhara Prasad J, *Mol Cryst & Liq Cryst (GB)*, **51** (1979) 317; **60** (1980) 153.

5 Shivaprakash N C, Rajalakshmi P K & Shashidhara Prasad J, *Liquid crystals of one- and two-dimensional order*, Vol. 11, edted by W Helfrich and G Heppke (Springer Verlag, Berlin-Heidelberg, New York), 1980, 72.

6 Boden N, Bushby R J & Clark L D, *Chem Phys Lett (Netherlands)*, **64** (1979) 519.

7 Shivaprakash N C & Shashidhara Prasad J, *Mol Cryst & Liq Cryst (GB)*, **74** (1981) 1815.

8 Shashidhara Prasad J & Shivaprakash N C, *Molecular structure and ordering in liquid crystals*, paper presented at the Fourth International Symposium on Ordered Fluids and Liquid Crystals held at Las Vegas, USA, during March 28-April 2, 1982; *Liquid crystals and ordered fluids* (Plenum Press, New York), Vol. 4 (In press).

9 Yasuniwa M, Taki Seiji & Takemura T, *Mol Cryst & Liq Cryst (GB)*, **60** (1980) 111.

10 Somashekar R, Revannasiddaiah D, Madhava M S, Subrahmanyam H S & Krishnamurti D, *Mol Cryst & Liq Cryst (GB)*, **45** (1978) 243.

11 Subrahmanyam H S & Krishnamurti D, *Mol Cryst & Liq Cryst (GB)*, **22** (1973) 239.

12 Subramhanyam H S, Prabha C S & Krishnamurti D, *Mol Cryst & Liq Cryst (GB)*, **28** (1974) 201.

13 Abdoh M M M, Shivaprakash N C & Shashidhara Prasad J, *J Phys Chem (USA)*, **86** (1982) 2349.

14 Hirschfelder J O, Curtiss C F & Bird R B, *Molecular theory of gases and liquids* (Wiley, New York), 1954, 974.

15 Margenau H & Kestner N R, *Theory of intermolecular forces* (Pergamon Press, London), 1969, 256.

Indian Journal of Pure & Applied Physics
Vol. 21, December 1983, pp. 741-742

Proton Magnetic Resonance Studies on 2-Methylbenzoxazole

K V R CHARY, K V G REDDY & B A SASTRY

Solid State and Molecular Physics Laboratory, Physics Department, Osmania University, Hyderabad 500007

and

G PONTICELLI & R PINNA

Istituto Di Chimica Generale, Inorganica Ed Analitica, Universita Di Cagliari, Via Ospedale 72, 09100 Cagliari, Italy

Received 14 *December* 1982

Proton magnetic resonance studies have been made on 2-methylbenzoxazole in the temperature range 77-300 K. Assuming C–C and C–H distances obtained from interatomic tables, the second moment (S_2) is calculated in the presence of CH_3 reorientation which is tallying with the experimental S_2 value in the temperature range 77-262 K. The fall of S_2 from $6\pm1G^2$ to $0.4\pm1G^2$ in the temperature range 262-300 K indicates general molecular reorientation. This reorientation is found to be associated with an activation energy of 10.0 kJ mol^{-1}.

In this note proton magnetic resonance (PMR) studies carried out in the temperature range 77-300 K on a frozen 2-methylbenzoxazole sample are presented. The 2-methylbenzoxazole which is in liquid form at 300 K is found to form many complexes with bivalent metal ions like cobalt(II), nickel(II), copper(II) and zinc(II)[1,2]. Another interesting feature with this compound is that it possesses methyl functional group which can reorient at favourable temperatures and this reorientation has significant effect on the width of the wide-line NMR signal and so also the second moment value. Also, the crystal structure of this compound in its frozen state has not been investigated. Hence, in view of these above features it is felt that the present PMR studies could provide substantial information about the structure and rigidity of the molecule and the molecular and/or intramolecular reorientation through the temperature dependence of the PMR second moment.

Materials and methods—Using analar grade benzoxazole, this sample was prepared by us and chemical analysis has been made for confirmation.

The PMR studies were undertaken on a laboratory-made wide-line NMR spectrometer at a fixed frequency of 12 MHz, whose details are given elsewhere[3]. The first derivative PMR signals were recorded at temperatures ranging from 77 to 300 K.

Results and discussion—The first derivative PMR signals of the complex under investigation were used to calculate the values of the second moment (S_2), at different temperatures, by standard methods[4]. The unit of the S_2 is 10^{-2} (mT)^2. The variation of S_2 of this compound with temperature is shown in Fig. 1. From this figure it is evident that the S_2 of 2-methylbenzoxazole is constant at 6.0 ± 1 in the temperature range 77-262 K and a rapid fall in S_2 from the above value to 0.4 ± 1 is noticed between 262-300 K. The above mentioned S_2 transition of 2-methylbenzoxazole indicates some kind of intramolecular or molecular reorientation.

In order to find the temperature below which the lattice of this compound is rigid, the theoretical rigid lattice second moment [S_2(rig)] has to be calculated and compared with the experimental S_2 at different temperatures. The theoretical S_2(rig) can be calculated by making use of the Smith's modified formula[5-7] of van Vleck[8]. Since the crystal structure of the sample under investigation is not known the intramolecular contribution (S_2') to S_2(rig) is estimated by Slitcher's method[9] and using the assumptions given below. In this method the interatomic distances are evolved by choosing the C–C side bond, C–C ring and C–H bond lengths as equal to 1.54, 1.39 and 1.10 Å respectively. In the present case, the above values are used to estimate the H–H distances in the benzene ring. The H–H distances in the single methyl group are taken as 1.79 Å on the basis of the tables of interatomic distances[10]. Using the above interatomic distances S_2' comes out to be 11.3. Since no crystal structure is available, a reasonable value for intermolecular contribution (S_2''rig) is obtained from Smith's method[6] where this S_2''(rig) is given as a function of the number of protons present in the sample. Since the number of protons in the present case is seven, from the above method the value of S_2''(rig) can be taken as 6.8. From the above assumptions the S_2(rig) comes out to be 17.8. But this is very much higher compared to the experimental value at 77 K (6.0 ± 1). Therefore, it is evident that our lowest attainable temperature was incapable of freezing out whatever

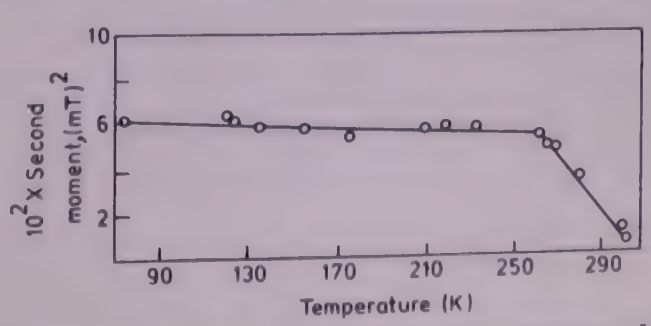

Fig. 1 –Variation of proton second moment with temperature for 2-methylbenzoxazole

motion that lead to a low S_2 value of 6.0 ± 1 in between 77 and 262 K. Similar discrepancy in S_2 has been noticed in the case of xylenes[11] and tetramethyl silane[6].

Since at low temperatures the whole molecule cannot undergo reorientation about any symmetry axis and as it is evident that there is no functional group other than the CH_3 group to undergo any reorientation, the low values of S_2 in the temperature range 77-262 K is interpreted as the result of rapid reorientation of the methyl group about their C_3 symmetry axis. This conclusion is qualified by estimating the S_2 in the presence of this group reorientation by standard procedure[12,13] which comes out to be 6.4. This value is very much consistent with the experimental S_2 value 6 ± 1 in the temperature range 77-262 K.

At temperatures higher than 262 K, the gradual decrease in S_2 suggests a slow onset of rotation of the molecule. At 300 K when the compound is in liquid state the value of S_2 comes out to be very small (~ 0.4) as expected.

The correlation frequencies associated with the S_2 transition are calculated from the modified Bloembergen *et al.*[14-16] equation which is shown below

$$\ln \nu_c = \ln \frac{\gamma M_2^{\frac{1}{2}}}{2\pi} - \ln \tan \frac{\pi}{2} \left[\frac{M - M_{HT}}{M_{LT} - M_{HT}} \right] \quad \ldots (1)$$

The constants in the above expression have their usual meanings. These reorientation frequencies are assumed to fit in the Arrhenius equation $\nu_c = \nu_0 \exp(-Ev/RT)$. Therefore, a plot of $\ln \nu_c$ versus $1000/T\,K^{-1}$ yields a straight line from which activation energy is calculated. In the present case it comes out to be 10.0 kJ mol^{-1}.

Conclusions—From the PMR studies on 2-methylbenzoxazole in the temperature range 77-300 K the following conclusions can be drawn: (1) the molecule appears to be not rigid even at 77 K due to the reorientation of the CH_3 group; (2) the coincidence of the theoretical S_2 for the reorientation of CH_3 group with the experimental value in the temperature range 77-262 K justifies the correctness of the assumptions made in finding out the interproton distances; and (3) the fall in S_2 in the temperature range 262-300 K is attributed to the onset of molecular reorientation and this is found to be associated with an activation energy of 10.0 kJ mol^{-1}.

We thank Prof. G Sivarama Sastry, Head of the Department of Physics for his interest in the present investigation. We express our gratitude to Prof. K Venkata Ramiah for his constant encouragement. We are grateful to the University Grants Commission, New Delhi for the financial assistance for carrying out this work.

References

1 Edward J D & Hughes M N, *J Chem Soc A (GB)*, (1969) 477.
2 Edward J D, Hughes M N & Rutt K J, *J Chem Soc A (GB)*, (1969) 2126.
3 Chary K V R, Reddy K V G & Sastry B A, *Indian J Phys Part A*, **56** (1982) 242.
4 Andrew E R, *Phys Rev (USA)*, **91** (1953) 425.
5 Smith G W, *J Chem Phys (USA)*, **36** (1962) 3081.
6 Smith G W, *J Chem Phys (USA)*, **42** (1965) 4229.
7 Smith G W, *J Chem Phys (USA)*, **43** (1965) 4325.
8 Van Vleck J H, *Phys Rev (USA)*, **74** (1948) 1168.
9 Slitcher C P, *Principles of magnetic resonance* (Harper & Row, New York) 1964, p. 61.
10 *Tables of interatomic distances and configurations in molecules and ions* (The Chemical Society, London) 1958.
11 Gupta R C, *J Prakt Chemie (Germany)*, **316** (2) (1974) 185.
12 Moskalev V V, *Sov Phys Solid-State (USA)*, **3** (1962) 2218.
13 Andrew E R & Eades R G, *Proc R Soc (London) Sec A (GB)*, **216** (1953) 398.
14 Bloembergen N, Purcell E M & Pound R V, *Phys Rev (USA)*, **74** (1948) 1184.
15 Abragam A, *Principles of nuclear magnetism* (Oxford University Press, Oxford) 1961, 456.
16 O'Reilly D E & Tsang T, *J Chem Phys (USA)*, **46** (1967) 1298.

Indian Journal of Pure & Applied Physics
Vol. 21, December 1983, p. 743

Photon Attenuation Coefficients in Compounds

D R SAMUEL SMILES, P V C SARMA, K PREMCHAND, B MALLIKARJUNA RAO & K PARTHASARADHI

Department of Nuclear Physics, Andhra University Visakhapatnam 530003

Received 17 *March* 1981; *revised received* 15 *March* 1983

Total photon attenuation coefficients are measured in a few compounds using HPGe detecting system on a good geometry set-up at 59.54 keV. These values are found to be, in general, in agreement with the available theoretical and semi-experimental data. The deduced total effective atomic numbers are found to be in agreement with those evaluated using theoretical expressions.

Most of the earlier experimental results on total attenuation coefficients of photons reported in literature are confined to elements and total cross-section estimates in organic and inorganic compounds are meagre. In addition, most of the available measurements are carried out by using either proportional counters or NaI(Tl) crystal detection systems. With the advent of solid state detectors, there is a renewed interest on these measurements in view of their high-resolution characteristic. Also, accurate theoretical estimates have been offered by Hubbel *et al.*[1] and Scofield[2] for the scattering and photoelectric processes respectively. Hence the total attenuation cross-sections in several inorganic compounds are estimated using an 80 cc HPGe detecting system. The experiments are carried out on a set-up similar to the one already reported[3] and in the same way. Total attenuation cross-sections for six compounds, viz. KCl, V_2O_5, LiF, B_2O_3, NaCl and $H_8O_2C_5$ are determined at 59.54 keV, employing monoenergetic gamma rays from a 14 mCi ^{241}Am sealed capsule obtained from Radio Chemical Centre, Amersham (UK). The absorbers are prepared by filling 99.9% pure amorphous compound in perspex rings of suitable thickness and closing them on either side with a thin mylar foil. In case of perspex ($H_8O_2C_5$), rods of suitable heights are used.

Table 1—Photon Attenuation Coefficients (in cm^2/g) in Compounds at 59.54 keV

Compound	Experimental value	Ref. (4)	Ref. (5)	Refs (1) and (2)
KCl	0.514±0.005	0.5127	0.5136	0.514
V_2O_5	0.560±0.005	0.5619	0.5570	0.5661
LiF	0.1780±0.0018	0.1797	0.1813	0.180
B_2O_3	0.1809±0.0018	0.1807	0.1818	0.1814
NaCl	0.3532±0.0036	0.3588	0.3604	0.3610
$H_8O_2C_5$	0.1920±0.0019	0.1931	0.1933	0.1930

Table 2—Effective Atomic Numbers in Compounds at 59.54 keV

Compound	Theoretical			Experimental (for total absorption process)
	Scattering	Photoelectric	Total absorption	
KCl	18.00	18.11	18.07	18.6±0.3
V_2O_5	12.29	19.26	16.88	16.7±0.3
LiF	6.00	8.17	6.23	6.45±0.12
B_2O_3	6.80	7.33	6.86	6.81±0.13
NaCl	14.00	15.22	14.58	14.80±0.29
$H_8O_2C_5$	3.59	6.66	3.74	3.60±0.07

The measured total photon attenuation coefficients with the theoretical estimates are presented in Table 1. The theoretical values in compounds are obtained by using the mass attenuation coefficients in individual elements employing the 'sum-rule'. From Table 1, it can be seen that the present experimental values are, in general, in agreement with the other sets of values and the 'sum-rule' is valid at this energy in these compounds.

Table 2 presents the experimental effective atomic numbers for total absorption processes obtained from the plots of atomic number versus the theoretical atomic cross-section in individual elements. The theoretical effective atomic numbers for total interaction are estimated by adding the numbers, evaluated for scattering and photoelectric processes using the theoretical expressions, in the respective cross-sectional weightages as already reported[6,7]. It can be seen that the present experimental effective atomic numbers are in agreement with theory within 4%.

References

1 Hubbell J H, Veigele Wm J, Briggs E A *et al.*, *Phys Chem Ref Data*, 4 (No. 3) (1975) 471.

2 Scofield J H, *Theoretical photoionization cross-section from* 1 *to* 1500 *keV* (University of California, Livermore, California 94550), UCRL-51326, January 12 (1973).

3 Radhakrishna Murty V, Sarveswara Rao K, Parthasaradhi K, *et al.*, *J Phys B (GB)*, **10** (1971) 3189.

4 Storm E & Israel H T, *Nuclear Data (USA)*, 7 (1970) 70.

5 Veigele Wm J, *Atomic Data* 5 (*USA*), **51** (1973).

6 Parthasaradhi K, *Indian J Pure & Appl Phys*, **6** (1968) 609.

7 Seshagiri Rao V & Parthasaradhi K, *Nucl Sci & Engg (USA)*, **42** (1970) 109.

Indian Journal of Pure & Applied Physics
Vol. 21, December 1983, pp. 744-746

Vibrational Spectra of 2, 4- & 2, 5-Dichloroanilines

S K SINGH* & R N SINGH
Department of Physics, Bihar University, L S College, Muzaffarpur

Received 29 *December* 1981; *accepted* 7 *December* 1983

The far infrared (20-600 cm^{-1}), infrared (200-4000 cm^{-1}) and laser Raman spectra (100-4000 cm^{-1}) of 2, 4- and 2, 5-dichloroanilines have been recorded using Fourier far IR spectrometer (model Polytec FIR 30), Perkin-Elmer (model 621) double beam grating spectrophotometer and He-Ne laser respectively. The vibrational spectra have been analysed assuming C_s point group.

The infrared spectra of 2, 4- and 2, 5-dichloroanilines have been studied by Srivastava[1] in the region 400-3800 cm^{-1}, of which only 21 observed absorption frequencies for the former and only 20 observed absorption frequencies for the latter have been reported. No assignments for the observed bands have been proposed by him. However, an attempt for the assignment of the observed frequencies in the spectra of 2, 5-dichloroaniline was made by Singh and Singh[2] in the same region. Earlier workers could observe only 50-70% of the expected normal modes in each molecule because they did not cover the FIR region of the spectra (i.e. below 400 cm^{-1}). A survey of the literature of the previous workers shows that the complete vibrational frequency data and their assignments for these two molecules have not been reported so far. The aim of this work is to re-investigate the vibrational spectra of these molecules and to propose complete assignments. The FIR region has been investigated for the first time for these two molecules to pick-up such fundamental frequencies which have not been reported so far. The He-Ne laser Raman spectra have also been recorded for the samples.

The compounds 2, 4- and 2, 5-dichloroanilines (in solid state) were obtained from Koch Light Laboratories Ltd, England, in pure form and used as such. The FIR spectra have been recorded on Fourier Far IR spectrometer (model Polytec FIR 30) in the region 20-600 cm^{-1}. The infrared spectra in solid phase with Nujol mull and also in CCl_4 solution have been recorded on Perkin-Elmer (model 621) double beam grating spectrophotometer in the region 200-4000 cm^{-1}. The Raman spectra have been recorded with samples in the powder form on Jobin Yovon Ramanor spectrometer consisting of double monochromater with concave holographic grating in the region 100-4000 cm^{-1}. The accuracy of measurements in the IR and Raman spectra is estimated to be within $\pm 5\ cm^{-1}$.

Assuming NH_2 group as mass point, 2, 4- and 2, 5-dichloroanilines would belong to C_s point group. The simplified model leads to 30 normal vibrations out of which 21 are planar (a') and 9 are non-planar (a''). In addition to these 30 ring vibrations, there would be 6 internal vibrations of the substituents group NH_2. The frequencies of the observed bands, their intensities, vibration number in Wilson's notations and assignments are given in Table 1. Assignments for the various observed bands have been made on the basis of the intensity of the bands and the data on related and similar molecules. All the modes of vibrations, because of C_s symmetry of the molecule, are both infrared and Raman active.

The three C—H stretching modes of vibrations (2, 20_a and 20_b) have been assigned at frequencies ν_3, ν_4 and ν_5; lying in the region 3000-3100 cm^{-1}. The C—X (X substitution) stretching modes (3, 7_a and 7_b) decrease considerably below 1200 cm^{-1} due to their mass dependence. The bands ν_{11}, ν_{27} and ν_{31} have been assigned to C—NH_2, C—Cl and CCl stretching frequencies respectively. These assignments find support from the work of Sharma and Dwivedi[3]. The bands with prominent intensities (ν_7, ν_8, ν_9 and ν_{10}) lying in the region 1608-1470 cm^{-1} have been assigned to C—C stretching frequencies. The vibration mode 14 (Kekule vibration) changes by a small magnitude with substitution and has been identified at ν_{12} ($\approx$1278 cm^{-1}). The frequency of mode 1 (ring breathing vibration) increases with the increase of mass number of the substituent and has been identified at ν_{18} ($\approx$1050 cm^{-1}).

In the case of asymmetric trisubstituted benzenes (C_s), the modes 3, 15 and 18_b are regarded as C—H in-plane bending vibrations[4] and these modes have been identified at frequencies ν_{13}, ν_{15} and ν_{17} respectively. The three C—X in-plane bending modes (18_a, 9_b and 9_a) have been assigned at frequencies ν_{14} (C—NH_2), ν_{30}(C—Cl) and ν_{34}(C—Cl). These assignments are in agreement with the data of Green *et al.*[5] as well as with that of other workers[6,7] for similar compounds.

The three C—C—C in-plane bending vibrations are denoted by 6_a, 6_b and 12 in Wilson's notations. For asymmetric trisubstitution with mixed substituents the frequency of normal mode 6_b is found to be greater than that of 6_a. In the present study, normal modes 6_b and 6_a have been identified at ν_{21} and ν_{23} respectively.

* Present address: Head of the Physics Department, D B College, Jaynagar 847 226

Table 1—Frequencies of Observed Bands, Their Intensities, Vibration Numbers in Wilson's Notation and Assignments

Molecule				Vib. No.	Species	Assignment
2, 4-DCA		2, 5-DCA				
IR	Raman	IR	Raman			
ν_1 3484(5.5)		3485(6)				$\nu_{as}(NH_2)$
ν_2 3408(4)		3405(7)				$\nu_s(NH_2)$
ν_3 3085(8)	3085(w)	3085(4)	3080(w)	2	a'	ν(C—H)
ν_4 3068(10)*	3060(m)	3060(4)	3050(w)	20_a	a'	ν(C—H)
ν_5 3030(1)*	3030(w)	3032(4)	3035(s)	20_b	a'	ν(C—H)
ν_6 1638(2)		1645(2)				$\delta_s(NH_2)$ Scissoring
ν_7 1608(9)*		1608(8.5)	1609(w)	8_b	a'	ν(C—C)
ν_8 1592(6)		1600(10)	1600(w)	8_a	a'	ν(C—C)
ν_9 1484(8.6)	1492(m)	1482(8)		19_b	a'	ν(C—C)
ν_{10}1470(10)*	1480(m)	1470(10)		19_a	a'	ν(C—C)
ν_{11}1298(6.5)	1300(m)	1303(5)	1308(w)	13	a'	ν(C—NH_2)
ν_{12}1281(9)	1275(s)	1290(5)*	1278(m)	14	a'	ν(C—C)Kekule Vibrn
ν_{13}1248(4.5)	1240(m)	1265(5)	1268(w)	3	a'	δ(C—H)
ν_{14}1155(5)	1162(w)	1150(4.5)		18_a	a'	δ(C—NH_2)
ν_{15}1130(5)	1122(m)	1142(4.5)		15	a'	δ(C—H)
ν_{16}1105(4.5)		1124(4)				$\delta_{as}(NH_2)$ Rocking
ν_{17}1085(5)	1080(w)	1086(5)*	1085(w)	18_b	a'	δ(C—H)
ν_{18}1050(6)	1058(m)	1048(5.1)*	1048(w)	1	a'	ν(C—C) Ring breathing
ν_{19}938(4)	930(w)	932(4)	922(s)	17_b	a''	γ(C—H)
ν_{20}873(6.4)	870(w)	898(6.4)	890(s)	5	a''	γ(C—H)
ν_{21}813(7.8)	822(s)	792(5.8)	790(w)	6_b	a'	δ(C—C—C)
ν_{22}806(5.4)		832(6.0)	825(w)	11	a''	γ(C—H)
ν_{23}732(6.0)	740(w)	733(3)		6_a	a'	δ(C—C—C)
ν_{24}708(6.4)	710(w)	718(4.4)	713(s)	4	a''	γ(C—C—C)
ν_{25}625(6.6)		620(5)				$\delta_{as}(NH_2)$ Wagging
ν_{26}578(6.4)	575(w)	575(5)	583(s)	16_a	a''	γ(C—C—C)
ν_{27}542(6.4)	538(m)	535(4.4)		7_b	a'	ν(C—Cl)
ν_{28}520(6)	525(s)	505(4.8)		12	a'	δ(C—C—C)
ν_{29}463(5.8)	455(w)	448(4.8)	445(m)	16_b	a''	γ(C—C—C)
ν_{30}435(6)	438(m)	434(5)	428(w)	9_b	a'	δ(C—Cl)
ν_{31}278(5.2)		270(3.7)	280(s)	7*a*	a'	γ(C—Cl)
ν_{32}210(5.8)		200(3,2)				(NH_2)Twisting
ν_{33}205(4.3)	207(s)	205(4.2)	207(m)	10_a	a''	γ(C—NH_2)
ν_{34}194(4)	200(s)	192(3.2)	188(s)	9_a	a'	δ(C—Cl)
ν_{35}182(3)	188(s)	180(3)	188(s)	10_b	a''	γ(C—Cl)
ν_{36}138(3.4)	140(s)	140(2.2)	145(m)	17_a	a''	γ(C—Cl)
ν_{37}3502		3508				(3068 435)*A*″&(3060 448)*A*″
ν_{38}2910		3395				(1608 1298)*A*′&(3085 310)*A*″
ν_{39}2725		2930				(1592 1130)*A*′&(1470) 2)*A*′
ν_{40}1875		2860				(1298 578)*A*″&(1600 1265)*A*′
ν_{41}1850		1919				(1050 806)*A*″&(1886 832)*A*″
ν_{42}1725		1858				(1592 138)*A*″&(1280 575)*A*″
ν_{43}1570		1698				(1130 435)*A*′&(1265434)*A*′
ν_{44}1406		1370				(1130 278)*A*″&(832 535)*A*′
ν_{45}1388		1268				(813 578)*A*′&(733 535)*A*′
ν_{46}1309		915				(732 578)*A*″&(733 180)*A*″
ν_{47}1228		850				(1085 138)*A*″&(575 270)*A*″
ν_{48}645		374				(435 205)*A*′&(180 192)*A*″
ν_{49}370						(182 × 2)*A*′
ν_{50}320						(138 + 182)*A*′

* Liquid phase reading (in CCl_4 solution);s = sharp; m = medium; w = weak; ν = stretching, δ = in-plane bending, γ = out-of-plane bending. In cols. 1 and 3, the figures in parentheses indicate intensity in the scale of 1 to 10.

The frequency of mode 12 drops considerably and has been identified at ν_{28} with prominent intensity.

The C—H out-of-plane bending vibrations are represented by normal modes 17_b, 5 and 11 in the case of asymmetric trisubstituted benzenes and these modes have been identified at frequencies ν_{19}, ν_{20} and ν_{22} respectively, lying in the region 950-800 cm^{-1}. The three C—X out-of-plane bending vibrations, denoted by normal modes 10_a, 10_b and 17_a, decrease considerably and have been assigned at ν_{33}, ν_{35} and ν_{38} respectively. These frequencies are within the frequency intervals established by Whiffen[8] and McMurry and Thornton[9]. Normal 4, 16_a and 16_b are the C—C—C out of plane bending vibrations of benzene. In the case of substituted benzenes, the frequency of mode 4 increases slightly from its magnitude in benzene and has been identified at ν_{24} in the present case. For asymmetric trisubstitution, Bentley and Wolforth[10] assigned one component 16_a between 530 and 590 cm^{-1} in the infrared spectrum of trialkyl benzenes, while the other component 16_b was assigned in the interval 430-450 cm^{-1}. Hence the assignments for modes 16_a and 16_b at frequencies ν_{26} and ν_{29} respectively stand justified.

The authors are grateful to Prof. B N Bhattacharya, Regional Sophisticated Instruments Centre, Indian Institute of Technology, Bombay, for kindly providing them with laser traces of the Raman spectra. The authors are also grateful to the Head, Regional Sophisticated Instruments Centre, Indian Institute of Technology, Madras and Prof. S M Verma, Chemistry Department, Banaras Hindu University, Varanasi, for their kind permission for recording FIR and IR spectra respectively.

References

1 Srivastava S L, *Indian J Pure & Appl Phys*, **5** (1967) 189.
2 Singh V B & Singh I S, *Indian J Pure & Appl Phys*, **6** (1968) 81.
3 Sharma S N & Dwivedi C P D, *Indian J Phys*, **50** (1976) 25.
4 Varsanyi G, *Vibrational spectra of benzene derivatives* (Academic Press, New York) 1969.
5 Green J H S, Harrison D J & Kynaston W, *Spectrochim Acta Part A (GB)*, **27** (1971) 793.
6 Singh R N & Prasad S C, *Spectrochim Acta Part A (GB)*, **34** (1978) 39.
7 Goel R K, Gupta S K & Sharma S N, *Pramana (India)*, **11** (1978) 541.
8 Whiffen D H, *Spectrochim Acta (GB)*, **7** (1955) 253.
9 McMurry H L & Thornton V, *Anal Chem (USA)*, **24** (1952) 318.
10 Bentley F F & Wolforth E F, *Spectrochim Acta (GB)*, **15** (1959) 165.

Indian Journal of Pure & Applied Physics
Vol. 21, December 1983, pp. 747-748

Absorption Spectra of Some Lanthanide Complexes: Pr^{3+}:L-Leucine & Mercaptopropionic Acid Ternary Complex

K TANDON
Chemistry Department, University of Jodhpur, Jodhpur
and
S P TANDON, M P BHUTRA,
KIRTY MATHUR & RITA BHARGAVA.
Physics Department, University of Jodhpur, Jodhpur

Received 31 *December* 1982

Slater-Condon, Racah and Landè interaction parameters, oscillator strength, Judd-Ofelt intensity parameters, nephelauxetic ratio and bonding parameter have been reported for Pr^{3+} ternary complex using L-leucine and mercaptopropionic acid as ligand in aqueous and dimethylformamide (DMF) solutions. These parameters have been compared with those for the free ion. Covalent bonding in the complex is indicated.

A number of rare-earth complexes with amino acids have been reviewed by Yatsimirskii *et al.*[1] and Forsberg[2]. Panyushkin *et al.*[3] have studied infrared absorption of some rare-earth complexes with α-amino acids. It is only recently that Bhutra and Gupta[4] have made spectral studies of Pr^{3+} complexes with cysteine and diols in the visible region.

The present note reports the absorption spectra of ternary complex of Pr^{3+} using L-leucine and mercaptopropionic acid as ligands in aqueous and DMF solutions. Various spectroscopic interaction and intensity parameters have been computed from the observed spectra.

The complex of Pr^{3+} with L-leucine and mercaptopropionic acid was prepared by the usual method[4]. Chemicals used were of AR Grade. The absorption spectra were measured on Carl-Zeiss VSU-2 Spectrophotometer in the region 360-600 nm in water and DMF solutions. The observed values of energy levels and oscillator strengths have been presented in Tables 1 and 2 respectively.

Table 1—Experimental and Calculated Energy Levels (in cm^{-1}) for Pr^{3+} Complex in Solution

Energy level	Solvent H_2O		Solvent DMF	
	E_{exptl}	$E_{calc.}$	E_{exptl}	$E_{calc.}$
$^1D_2$	17007	17169	16949	17121
$^3P_0$	20833	20865	20790	20826
$^3P_1$	21413	21361	21322	21278
$^3P_2$	22573	22502	22472	22399
rms deviation		93.0		97.65

Table 2—Experimental and Calculated Oscillator Strengths for Pr^{3+} Complex in Solutions

Energy levels	Solvent water $P\times10^{-6}$		Solvent DMF $P\times10^{-6}$	
	Exptl	Calc.	Exptl	Calc.
$^1D_2$	3.60	3.60	4.37	4.37
$^3P_0$	1.74	2.91	3.07	3.83
$^3P_1$	4.15	2.95	4.65	3.88
$^3P_2$	11.47	11.47	11.97	11.97
rms deviation	0.84		0.54	

Energy parameters—The initial set of parameters may be evaluated by expressing the energy as a Taylor series expansion. For the jth level it is given by:

$$E_j(F_k, \zeta_{4f}) = E_{0j}(F_k^0 \zeta_{4f}^0) + \sum_{k=2,4,6} \frac{\partial E_j}{\partial F_k}\Delta F_k + \frac{\partial E_j}{\partial \zeta_{4f}}\Delta\zeta_{4f} \quad \ldots (1)$$

where E_{0j} is the zero order energy of the jth level. Substituting the observed energy value E_j, zero order energy value E_{0j} and partial derivatives for the free ion, first best value of F_2, F_4, F_6 and ζ_{4f} parameters are calculated by partial multiple regression method. Using these parameters, zero order energy values, the energy values E_j for different levels of Pr^{3+} ion in both the solvents have been computed. The observed and computed values of E_j are collected in Table 1. The F_k parameters are also related to another set of energy parameters known as Racah parameters E^k which have also been calculated and included in Table 3 along with other parameters.

Intensity parameters—The experimental oscillator strengths for various transitions have been computed by using the relation

$$P = 4.6\times10^{-9}\times\varepsilon_{max}\times\Delta\nu_{1/2} \quad \ldots (2)$$

where ε_{max} is the molar extinction coefficient and $\Delta\nu_{1/2}$ is the bandwidth for the respective transition.

Theoretically, the oscillator strength P_{calc} of the induced dipole transition, according to Judd-Ofelt relation can be expressed as:

$$P_{calc} = |U^{(2)}|^2 T_2 + |U^{(4)}|^2 T_4 + |U^{(6)}|^2 T_6 \quad \ldots (3)$$

The values of T_λ parameter have been computed from Eq. (3) using partial multiple regression method[5], where the values of reduced matrix elements have been taken from Carnall[6]. The values of T_λ-parameter for Pr^{3+} complexes with L-leucine and mercapto-

Table 3—Observation of the Parameters of Pr^{3+} Complex in Solution

Parameter	Free ion	H_2O	DMF
F_2	322.09	312.44	312.35
F_4	44.46	43.13	43.12
F_6	4.866	4.72	4.72
E^1	4729	4587.22	4585.91
E^2	24.79	23.995	23.988
E^3	478.14	463.79	463.66
ζ_{4f}	741.00	677.1497	657.64
β		0.9700	0.9698
$b^{1/2}$		0.1224	0.1229
$T_2 \times 10^9$		5.5	19.3
$T_4 \times 10^9$		0.81	1.07
$T_6 \times 10^9$		3.53	3.65
T_4/T_6		0.229	0.293

propionic acid in water and DMF have been reported in Table 3. The calculated values of oscillator strengths for various transitions are included in Table 2.

Bonding and nephelauxetic ratio (β)—On complexation the expansion of central ion takes place. This effect of expansion is known as nephelauxetic effect and has been studied by various workers[7-9]. The bonding parameter $b^{1/2}$ has been calculated using the relation reported earlier[7]. Values of β and $b^{1/2}$ have been included in Table 3.

Discussion—A comparison of the observed and calculated values of energy levels (Table 1) shows that the rms deviations are 93.0 cm^{-1} for the Pr^{3+} complexes in aqueous solution and 79.6 cm^{-1} in DMF solution. These values indicate good agreement with theoretical and experimental energy values.

The interelectronic repulsion F_k and E^k and Lande ζ_{4f} parameters exhibit a decrease from the values of corresponding parameters of Pr^{3+} free ion (Table 3). This is due to the decrease in interelectronic repulsion and spin-orbit interaction due to the expansion of the central metal-ion orbital on complexation. The positive $b^{1/2}$ values indicate covalent bonding of the complexes under study.

The ratio of T_4/T_6 is nearly constant which suggests that the structure of the complexes in different solvents remains invariant.

References

1 Yatsimirskii K B, Kostroming N A, Sheka Z A *et al.*, *The chemistry of complexes of the rare earth elements*, translated from Russian (Naukova Dumka, Kiev) 1966.

2 Forsberg J H, *Coord Chem Rev (Netherlands)*, **10** (1973) 195.

3 Panyushkin V T, Garnovskii A D, Osipov O A & Pozharskii A F, *Zh Obshch Khim (USSR)*, **87** (1967) 312.

4 Bhutra M P & Gupta A K, *Indian J Pure & Appl Phys*, **21** (1983) 374.

5 Goulden Cyril H, *Method of statistical analysis* (Asia Publishing House, Bombay) 1964. ch 8, p 134.

6 Carnall W T, *Handbook of physics and chemistry of rare earths* (North Holland, Amsterdam), **3** (1979) 171.
Judd B R, *Lanthanide and actinide chemistry and spectroscopy*, ACS Symposium Series, Vol 131, edited by N M Edelstein (American Chemical Society, Washington) 1980, 267.

7 Tandon S P, Mehta P C, *J Chem Phys (USA)*, **52** (1970) 4313.

8 Karaker D G, *J Inorg & Nucl Chem (GB)*, **33** (1971) 3713.

9 Peacock R D, *Structure and bonding* (Springer-Verlag, Berlin), **22** (1975) 88.

Indian Journal of Pure & Applied Physics
Vol. 21, December 1983, pp. 749-751

Ultraviolet Absorption Spectra of 2, 3- & 3, 5-Dichloroanilines in Vapour Phase

R K GOEL & S K GUPTA*
Department of Physics, D N College, Meerut 250002
and
R M P JAISWAL
Department of Physics, Kurukshetra University, Kurukshetra 132119

Received 7 *February* 1981; *revised received* 12 *April* 1983

The near ultraviolet absorption spectra of 2, 3- and 3, 5-dichloroanilines corresponding to $^1A_{1g} \rightarrow {}^1B_{2u}$ and $^1A_{1g} \rightarrow {}^1B_{1u}$ transitions of benzene have been recorded in vapour phase. The spectra have been analyzed in terms of some ground and excited state fundamentals. The assignments of fundamental frequencies to probable modes of vibration and red shift of 0, 0 bands are discussed.

The electronic absorption spectrum of aniline in vapour phase has been studied by Ginsberg and Matsen[1]. Apart from other substituted anilines, the electronic spectra of di- and trichloroanilines have been studied by many workers[2-5]. In continuation of this work, the present communication reports the electronic absorption spectra of 2, 3- and 3, 5-dichloroanilines in vapour phase which have not been reported earlier.

The near ultraviolet absorption spectra of 2, 3- and 3, 5-dichloroaniline molecules (hereafter referrred to as 2, 3-DCA and 3, 5-DCA respectively) have been photographed on Russian NCπ-30 spectrograph with a dispersion of 16 Å/mm at 3100 Å and 9 Å/mm at 2500 Å, varying the temperature between 25 and 70°C and path-length from 50 to 120 cm. The band heads were measured on a comparator (of Optical Instrument Co., with a least count of 0.0001 cm) with an accuracy of ± 5 cm^{-1}. In the present study, both the systems corresponding to $^1A_{1g} \rightarrow {}^1B_{2u}$ (2600 Å) and $^1A_{1g} \rightarrow {}^1B_{1u}$ (2100 Å) system of benzene have been photographed and analyzed.

For $^1A_{1g} \rightarrow {}^1B_{2u}$ system, the very strong bands at 33460 and 33393 cm^{-1} towards the longer wavelength side have been assigned as 0, 0 bands in 2, 3-DCA and 3, 5-DCA respectively. Many of the fundamentals observed in both molecules (Tables 1 and 2) find support from the literature values[6].

Evans[7] has suggested the occurrence of NH_2 torsion at around 245 cm^{-1} and Sharma and Dwivedi[8] assigned this mode at 242 cm^{-1}. In view of these, the

Table 1—Analysis of the Electronic Absorption Bands of 3, 5-Dichloroaniline

Intensity*	Position, cm^{-1}	Assignment
	$^1A_{1g} \rightarrow {}^1B_{2u}$ (2600 Å) System	
vw	33180	$0-5\times44$
vw	33199	$0+272-2\times44$
m	33265	$0-3\times44$
ms	33305	$0-2\times44$
s	33349	$0-44$
vs	33393	0, 0
vvw	33486	$0+223-3\times44$
w	33516	$0+223-2\times44$
w	33555	$391-5\times44$
s	33580	$0+223-44$
s	33616	$0+223$
s	33665	$0+272$
mw	33701	$0+391-2\times44$
mw	33739	$0+391-44$
s	33784	$0+391$
m	33831	$0+2\times223$
ms/s	33868	$0+556-2\times44$
s	33900	$0+507$; $0+556-44$
s	33949	$0+556$
vw	34010	$0+391+223$
w	34035	$0+726-2\times44$
ms	34074	$0+726-44$
s	34119	$0+726$
ms/s	34156	$0+556+223$
ms	34184	$0+878-2\times44$
s	34217	$0+878-44$
s	34271	$0+878$
m	34312	$0+726+223-44$
ms	34351	$0+726+223$
m	34421	$0+1236-213$; $0+2\times507$
m	34488	$0+1137-44$
s	34530	$0+1137$
ms	34579	$0+1236-44$
s	34629	$0+1236$
m	34673	$0+726+556$
s	34738	$0+1345$
s	34808	$0+1137+272$
m	34868	$0+1236+223$
m	34904	$0+3\times507$
m	34951	$0+878+726-44$
ms	34964	$0+1236+391-44$
ms	34987	$0+878+726$
msb	35529	$0+1415+726$
msb	35639	$0+1415+878-44$
	$^1A_{1g} \rightarrow {}^1B_{1u}$	(2100 Å) System
sb	39503	$0-239$
vsb	39742	0, 0
vsb	40007	$0+264$
vsb	40245	$0+503$
msb	40467	$0+725$

* vw—very weak, w—weak, m—medium, s strong, vs—very strong, vsb—very strong and broad, msb—medium strong and broad, vvw—very very weak

* Department of Physics, K K Jain College, Khatauli 251201

Table 2—Analysis of the Electronic Absorption Bands of 2, 3-Dichloroaniline

Intensity*	Position, cm^{-1}	Assignment	Intensity*	Position, cm^{-1}	Assignment
$^1A_{1g} \rightarrow {}^1B_{2u}$ (2600 Å) System			$^1A_{1g} \rightarrow {}^1B_{1u}$ (2100 Å) System		
vw	33253	—	w	39060	0−243
vs	33460	0	wb	39303	0
msb	33706	0+246	msb	39485	0+182
msb	34192	0+732	mwb	39846	0+543
msb	34681	0+1221	wb	40052	0+748
wb	35226	—	wb	40319	0+1016
w	35516	—			
wb	36293	—			
wb	36673	—			

* See Table 1

Table 3—Correlation of the Fundamental Vibrational Frequencies of 3, 5- & 2, 3-DCA in IR, Raman and UV Spectra and Their Assignments

(All values in cm^{-1})

3, 5-DCA			2, 3-DCA				Assignment†
IR	Electronic		IR	Raman	Electronic		
	GS	ES			GS	ES	
	239*	223	—	—	243*	182*	NH_2 torsion
297	—	272	299	282	—	246	β(C−Cl)
427	—	391	—	—	—	—	C−C o.p.b.
437‡							
578	—	507	582	581	—	—	β(C−C)
702	—	556	—	—	—	—	δ(C−C)
797	—	726	767	779	732	732	C−C−C trigonal bend
989	—	878	997	985	—	—	Ring breathing
1272	—	1137	—	—	—	—	ν(C−C)
1302	—	1236	1312	1307	—	1221	ν(C−NH_2)
1445	—	1345	—	—	—	—	ν(C−C)

* In second system ($^1A_{1g} \rightarrow {}^1B_{1u}$)

† ν, stretching, β, in-plane bending, δ, out-of-plane deformation

‡ Raman value

excited state (ES) value of 223 cm^{-1} in 3, 5-DCA and 182 cm^{-1} (from $^1A_{1g} \rightarrow {}^1B_{1u}$ system) in 2, 3-DCA have been assigned to NH_2 torsional mode, which also find support from the ground state (GS) values of 239 and 243 cm^{-1} respectively.

The strong band towards shorter wavelength side having a separation of 878 cm^{-1} in 3, 5-DCA explains quite a good number of observed bands. It has been taken to represent the ring breathing mode. Its ground state counterpart could not be observed but it finds support from the corresponding IR and Raman frequencies[9]. In view of the assignments of Singh[11], Sharma *et al.*[12] and Dwivedi and Sharma[13], the GS value of 44 cm^{-1} in 3, 5-DCA has been taken as a difference band, such as between ES fundamental 391 cm^{-1} and its GS counterpart at 427/437 cm^{-1} (Table 3). The other fundamentals with the corresponding IR and Raman values along with their assignments are shown in Table 3.

In the present study, it is also interesting to observe the second system ($^1A_{1g} \rightarrow {}^1B_{1u}$) around 2500Å in both the molecules. The bands at 39742 and 39303 cm^{-1} in this system for 3, 5-DCA and 2, 3-DCA respectively have been assigned as 0, 0 band. However, the bands observed were broad and diffuse in this system. Although, the previous workers[2-4] could not observe this system in other isomers of dichloroanilines but Amma *et al.*[14] and Nair *et al.*[15] have observed this additional system in other benzene derivatives.

The 0, 0 bands of 3, 5-, 2, 3-, 2, 5- and 3, 4- DCAs are at 33393, 33460, 33114 and 32327 cm^{-1} respectively while that of aniline is at 34037 cm^{-1}. Thus the red shift from aniline is in the order 3, 4- > 2, 5- > 3, 5- > 2, 3-DCA. A similar trend has been observed by Varadarajan and Kalkar[16] for dichlorotoluenes.

The authors are thankful to Prof. N Nath, Head of the Physics Department, Kurukshetra University, Kurukshetra for providing necessary facilities and

to the University Grants Commission, New Delhi for financial assistance.

References

1 Ginsberg N & Matsen F A, *J Chem Phys (USA)*, **13** (1947) 167.

2 Sharma D & Srivastava S L, *Indian J Pure & Appl Phys*, **5** (1967) 305.

3 Rao C G R, Reddy B R K & Rao P T, *Indian J Pure & Apply Phys*, **8** (1970) 764.

4 Singh S Nath & Singh S N, *Indian J Pure & Appl Phys*, **9** (1971) 138.

5 Tripathi G N R & Pandey V M, *Indian J Pure & Appl Phys*, **13** (1975) 860.

6 Rai J N & Maheswari R C, *Indian J Pure & Appl Phys*, **9** (1971) 27.

7 Evans J C, *Spectrochim Acta (GB)*, **16** (1960) 428.

8 Sharma S N & Dwivedi C P D, *Indian J Phys*, **50** (1976) 25.

9 Goel R K, Gupta S K, Jaiswal R M P & Garg P P, *Indian J Pure & Appl Phys*, **18** (1980) 223.

10 Pandey S M & Singh S J, *Curr Sci (India)*, **43** (1974) 713.

11 Singh S J, *Spectrosc Lett (USA)*, **9** (1976) 377.

12 Sharma S N, Sinha R P & Dwivedi C P D, *Indian J Pure & Appl Phys*, **14** (1976) 838.

13 Dwivedi C P D & Sharma S N, *Spectrosc Lett (USA)*, **7** (1974) 329.

14 Amma R A, Nair K P R & Rai D K, *Appl Spectrosc (USA)*, **23** (1969) 616.

15 Nair K P R, Amma R A & Srivastava M P, *Appl Spectrosc (USA)*, **23** (1969) 550.

16 Varadarajan T S & Kalkar A K, *Indian J Pure & Appl Phys*, **13** (1975) 125.

Indian Journal of Pure & Applied Physics
Vol. 21, December 1983, pp. 752-754

Infrared & Laser Raman Spectra of Some Diaminotoluenes

R K GOEL
Department of Physics, D N College, Meerut 250002
and
M L AGARWAL
Department of Physics, D S College, Aligarh

Received 24 *February* 1983; *revised received* 22 *August* 1983

The infrared absorption spectra of 2,4-, 2,6- and 3,4- diaminotoluenes have been recorded on Perkin Elmer 577 spectrophotometer in the region 200-4000 cm^{-1}. The laser Raman spectra of these molecules have been recorded in Cary 82 Raman spectrometer, using krypton ion laser of 6471 Å. The spectra have been analyzed assuming C_{2v} point group for 2, 6-diaminotoluene and C_s for the other two molecules, and the assignments for the observed fundamental modes have been made.

The vibrational spectra of several methylbenzenes were studied by Pitzer and Scott[1], Wilmushurst and Bernstein[2], Green *et al.*[3] and Mooney[4]. The vibrational spectra of various aminotoluenes have also been reported in literature[5-7]. No work seems to have been done on diaminotoluenes. The present note reports the infrared absorption spectra and laser Raman spectra of 2, 4-, 2, 6- and 3, 4-diaminotoluenes. The present assignments are indispensable for the calculation of thermodynamic functions of the molecules and of frequencies with changes in mass and force constants.

The pure chemicals, 2,4-, 2,6- and 3,4-diaminotoluenes (hereafter referred to as 2, 4-DAT, 2, 6-DAT and 3, 4-DAT respectively) obtained from M/s Tokyo Kasei Kogyo Co. Ltd, Japan, were used as such without further purification. The infrared spectra were recorded on Perking Elmer 577 spectrophotometer in the region 200-4000 cm^{-1} in KBr pellet and nujol mull. The laser Raman spectra of the three molecules were recorded on Cary 82 Raman spectrometer using krypton ion laser of 6471 Å, power 80 mW and slit width 3 cm^{-1}. The positions of the bands along with their assignments for the three diaminotoluenes are given in Table 1.

All the three molecules have been taken to belong to C_s point group for the sake of comparison and convenience in analyzing the spectra.

C–C *vibrations*—In tri-substituted benzenes[8], the frequency of one of the two ring modes ν_1 and ν_{12} reduces up to 820 cm^{-1} while the other remains around 1000 cm^{-1}. As ν_1 vibration is totally symmetric, it should appear as a very strong and

Table 1—Assignments of Observed Fundamental Frequencies (in cm^{-1}) in 2, 6-, 2, 4- and 3, 4-Diaminotoluenes

Vibration number	2, 6-DAT			2, 4-DAT		3, 4-DAT		Assignment**
	Sym. species	IR†	Raman‡	IR†	Raman‡	IR†	Raman‡	
2	a′	3070(vvw)	—	3105(w)	—	3090(vw)	—	ν(C–H)
20a	a′	3058(vw)	3038(29)	3078(w)	—	3060(vw)	—	ν(C–H)
8b	a′	1592(m)	1599, 1597 (61)	1605(ms)	—	1600(m)	—	ν(C–C)
19b	a′	1495(ms)	1498, 1495 (26)	1500(mb)	—	1505(m)	—	ν(C–C)
13	a′	1185(vvs)	—	1184(vvs)	—	1170(sb)	—	ν(C–CH_3)
99	a′	1090(vvw)	—	1090(vvw)	—	—	—	C–H i.p.b.
7a	a′	1380(vs)	—	1378(vvs)	—	1380(vvs)	1390(45)	ν(C–NH_2)
12	a′	860(vs)	—	852(vvs)	—	888(s)	—	C–C–C trigonal bending
1	a′	1056, 1038 (vs)	1054(99)	1033(vs)	—	1042(sb)	—	ν(C–C) ring breathing
6a	a′	—	670(75)	710, 700 (mb)	—	695(ms)	—	C–C i.p.b.
18b	a′	—	—	—	—	—	—	—
20b	a′	3010(vw)	—	3050(mw)	—	3015(vvw)	—	ν(C–H)
8a	a′	1582(ms)	1587, 1585, 1583 (70)	1580(s)	—	1592(mb)	—	ν(C–C)
19a	a′	1450(ms)	—	1450(sb)	—	1455(m)	—	ν(C–C)
14	a′	1318(sb)	1311(99)	1312(vvs)	—	—	—	ν(C–C). Kekule

(*Contd*)

Table 1 – Assignments of Observed Fundamental Frequencies (in cm^{-1}) in 2, 6-, 2, 4- and 3, 4-Diaminotoluenes—*Contd*

Vibration number	2, 6-DAT			2, 4-DAT		3, 4-DAT		Assignment**
	Sym. Species	IR†	Raman‡	IR†	Raman‡	IR†	Raman‡	
7b	a′	1288(vvs)	—	1295(vvs)	—	1292(vvs)	—	ν(C–NH_2)
3	a′	—	—	1223(vvs)	—	1248(vvs)	—	C–H i.p.b.
9b	a′	1150, 1145 (sb)	—	1148(vvs)	—	1160(m)	—	C–H i.p.b.
6b	a′	610m	—	622, 618 (m)	—	—	518(22)	C–C i.p.b.
15	a′	—	353, 351 (51)	—	—	—		C–CH_3 i.p.b.
18a	a′	310*(m)	—	—	330(25)	—	—	C–NH_2 i.p.b.
17	a″	785(mw)	—	800(s)	—	808(mw)	—	C–H o.p.b.
16a	a″	—	497, 494 (38)	495, 490 (m)	—	—	498(2)	C–C o.p.b.
10a	a″	—	—	215(m)	—	220, 215 * (mw)	—	C–NH_2 o.p.b.
4	a″	715(mb)	—	720(ms)	—	715(s)	—	C–C o.p.b.
17b	a″	920(s)	—	930(s)	—	938(s)	—	C–H o.p.b.
11	a″	—	—	765(m)	754(89)	745(m)	—	C–H o.p.b.
16c	a″	—	—	390*(m)	—	398*(m)	—	C–C o.p.b.
10b	a″	—	—	—	120(14)	—	112(75)	C–NH_2 o.p.b.
5	a″	300*(mw)	—	295*(mm)	—	300, 297 (15)	—	C–CH_3 o.p.b.
NH_2 group vibrations		3412(ms)	—	3442(vs)	—	—	—	ν(N–H) asym.
		3340(vvs)	—	3355(s)	—	3365(vsb)	—	ν(N–H) sym.
		3320(m)	—	3308, 3292 (ms)	—	—	—	ν(N–H) sym.
		3240(mw)	—	3210(s)	—	—	—	ν(N–H) sym.
		1630(ms)	—	—	—	1620(s)	—	NH_2 scissoring
		1620(ms)	—	1618, 1615 (vw)	—	1615(ms)	—	NH_2 scissoring
		1150, 1146 (sb)	—	1148(vvs)	—	1160(m)	—	NH_2 twisting
		—	—	1075(sb)	—	1080(s)	—	NH_2 twisting
		575(vw)	—	570(mw)	—	570(sb)	575, 573 (22)	NH_2 wagging
		—	261(12)	—	—	255*(m)	—	NH_2 torsion
		235*(s)	247(35)	235*(ms)	—	240(ms)	241, 239 (28)	NH_2 torsion
CH_3 group vibrations		2915(m)	—	2938(mw)	—	2940(vvw)	—	ν(C–H) asym.
		2895(m)	—	2915(m)	—	2930(mw)	—	ν(C–H) asym.
		2860, 2852 (w)	—	2850(m)	—	2865(vw)	—	ν(C–H) sym.
		1475(ms)	—		—	1495(vw)	—	C–H asym. def.
		1470(m)	—	1460(sb)	—	1465(m)	—	C–H asym. def.
		—	—	1405(vvw)	—	1410(vvw)	—	C–H sym. def.
		—	—	1075(sb)	—	1080(s)	—	CH_3 rocking
		985(s)	—	960(s)	960(18)	950(m)	946(30)	CH_3 rocking
		285*(mw)	283, 279 (33)	270*(m)	—	—	—	CH_3 torsion

† Visual intensities: s, strong; m, medium; v; very; b, broad; w, weak

‡ Intensities (based on a maximum value of 100) are shown in parentheses.

* KBr values

** i.p.b., in-plane bending; o.p.b, out-of-plane bending; a′, in-plane; a″, out-of-plane; and ν, stretching

polarized band in the Raman spectra. Only one very strong Raman band has been observed at 1054 cm^{-1} in 2, 6-DAT in this region. In view of these, the very strong infrared bands observed at 1033, 1056/1038 and 1042 cm^{-1} have been assigned to ν_1 mode in 2, 4-DAT, 2, 6-DAT and 3, 4-DAT respectively, while those at 852, 860 and 888 cm^{-1} to ν_{12} mode respectively. These find support from the literature values[9].

A group of four bands between 1400 and 1650 cm^{-1} characterize the spectra of substituted benzenes, i.e., there appear two doubly degenerate vibrations e_{2g} (1595) and e_{1u} (1485) (vibrations 8 and 19 respectively according to Wilson's notation), and one non-degenerate vibration b_{2u} (1310), i.e. ν_{14} vibration of benzene, which have been attributed to C–C stretching vibrations and all these frequencies are known to remain practically unaffected by substitution; however, the doubly degenerate vibrations under reduced symmetry C_s split into two components. The component vibrations 8a, 8b, 19a, 19b and 14 have been observed at 1582 (1585 R*), 1592 (1599 R*), 1450, 1495 and 1318 cm^{-1} in 2, 6-DAT; at 1580, 1605, 1450, 1500, 1312 cm^{-1} in 2, 4-DAT; and at 1592, 1600, 1455, 1505 cm^{-1} (5th value not observed in this molecule) in 3, 4-DAT respectively. These are in agreement with the values given in literature[9–11].

C–X *vibrations*—As a result of substitution at positions 1, 2 and 6 of the ring, the stretching vibrations ν_{13}, ν_{7a} and ν_{7b} become X-sensitive. In substituted anilines, strong C–NH_2 vibration appears near 1300 cm^{-1} (Ref. 12), but because of the two NH_2 groups, one of the two C–NH_2 stretching frequencies may be modified. As such, the bands observed as 1288, 1380 cm^{-1} in 2, 6-DAT, at 1295, 1378 cm^{-1} in 2, 4-DAT, and at 1292, 1380 (1390 R*) cm^{-1} in 3, 4-DAT have been taken to represent the C–NH_2 stretching modes. A frequency around 200 cm^{-1} has been assigned to C–NH_2 out-of-plane vibration by many workers[3,6]. On lines similar to the stretching mode, the two C–NH_2 out-of-plane modes have been identified at 215, 120 cm^{-1} in 2, 4-DAT, and at 220, 112 cm^{-1} in 3, 4-DAT.

Studies on the spectra of toluene and substituted toluenes[2,4,5] show that there appears a strong band around 1200 cm^{-1} which involves C–CH_3 valence oscillation. In view of this, the bands observed at 1185, 1184 and 1170 cm^{-1} have been identified as the C–CH_3 stretching mode in 2, 6-DAT, 2, 4-DAT and 3, 4-DAT respectively. It is also in agreement with literature values[13]. The other C-*X* modes are shown in Table 1 in their respective regions.

Group vibrations—In view of the relation of Bellamy and Williams[14], the bands observed at 3412, 3320 cm^{-1} in 2, 6-DAT, and those at 3442, 3308 cm^{-1} in 2, 4-DAT have been identified as the asymmetric N–H stretching modes, while the corresponding symmetric stretching modes have been identified at 3340, 3240 cm^{-1} in 2, 6-DAT, and at 3355, 3210 cm^{-1} in 2, 4-DAT respectively. Only one band (3365 cm^{-1}) has been observed in this region in 3, 4-DAT, which has been assigned to N–H symmetric stretching mode. Evans[15] assigned a band around 490 cm^{-1} as the first overtone of NH_2 torsion about C–N bond. In the present case, the bands at 261,247 cm^{-1} in 2,6-DAT, at 235 cm^{-1} in 2, 4-DAT, and at 255, 241 cm^{-1} in 3, 4-DAT have been assigned to NH_2 torsional modes.

The C–H stretching and bending vibrations are well assigned in their respective regions in Table 1.

Owen and Hester[16] assigned the CH_3 torsion in the region 177-240 cm^{-1} in various monohalogenated anisoles, while Green *et al.*[3] assigned this mode at around 200 cm^{-1} in methyl substituted benzenes. In the present study, this mode has been identified at 285 (283 R*) and 270 cm^{-1} in 2, 6-DAT and 2, 4-DAT respectively. It is also supported from the work of Tylli *et al.*[17] who assigned the methy torsion around 280 cm^{-1}.

The authors are thankful to Dr L H Jones, Los Alamos Scientific Laboratory, University of California, New Mexico, for providing the facilities for Raman spectra in his laboratory. One of the authors (MLA) is also thankful to the University Grants Commission, New Delhi, for the financial assistance.

R*, Raman frequency

References

1 Pitzer K S & Scott D W, *J Am Chem Soc (USA)*, **65** (1943) 803.
2 Wilmshurst J K & Bernstein H J, *Can J Chem (Canada)*, **35** (1957) 911.
3 Green J H S, Harrison D J & Kynaston W, *Spectrochim Acta Vol A (GB)*, **27** (1971) 793, 807.
4 Mooney E F, *Spectrochim Acta (GB)*, **20** (1964) 1343.
5 Singh S J & Pandey S M, *Indian J Pure & Appl Phys*, **12** (1974) 300.
6 Sharma S N & Dwivedi C P D, *Indian J Pure & Appl Phys*, **13** (1975) 570.
7 Kydd R A & Krueger P J, *J Chem Phys (USA)*, **72** (1980) 280.
8 Tripathi R S, *Indian J Pure & Appl Phys*, **6** (1968) 698.
9 Singh R N & Prasad S C, *Indian J Pure & Appl Phys*, **15** (1977) 264.
10a Goel R K, Gupta S K & Sharma S N, *Pramana (India)*, **11** (1978) 541.
b Goel R K, Kansal M P & Sharma S K, *Acta Phys Pol A (Poland)*, **58** (1980) 453.
11 Varsanyi G, *Vibrational spectra of benzene derivatives* (Academic Press, New York), 1969.
12 Singh V B, Singh R N & Singh I S, *Spectrochim Acta (GB)*, **22** (1966) 927.
13 Goel R K, Sharma S D, Kansal K P & Sharma S N, *Indian J Pure & Appl Phys*, **18** (1980) 930.
14 Bellamy L J & Williams R L, *Spectrochim Acta (GB)*, **9** (1957) 341.
15 Evans J C, *Spectrochim Acta (GB)*, **16** (1960) 428.
16 Owen N L & Hester R E, *Spectrochim Acta Vol A (GB)*, **25** (1969) 343.
17 Tylli H, Konschin H & Carola G F, *J Mol Struct (Netherlands)*, **55** (1975) 157.

INSTRUCTIONS TO AUTHORS

SCOPE

The journal welcomes, for publication, full papers and short notes, reporting significant new results of research, in all areas of physics except space physics. The applied fields covered are electronics, electrical engineering, instrumentation and applied mathematics. However, papers in applied mathematics with emphasis on only derivation and proofs and having no direct physical significance, will not be considered. Review articles are not published normally.

SUBMISSION OF MANUSCRIPT

Manuscripts for consideration should be submitted, *in duplicate*, to Editor, Indian Journal of Pure & Applied Physics, Publications & Information Directorate, Hillside Road, New Delhi 110012. They should neither have been already published nor be under consideration elsewhere.

Manuscripts should be in English and typewritten on only one side of good quality paper, in double space, with adequate margin on all four sides. One original and one carbon or photo-copy, each complete in all respects including abstract, illustrations, appendixes, etc. are to be submitted.

PREPARATION OF MANUSCRIPT

Authors may consult recent issues of the Journal to familiarize themselves with the general style and practices adopted in regard to the various elements of a paper.

General

Manuscript should be presented in as concise a form as possible. Good attention should be given to spelling and grammar. In giving names of chemical compounds and structures, abbreviations of units of measurements, symbols and notations, the style and practices recommended by the IUPAP and IUPAC, should be followed.

Frequently repeating combinations of words, e.g. electric field gradient (EFG), junction field effect transistor (JFET), stimulated Raman emission (SRE), should be abbreviated subsequently, indicating the abbreviated form in parenthesis, as shown, at the place of their first occurrence.

Pages should be numbered consecutively and arranged in the following order: Title, authors' names with their institutional affiliations and abstract, along with relevant footnotes whenever necessary (on a separate sheet); introduction; experimental details/theory/method/analysis; results; discussion; conclusion(s); acknowledgement; references and appendixes. Tables, captions for figures (with legends) and appendixes should be typed *on separate sheets* and attached at the end of the manuscript.

Title

The title should be neither too brief/general nor unnecessarily long. It should reflect the content of the paper so as to derive the maximum advantage in indexing. If a paper forms part of a general series, a specific subtitle, indicating the particular aspect of the work covered in the paper, should be provided.

A short running title for the paper, the broad subject heading under which it should be classified in the contents page (authors may consult recent numbers of the journal for this purpose), and the author (indicated by an asterisk on the relevant author's name) and address for correspondence, should also be provided on the title page.

Abstract

The abstract, usually not exceeding 200 words, should indicate the scope and significant content of the paper, highlighting the principal findings and conclusions. It should be in such a form that abstracting periodicals can use it without modification.

Introduction

Long and elaborate introduction should be avoided. It should be brief and state the exact scope of the study in relation to the present status of knowledge in the field. Literature review should be limited strictly to what is necessary to indicate the essential background and the justification for undertaking the study.

Materials, methods, apparatus, etc.

The sources of materials and their purity, methods of preparation, procedure for measurements and their accuracies, etc. should be clearly stated to enable any other worker to repeat the work if necessary. New methods, techniques, theories, etc. should be described in adequate detail; but if they are well known, a mere literature reference to them will do; differences from standard ones, improvements or innovations should, however, be clearly mentioned.

Results

Only such primary data as are essential for understanding the discussion and main conclusions emerging from the study should be included. All secondary data as are of interest to a specific category of readership *should not be included* in the paper. Such data should be retained by the authors for supply, on request, to any interested research worker. A footnote to this effect may be inserted at the relevant place in the paper.

The results must be presented in a coherent sequence in a unified logical structure, avoiding repetition or confusion. Limitations of the results should be clearly stated.

The same data should not be presented in both tabular and graphic forms. Only such tables and figures as are essential should be included. Simple linear plots that can easily be discussed in the text, should not be included. Infrared, ultraviolet, NMR and other spectra, DTA curves, etc. should be included only if they pertain to new compounds and/or are essential to the discussion; otherwise only significant numerical data should be given in the text or in a table.

Discussion

Long rambling discussion should be avoided. The discussion should deal with the interpretation of results without repeating information already presented under results. It should relate new findings to the known and include logical deductions. A separate section on 'conclusions' can be given only when they are well established and of outstanding significance. Mere observation of qualitative trends of results should be distinguished from firm conclusions. Also, limitations, if any, to the conclusions should be clearly pointed out.

Mathematical portions

Special attention should be given to the mathematical portions of the paper. Equations must be well separated from the text and written clearly with good separation between the successive lines. The usual norms of breaking long mathematical expressions should be adhered to. Equations should be numbered consecutively in Arabic numerals with the number in parenthesis near the right hand margin. Superscripts and subscripts should be clearly indicated in pencil by V and Λ sign respectively. Capital and small letters,

particularly of the same letter when both occur, as well as letters or *symbols likely to be confused* one for the other, *should be* clearly *distinguished*. Special characters (e.g. Greek, script, vector, tensor, etc.) required must be indicated by marginal notes. Letters and symbols which should appear in bold face must be clearly indicated. To simplify typesetting: (i) long and complicated mathematical expressions which are frequently repeated should be replaced with single letter/symbol, *without clashing with the others used* in the paper; (ii) the "exp" form of complex exponential functions should be used; and (iii) to simplify fractions, the solidus (/) is to be used and fractional exponents are to be used instead of root signs, e.g.

write $\exp\{-i\omega_0(t_1-t_2)/2\}$ and *not* $e^{-i\omega_0(t_1-t_2)/2}$

write $(4\omega_{pl}K_{3\lambda}^2/\tilde{\omega}K_D^2)^{1/2}$ and *not* $\sqrt{\dfrac{4\omega_{pl}K_{3\lambda}^2}{\tilde{\omega}K_D^2}}$

Tables

Tables should be numbered consecutively in Arabic numerals and *should bear brief titles. Column headings should be brief.* Units of measurement should be abbreviated and placed below the headings. Nil results should be indicated and distinguished clearly from absence of data. Inclusion of structural formulae inside the tables should be avoided as far as possible. Tables should be referred to in the text by numbers and not by terms like 'above', 'below', 'preceding' or 'following'. Results should not be presented to a greater accuracy than that of the method employed.

Illustrations

The number of illustrations should be kept to the minimum. Wherever possible, e.g. a number of individual analogous figures referring to different variables, substances, molecules, etc. may be combined into one composite figure. All illustrations should be numbered consecutively in Arabic numerals. *Captions and legends* to the figures should be *self-explanatory*. Line drawings should be made with Indian ink on white drawing paper/cellophane sheet/tracing cloth, and drawn to approximately twice the printed size.

The lettering should be uniform, preferably in stencil, so as to be *not less than* 1.5 *mm after reduction* widthwise to full page size (165 mm) or column size (80 mm). The size of geometrical shapes (used to distinguish different graphs), dots, lines, etc. should be sufficiently *large to permit* the necessary *reduction without loss of detail*. In the case of photographs, *prints must be on glossy paper and contrasty*. If an illustration is taken from another publication, reference to the source should be given and prior permission secured. Illustrations should be referred to in the text by numbers and not by terms like 'above', 'following' etc.

Acknowledgement

Acknowledgements should not be exuberant and must be made only to real assistance rendered in connection with the work reported in the paper.

References

References cited should be limited to the absolute minimum (particularly in the case of short notes) based on their essential relevance. In the text, references to literature should be *numbered consecutively, in the order of their first occurrence*, and should be indicated by superscript Arabic numbers at the relevant places; as far as possible the placement of references on numerals or other symbols should be avoided; in such cases the reference may be given in parenthesis in running text, e.g. "this yielded for n a value of 2.3 (Ref. 5)". Full bibliographic details for all the references mentioned in the text should be listed in serial order at the end of the paper.

In citing references to research papers, names and initials of authors should be followed, in order, by the title of the periodical in the abbreviated form (underlined), the volume number (two lines underneath), the year within circular brackets and the page number [e.g. Chandra B P & Shrivastava K K, *J Phys & Chem Solids (GB)*, 39 (1978) 939]. For names of periodicals, the abbreviations followed by the *Physics Abstracts* should be used. For periodicals not covered by *Physics Abstracts*, the title abbreviations should be according to the *Bibliographic Guide for Editors and Authors*, 1974, published by the American Chemical Society, Washington DC, USA; additionally the country from which the journal is published should be given in parenthesis immediately after the title abbreviation. If a paper has been accepted for publication, the names of the authors and the journal (with volume number and year, if known) should be given followed by the words "in press" [e.g. Wahi P K & Patel N D, *Can. J Spectrosc (Canada)*, in press.].

In references containing *up to four authors*, the *names of all* the *authors* with their respective initials should *be given*. The abbreviations *et al.*, idem and ibid should be avoided. When there are more than four authors, *only* the names of the *first three authors* with their respective initials should *be given*, followed by the words '*et al.*'

Reference to a book should include details in the following order: name and initials of authors, the title of the book (underlined), name of publisher and place of publication within circular brackets and year and page (s) [e.g. Clayton G B, *Operational amplifiers* (Newnes-Butterworths, London), 4th Edn, 1977, 26]. If the reference is to the work of an author published in a book by a different person, the fact that it is cited from the source book should be clearly indicated [e.g. Turnhout Van J, 'Thermally stimulated discharge of electrets' in *Topics in applied physics*: Vol. 33—*Electrets*, edited by C M Sessler (Springer Verlag, Berlin), 1980, 130].

Proceedings of conferences and symposia should be treated in the same manner as books. Reference to a paper presented at a conference, the proceedings of which are not published, should include, in the following order, names and initials of authors, title of the paper (underlined), name of the conference, and where and when it was held (e.g. Herczeg P, *Symmetry-violating kaon decays*, paper presented to the International Conference on High Energy Physics and Nuclear Structure, Vancouver, Canada, 13-17 August 1979).

Reference to a thesis should include the name of the author, title of the thesis (underlined), university or institution to which it was submitted and year of submission (e.g. Mehrotra S N, *Many-body techniques and their applications to interacting bosons*, Ph D thesis, Ranchi University, 1976).

Reference to a patent should include names of patentees, country of origin (underlined) and patent number, the organization to which the patent has been assigned (within circular brackets), date of acceptance of the patent and reference to an abstracting periodical where available [e.g. Labes M M, *US Pat.* 4,066,567 (to Temple University), 3 January 1978; *Chem. Abstr.*, **88** (No. 20) (1978), 138350 n].

PROOFS & REPRINTS

Authors will receive galley proofs and a reprint order form. The galley proofs, indicating the essential corrections, should be returned to the Editor without delay, enclosing the reprint order form. Authors are given 25 *free reprints* for each paper. *Extra* reprints can be had *at cost. If the reprint order is not received with the corrected proofs, it will be presumed that the author needs no extra reprints.* Later requests for *more* reprints cannot be complied with. Covers for reprints cannot be provided.

THE WEALTH OF INDIA

An Encyclopaedia of Indian Raw Materials and Industrial Products, published in two series: **(i) Raw Materials**, and **(ii) Industrial Products**.

RAW MATERIALS

The articles deal with Animal Products, Dyes & Tans, Essential Oils, Fats & Oils, Fibres & Pulps, Foods & Fodders, Drugs, Minerals, Spices & Flavourings, and Timbers and other Forest products. Names in Indian languages, and trade names are provided.

For important crops, their origin, distribution, evolution of cultivated types, and methods of cultivation, harvesting and storage are mentioned in detail. Data regarding area and yield and import and export are provided. Regarding minerals, their occurrence and distribution in the country and modes of exploitation and utilization are given. The articles are well illustrated. Adequate literature references are provided.

Eleven volumes of the series covering letters A – Z have been published.

Vol. I(A-B) Rs. 80.00; Vol. II (C) Rs. 95.00; Vol. III (D-E) Rs.105.00; Vol.IV (F-G) Rs. 65.00; Vol. IV: Suppl. Fish & Fisheries Rs. 40.00; Vol. V (H-K) Rs. 75.00; Vol. VI (L-M) Rs. 90.00; Vol. VI: Suppl. Livestock Rs. 60.00; Vol. VII (N-Pc) Rs. 30.00; Vol. VIII (Ph-Re) Rs. 86.00; Vol. IX (Rh-So) Rs.104.00; Vol. X (Sp-W) Rs. 225.00; Vol. XI (X-Z) Rs. 115.00.

INDUSTRIAL PRODUCTS

Includes articles giving a comprehensive account of various large, medium and small scale industries. Some of the major industries included are: Acids, Carriages, Diesel Engines, Fertilizers, Insecticides & Pesticides, Iron & Steel, Paints & Varnishes, Petroleum Refining, Pharmaceuticals, Plastics, Ship & Boat-building, Rubber, Silk, etc.

The articles include an account of the raw materials and their availability, manufacturing processes, and uses of products, and industrial potentialities. Specifications of raw materials as well as finished products and statistical data regarding production, demand, exports, imports, prices, etc., are provided. The articles are suitably illustrated. References to the sources of information are provided.

Nine volumes of the series covering letters A – Z have been published.

Part I (A-B) Rs. 54.00; Part II (C) Rs. 64.00; Part III (D-E) Rs. 25.00; Part IV (F-H) Rs: 25.00; Part V (I-L) Rs. 30.00; Part VI (M-Pi) Rs. 28.00; Part VII (Pl-Sh) Rs. 60.00; Part VIII (Si-Ti) Rs. 66.00; Part IX (To-Z) Rs. 80.00.

HINDI EDITION: BHARAT KI SAMPADA—PRAKRITIK PADARTH

Vols. I to VI and two supplements of Wealth of India—Raw Materials series in Hindi already published.

Published Volumes:

Vol. I (अ-औ) Rs. 38; Vol. II (क) Rs. 36; Vol. III (ख-न) Rs. 36; Vol. IV (प) Rs. 83; Vol. V (फ-मेरे) Rs. 60; Vol. VI (मेल-ह) Rs. 80.

Supplements:

Fish & Fisheries (Matsya & Matsyaki) Rs. 49; Liverstock (*Pashudhan aur Kukkut Palan*) Rs. 34.

Vols. VII to XI under publication.

Please contact:

Manager (Sales & Advertisement)

PUBLICATIONS & INFORMATION DIRECTORATE, CSIR

Hillside Road, New Delhi 110012

RN 7092/63

CSIR PUBLICATIONS

WEALTH OF INDIA

An encyclopaedia of the economic products and industrial resources of India issued in two series

RAW MATERIALS SERIES—contains articles on plant, animal and mineral resources

	Rs	$	£
Vol. I (A-B)	80.00	30.00	13.00
Vol. II (C)	95.00	33.00	17.00
Vol. III (D-E)	105.00	32.00	20.00
Vol. IV (F-G)	65.00	27.00	12.00
Supplement (Fish & Fisheries)	40.00	16.00	7.00
Vol. V (H-K)	75.00	28.00	12.50
Vol. VI (L-M)	90.00	34.00	15.00
Supplement (Livestock)	60.00	18.00	6.00
Vol. VII (N-Pe)	30.00	9.00	3.00
Vol. VIII (Ph-Re)	86.00	32.00	14.00
Vol. IX (Rh-So)	104.00	35.00	19.00
Vol. X (Sp-W)	225.00	75.00	42.50
Vol. XI (X-Z)	115.00	38.50	22.00

INDUSTRIAL PRODUCTS SERIES—deals with major, small-scale and cottage industries

Part I (A-B)	54.00	20.00	9.00
Part II (C)	64.00	24.00	11.00
Part III (D-E)	25.00	7.50	2.50
Part IV (F-H)	25.00	7.50	2.50
Part V(I-L)	30.00	9.00	3.00
Part VI (M-Pi)	28.00	8.00	2.80
Part VII (Pl-Sh)	60.00	18.00	6.00
Part VIII (Si-Ti)	66.00	27.00	10.00
Part IX (To-Z)	80.00	34.00	12.00

BHARAT KI SAMPADA (Hindi Edition of Wealth of India, Raw Materials):

Vol. I (अ-औ)	38.00	16.00	6.50
Vol. II (क)	36.00	15.00	6.00
Vol. III (ख-न)	36.00	15.00	6.00
Vol. IV (प)	83.00	34.00	16.00
Vol. V (फ-मेरे)	60.00	22.00	10.00
Vol VI (मेल-ह)	80.00	27.00	13.00
Livestock (Kukkut Palan)	34.00	15.00	6.00
Fish & Fisheries (Matsya aur Matsyaki)	49.00	21.00	8.00
A Dictionary of Generic & Specific Names of Plants and Animals Useful to Man with their English and Latin pronunciation in Devanagari.	30.00	11.00	5.00

OTHER PUBLICATIONS

	Rs	$	£
Proceedings seminar on primary communications in Science & Technology in India by Sh. R.N. Sharma & S. Seetharama	52.00	17.50	9.00
Flora of Delhi by J.K. Maheshwari	28.00	8.00	2.80
Indian Fossil Pteridophytes by K.R. Surange	23.00	8.00	2.30
Indian Thysanoptera by T.N. Ananthakrishnan	26.00	8.00	2.60
The Millipede Thyropygus by G. Krishnan	12.00	3.50	1.20
Drug Addiction with special reference to India by R.N. Chopra & I.C. Chopra	12.00	3.50	1.20
Glossary of Indian Medicinal Plants by R.N. Chopra & I.C. Chopra	35.00	13.00	6.00
Fluidization & Related Processes	12.00	4.00	1.20
Evolution of Life by M.S. Randhawa, A.K. Dey, Jagjit Singh & Vishnu Mitre	22.50	7.00	2.25
Collected Scientific Papers of Meghnad Saha	30.00	9.00	3.00
Proteaceae by C. Venkata Rao	34.00	11.00	3.40
Pinus by P. Maheshwari & R.N. Konar	30.00	11.00	5.00
Cellulose Research I	3.00	0.90	0.30
Cellulose Research II	6.00	1.75	0.60
Chemical Process Design	9.00	2.50	0.90
Low Temperature Carbonization of Non-coking Coals & Lignites & Briquetting Coal Fines:			
Vol. I	17.50	5.50	1.75
Vol. II	17.50	5.50	1.75
Nucleic Acids	10.00	3.00	1.00
IGY Symposium: Vol. I	9.00	2.50	0.90
IGY Symposium: Vol. II	9.00	2.50	0.90
CNS Drugs	16.50	5.00	1.65
Kinetics of Electrode Processes & Null Points of Metals	2.50	0.75	0.25
Indian Sardines by R.V. Nair	22.00	7.00	2.20
Termite Problems in India	9.00	3.00	0.90
Loranthaceae by B.M. Johri & S.P. Bhatnagar	32.00	11.00	3.20
Abies and Picea by K.A. Chowdhury	14.00	6.00	2.10
Gnetum by P. Maheshwari and Vimla Vasil	20.00	6.00	2.00
Aquatic Angiosperms by K. Subramanyam	20.00	6.00	2.00
Supplement to Glossary of Indian Medicinal Plants by R.N. Chopra, I.C. Chopra & B.S. Varma	18.00	7.00	3.00
Herbaceous Flora of Dehra Dun by C.R. Babu	144.00	60.00	22.00
Diosgenin and Other Steroid Drug Precursors by Y.R. Chadha & Miss L.V. Asolkar	36.00	13.00	6.00
Research & Development Management by Inder Dev	25.00	10.00	—
Rural Development and Technology—A Status Report-cum-Bibliography by P.R. Bose & V.N. Vashist	100.00	38.00	17.00

Packing and Postage extra

Please contact:

Manager (Sales & Advertisement)

PUBLICATIONS & INFORMATION DIRECTORATE, CSIR

Hillside Road, New Delhi 110012

Printed & Published by D.S. Sastry, Editor, Publications & Information Directorate (PID)
Hillside Road, New Delhi 110012, at PID Photocomposition Unit

D(C)540